Bedrock Structural Influences on River Morphology

by

Michael J. Curran

BA, Colorado College, 2013

Thesis Submitted in Partial Fulfillment of the
Requirements for the Degree of
Master of Science

in the
Department of Geography
Faculty of Environment

SIMON FRASER UNIVERSITY
Spring 2020

Approval

Name:	**Michael Curran**
Degree:	**Master of Science**
Title:	**Bedrock Structural Influences on River Morphology**
Examining Committee:	**Chair:** Rosemary Collard Assistant Professor
	Jeremy G. Venditti Senior Supervisor Professor
	John J. Clague Supervisor Professor Emeritus
	Doug Stead Supervisor Professor
	Allison Pfeiffer External Examiner Assistant Professor Department of Geology Western Washington University
Date Defended/Approved:	April 16, 2020

Abstract

Bedrock rivers largely set the pace for landscape evolution in unglaciated terrain and yet little is known about what controls their morphologies. I examine the role that geologic structure plays in the alignment and morphology of bedrock canyons at different scales. At the watershed scale, I examine the striking alignment of the Fraser River with the Fraser River Fault zone and its largely unmapped secondary fault structures. I explore how large sediment inputs affect bedrock canyons alignment and their morphological characteristics. At the reach scale, I investigate how geological structure influences bedrock canyon width. I find that width constrictions coincide with dominant sub-horizontal joint sets whereas widenings coincide with dominant sub-vertical joint sets. I consider this in the context of sequential constrictions and widenings and propose a conceptual model where sub-vertical jointing makes canyon walls more susceptible to failure due to river undercutting than horizontal jointing.

Keywords: bedrock rivers, structural control, Fraser River, fluvial geomorphology

Acknowledgements

I would like to thank my senior supervisor, Dr. Jeremy Venditti for the continued encouragement and the guided freedom with which I could explore and learn. I have learned so much under your tutelage.

I would also like to thank the entire River Dynamics Lab group for providing a positive and creative community and a supportive forum in which to voice ideas. Fellow graduate students Max Hurson, Tingan Li, Kyle Kusack, and Morgan Wright, thank you for all the engaging conversations in the lab and the occasional escapes to see the sun. Post-docs Dr. Lizzie Dingle and Dr. Ryan Bradley, thank you for providing much-needed guidance and helping to promote a positive atmosphere in the lab.

I would like to thank all the faculty, staff, and students in the Geography and Environmental Science Departments for their continued support, especially B-Jae Kelly, John Ng, and Justin Song for all their help with equipment and software.

Finally, I would like to thank my family and friends for their unfailing support, encouragement, and guidance in everything I do.

Table of Contents

List of Tables

List of Figures

List of Acronyms

YF	Yalakom Fault
FRF	Fraser River Fault
FRFz	Fraser River Fault zone
Km	kilometer
m.y.	million years
Ma	million years ago
m	meters
s	second
Q	discharge
w	width
h	depth
LiDAR	Light Detection and Ranging
DEM	digital elevation model
RK	river kilometers upstream of the ocean
CPW	constriction-pool-widening
UAV	unmanned aerial vehicle
GPS	global positioning system
DGPS	differential global positioning system
RTK	real-time kinematic
SfM	structure from motion
GCPS	ground control points

Chapter 1.

1.1. Introduction

Bedrock rivers are the interface between surface hydrology and geology. When actively eroding, they are influenced by, and often aligned with, the structure of the rock they incise. Structural controls on river networks are well-documented, and river reaches commonly align with visible structures (Figure 1a-c; Zernitz, 1932; Judson & Andrews, 1955; Maarouf, 1983). At reach scale, the orientation and spacing of discontinuities in rock can influence incision rates and thus affect the style of erosion at the riverbed and margins (Figure 1b, c) (Whipple et al., 2000; Chatanantavet & Parker, 2009). Yet, despite recognition that rock structure can influence river alignment, there has been little work documenting how closely rivers align with structural forms and faults across scales.

At the synoptic scale, rivers commonly align with large-scale structural forms and faults, suggesting a “tectonic predesign” to erosional features in a landscape (Eyles et al., 1997). The geometry of rivers has been used to infer the locations and movements of faults both in planform and profile (e.g. Molnar and Tapponier, 1975, Burbank and Anderson, 2001, Gallen and Wegmann, 2017). Different fault types can control the alignment of rivers in different ways. For example, fold-and-thrust belts generally create rectangular drainage patterns, with transverse gorges in bedrock where rivers cut across mountain ranges (Figure 1a; Scheidegger, 2004). In contrast, strike-slip faults can create complex patterns in a river’s alignment because they can express themselves as convoluted suites of transverse, normal, and thrust faults (Sengor, 2017).

At a smaller scale, structurally controlled river channels are commonly a patchwork of alluvial and bedrock reaches that align imperfectly with the larger scale structure (Rennie et al., 2018). Alluvial reaches may bypass controlling faults, and bedrock reaches align differently based on local changes in bedrock structure and/or exogenic perturbations such as landslides. At this scale, rock structure can affect canyon morphology in a variety of ways. Faults may control the location of tributaries whose fans create steep reaches and deep scoured pools in the fractured rock below (Dolan et al., 1978). Local jointing affects the geometry of constrictions and downstream pool geometry, and greater joint density on channel walls may correspond to deep pools (Wohl and

Legleiter, 2003). The vertical spacing of straths on canyons walls may correlate with the spacing of horizontal joint surfaces (Wohl, 2008), and reach-scale river width commonly differs with joint spacing due to differing susceptibilities to plucking versus abrasion (Spotilla et al., 2015).

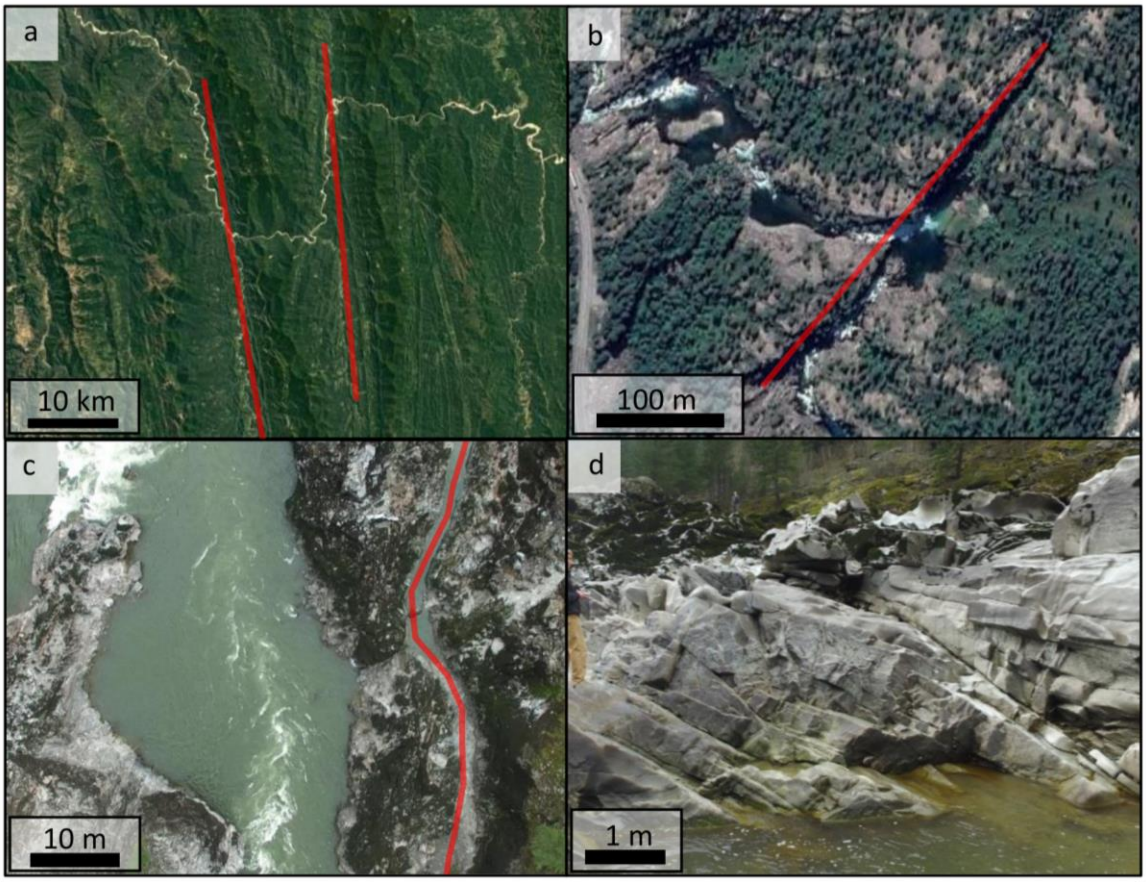

Figure 1. Structural controls on river alignment. a) Large-scale structural control of river form on the Rio Grande o Gaupay, Bolivia. b) Reach-scale control of channel alignment on the Rauma River, Norway. c) Small-scale structural controls in the Fraser River, British Columbia, Canada. d) Structural influence at the process-scale (note plucking along joint planes in the foreground and abrasional features in background) in the Fraser River, British Columbia, Canada.

At the process scale, joint spacing and orientation partly control incision rates by modulating the dominance of plucking and abrasion. Fracture-controlled plucking of blocks can be more effective than abrasion by orders of magnitude (Whipple et al., 2000; Chatanantavet & Parker, 2009; Beer et al., 2017). Additionally, the geometry of fractures can influence the type of plucking that occurs (vertical, horizontal, sliding, or toppling), which, in turn, can affect erosion rates as shown in studies of knickpoint retreat (Dubinksi & Wohl, 2013; Lamb et al., 2015).

Here I explore how large-scale orientation of the Fraser River in southwest and south-central British Columbia is controlled by the orientation of Fraser River Fault zone (FRFz), and how secondary faulting associated with wrench faulting affects the alignment of individual bedrock-bound canyons. I also explore how landslides and other major episodic sediment inputs affect canyon alignment and morphology.

1.2. Study Area

The Fraser River flows 1375 km from its headwaters in the Rocky Mountains to its delta on the southwest coast of British Columbia near Vancouver (Figure 2). The watershed has an area of ~232,000 km^2 and drains parts of the Rocky, Coast, Cariboo, and Cascade mountain ranges, as well as much of the southern Interior Plateau of British Columbia. The mean annual discharge and mean annual flood at Hope, where the river exits the mountain front and begins to deposit its sediment load, are respectively 2830 m^3s^{-1} and 8766 m^3s^{-1} (Venditti et al., 2015). The river underwent a major reorganization in the Middle Pleistocene when a formerly north- and east-draining watershed was captured by a smaller south-flowing proto-Fraser River (Andrews et al., 2012). The watershed has been subjected to multiple continental glaciations, with the disappearance of the last ice sheet and establishment of the present drainage about 11,000 years ago (Clague, 1981).

Glaciers and the ice sheet that repeatedly covered British Columbia during the Pleistocene Epoch modified the Fraser River watershed. The configuration and flow of the last ice sheet were strongly controlled by topography; lobes of this ice sheet flowed south down all of the major valleys of southern British Columbia, including the Fraser Canyon, and into the northwestern conterminous United States (Clague, 1981), widening and deepening these valleys. Glacioisostatic rebound at the end of the Pleistocene elevated the land surface several hundred meters between about 14,500 and 12,000 years ago (James et al., 2000; Clague and James, 2002). Glacier erosion and debuttressing of valley slopes by the thinning and retreating ice likely caused landslides that reached the valley floor and locally altered the course of the river. Glacier ice flowing out of the Seton, Stein, Thompson, and Nahatlatch valleys also likely broadened the Fraser Valley at their confluences (Howes, 1975; Ryder and Church, 1986).

The Fraser Canyon is a geographic region with varied boundary types. The reach that extends from Soda Creek (RK 565; river kilometers upstream of the ocean) on the north to Yale (RK 190) in the south has 42 individual, named bedrock canyons that make up 16% of the total length (Figure 2; Table 1). However, the river is bedrock-bound (bedrock on both banks) for 25.5% of the length (Rennie et al., 2018). Another 28.8% is bedrock-constrained (bedrock on one bank).

The Fraser Canyon has been subjected to recent orogenic uplift of the Coast and Cascade mountain ranges and to episodic and ephemeral isostatic depression and rebound associated with the growth and decay of the Cordilleran ice sheet (Clague and James 2002). Both mountain ranges experienced a pulse of rapid exhumation during the late Miocene (8-12 Ma) with uplift rates between 0.5-1.0 km/m.y. (Parrish, 1983; Reiners et al., 2002). The two mountain ranges are divided by the Fraser River Fault zone (FRFz), which is a 570 kilometers long right-lateral transform fault that strikes NW-SE along the Fraser River from the Chilcotin River (Figure 2) into Washington State. Bedrock on opposite sides of the FRFz were offset 80-100 km between 46.5 and 34 Ma (Coleman & Parrish, 1991). The fault zone comprises numerous fault strands and secondary structures that accommodated the Paleogene displacements. Limited mapping of the secondary structures within the fault zone show signatures of wrench faulting. Reactivation of older structures (e.g. Hope, Pasayten, and Yalakom faults), likely contribute further complexity to the fault zone (Coleman and Parrish, 1991).

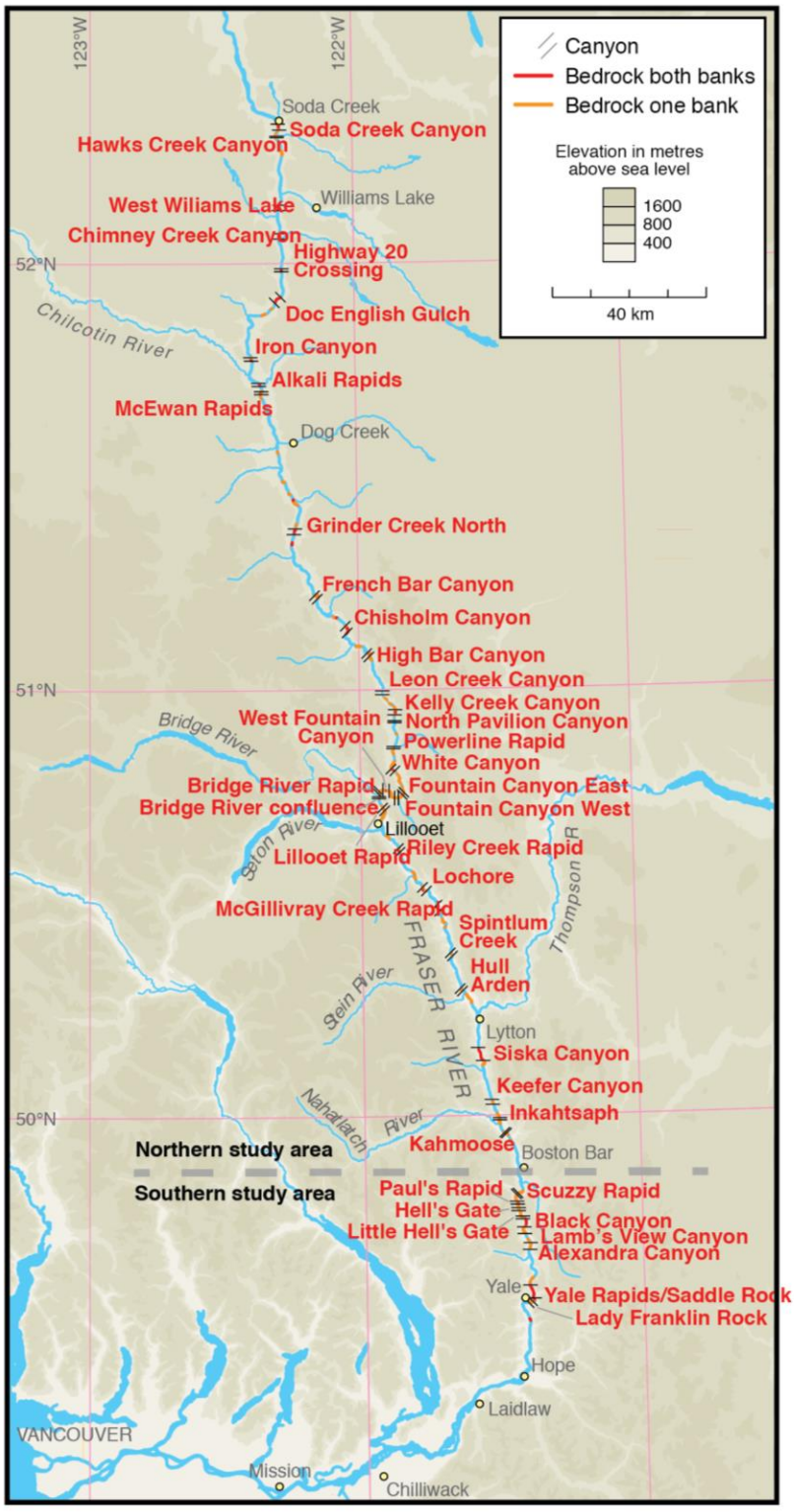

Figure 2. Map of the 42 bedrock-bound canyon reaches that constitute the study area.

Table 1.Characteristics of the 42 named bedrock-bound canyons in the study area.

canyon name	canyon type	mean azimuth	mean valley wall slope (°)	mean slope	length (m)	mean width (m)	mean depth (m)
Soda Creek	epigenetic	285	11.9	0.0011	1779.9	81.5	10.1
Hawks Creek	epigenetic	264	8.3	0.0005	259.2	109.1	9.4
West Williams Lake	unknown	248	13.3	0.0010	1434.2	110.9	9.7
Chimney Creek	epigenetic	280	15.6	0.0010	1390.4	78.2	17.7
Highway 20 Crossing	unknown	283	11.9	0.0003	250.4	116.2	11.2
Doc English Gulch	unknown	219	16.0	0.0010	3203.5	99.8	11.2
Iron	epigenetic	291	20.6	0.0007	923.3	68.4	21.2
Alkali Rapids	epigenetic	296	14.3	0.0010	760.1	101.2	13.7
McEwan Rapids	epigenetic	237	16.9	0.0012	771.3	78.8	19.0
Grinder Creek North	epigenetic	246	16.7	0.0009	1631.6	128.4	12.8
French Bar	unknown	317	18.0	0.0018	1860.3	144.9	10.0
Chisholm	unknown	284	15.5	0.0005	2065.8	84.5	12.7
High Bar	epigenetic	318	15.0	0.0012	1511.1	100.3	10.9
Leon Creek	epigenetic	278	19.7	0.0017	898.2	63.7	11.7
Kelly Creek	unknown	251	19.1	0.0016	1403.9	71.6	16.4
North Pavilion	unknown	287	18.8	0.0017	512.9	51.0	18.6
Powerline Rapid	unknown	247	17.5	0.0012	520.2	90.7	11.8
White	unknown	339	21.4	0.0009	1098.6	94.0	16.9
Fountain East	fault controlled	229	20.9	0.0026	826.0	77.4	13.6
Fountain West	fault controlled	182	18.6	0.0010	1065.0	80.5	19.1
West Fountain	fault controlled	174	22.2	0.0023	1634.9	91.7	14.5
Bridge River Rapids	fault controlled	N/A	21.2	0.0000	N/A	N/A	N/A
Bridge River Confluence	fault controlled	260	19.9	0.0012	362.0	62.1	21.4
Lillooet Rapid	epigenetic	291	14.0	0.0003	1898.7	88.6	18.0
Riley Creek Rapid	unknown	295	12.3	0.0006	1065.8	110.8	11.9
Lochore-Nesikep	epigenetic	326	16.2	0.0008	1594.7	81.0	13.2
McGillivray Creek Rapid	epigenetic	309	15.4	0.0010	1819.0	79.3	14.6
Spintlum Creek Rapid	epigenetic	301	16.7	0.0005	1592.7	111.1	8.2
Hull Arden Creek	unknown	294	17.1	0.0011	1981.0	94.1	13.2
Siska	fault controlled	295	18.5	0.0009	4297.9	66.5	23.7
Keefer	epigenetic	300	16.5	0.0005	1550.1	132.7	17.6
Inkahtsaph	unknown	265	14.9	0.0008	544.5	100.2	30.1
Kahmoose	unknown	344	15.6	0.0008	490.1	88.1	27.9
Scuzzy Rapid	fault controlled	210	23.0	0.0021	439.0	83.5	13.1
Paul's Rapid	fault controlled	294	25.7	0.0019	833.2	73.5	24.4
Hell's Gate	fault controlled	N/A	28.8	0.0000	N/A	N/A	N/A
Little Hell's Gate	fault controlled	300	29.5	0.0026	1318.8	126.8	11.3
Black	fault controlled	281	23.3	0.0015	2794.7	83.4	19.5
Black to Alexandra	fault controlled	292	21.8	0.0012	2590.9	171.5	16.0
Alexandra	unknown	317	15.5	0.0004	824.5	119.5	25.1
Yale Rapids	fault controlled	289	24.4	0.0017	4929.0	112.2	18.1

1.3. Methods

I examined the reach orientation of the Fraser River by creating a channel centerline following Dilts (2015) and a polygon of the banklines collected from satellite imagery (The Freshwater Atlas, Province of British Columbia, accessed 18/7/2018). The centerline was smoothed with a bezier curve and divided into 10 m segments. Orientations were determined as the azimuth between end points. I categorized azimuths to generate rose diagrams for alluvial, bedrock-constrained, and bedrock-bound reaches. I grouped river orientations following the classification in Rennie et al. (2018) as being either alluvial, bedrock-constrained, or bedrock-bound. I further divided the bedrock canyon segments into northern and southern regions (Figures 1, 4). The southern region is characterized by nearly continuous bedrock-bound reaches, while the northern region has smaller and more discontinuous canyons.

Mapped faults within 2 kilometers of the river centerline (BC Digital Geology, Province of British Columbia, accessed 12/6/2018) were divided into 1 km sections, and their orientations calculated the same way. I identified and traced previously unmapped lineaments within a 2 km radius of the river centerline using 2 m (LiDAR collected Dec. 7, 2016) and 25 m (Province of British Columbia) digital elevation models (DEMs) and satellite imagery (Landsat/Copernicus, Maxar Technologies, Province of British Columbia, District of Lillooet accessed in Google Earth, Bing Imagery, 1/5/2018-1/12/2019). The inferred locations of major faults (mapped in BC Digital Geology, Province of British Columbia, accessed 12/6/2018) were used to determine the expected orientations of secondary structures (Figure 3a) associated with them.

I compared the alignment of the river with the main FRFz. Wrench faulting theory (Wilcox et al., 1973) suggests that the secondary faulting should occur on the five planes of Reidel shearing: 1) (R) shears 15^{o} in a clockwise direction from the orientation of the principal displacement (θ), 2) antithetic (R') shears 75^{o} clockwise from θ, 3) synthetic P shears 45^{o} anticlockwise from θ, 4) tension gashes and normal faults orthogonal to θ, and 5) Y shears parallel to θ (Figure 3a).

The satellite imagery and DEMs were also used to map landslides and lateral sediment inputs bordering each of the 42 named bedrock-bound canyons. I then used these

features to categorize some canyons as epigenetic gorges, which are created when a river is forced to incise bedrock adjacent to its channel by sedimentary processes such as landslides or rapid aggradation (Ouimette et al., 2008). I classified bedrock-bound canyons that were not epigenetic as fault controlled and left some unclassified if their origin was ambiguous.

The morphological characteristics of all 42 named bedrock-bound canyons were determined from data presented in Rennie et al. (2018). River depths were determined with an acoustic Doppler coupling profiler, and water surface slope was mapped using a Wide Area Augmentation Strategy DGPS (see Rennie et al., 2018 for details). I separately measured average surrounding valley slope and determined lengths and widths of the canyons using the satellite imagery and DEMs. I calculated valley slope as the average slope within a 750 m perpendicular distance from the channel centerline. I made statistical comparisons of the epigenetic and fault controlled canyon types using non-parametric correlation methods between canyon type and each morphologic characteristic. I explored whether the orientation distributions were Von Mises (circular normal) distribution using the Watson Test of Uniformity. I estimated whether the circular fault and river alignment distributions were statistically different by using the Watson Two-Test of Homogeneity.

1.4. Results

1.4.1. Orientations by channel type

The orientations of 10 m reaches of the Fraser River grouped by reach type (alluvial, bedrock-constrained, bedrock-bound) have a dominant NW-SE orientation that parallels the strike of the FRFz (Figure 3b, c & d). Statistically, they are non-normal ($p < 0.01$), and visually, their multiple modes align weakly with the expected orientations of secondary structures associated with the fault (Figure 3b, c, d). The largest mode of the alluvial segments has an orientation similar to the main trend of the fault zone (11.1% fall within $\pm$ 3^{o}), but the distribution contains other modes that lie between other structure orientations (Figure 3a). The bedrock-constrained reaches cluster around the main direction of the FRFz (12.3% fall within $\pm$ 3^{o}) (Figure 3b). However, they also have multiple modes that do not align with this direction and that have distributions that are statistically

different (Watson's Two Test of Homogeneity; $p < 0.01$), depending on whether they are constrained on the right or left bank. Only 6.6% of the bedrock-bound reaches fall within $\pm$ 3º of the FRFz orientation (Figure 3d). The distributions include four other modes. Two are at 15º and 29º from the largest mode and lie between the orientations predicted from wrench fault theory (Figure 3a). The other two modes align well with orientations predicted from wrench fault theory at 49º and 74º from the magnitude of the largest mode.

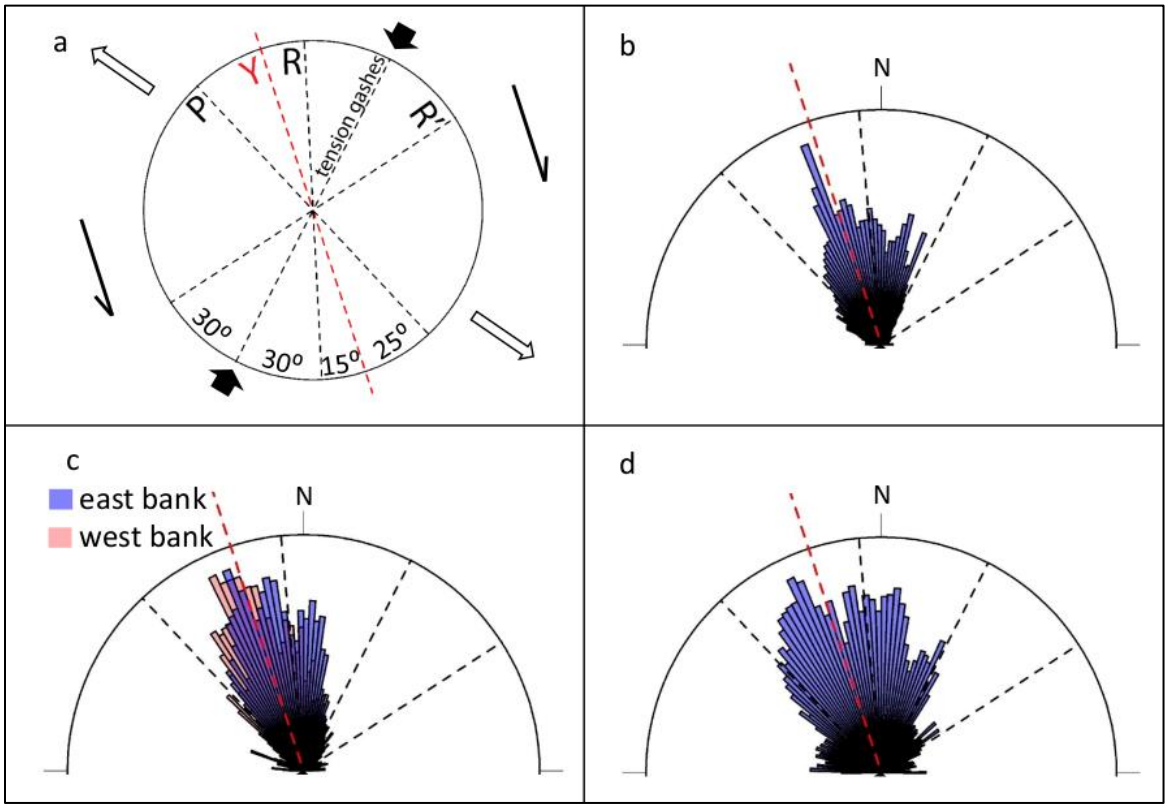

Figure 3. Rose diagrams showing orientations of 10 m segments of the Fraser River in different reach types with expected orientations of secondary structures associated with the Fraser River Fault overlain. A) Model of deformation for the FRFz with the dashed lines showing expected orientations of secondary structures (P,Y,R,R'-type Reidel shears, and tension gashes). Half-arrows indicate direction of shear. B) Alluvial reaches. C) Bedrock-constrained reaches colored by which bank is bedrock. D) Bedrock-bound reaches.

1.4.2. Orientations of bedrock-bound reaches by region

I would expect to see a stronger relation between river orientation and bedrock structure where the river is bedrock-bound, because it is incising directly into rock. A stronger

relation between the named bedrock-bound canyon orientations and fault structures is evident when data are separated between the northern region with more discontinuous canyons and southern region with more continuous canyons (Figure 4). In the south, the FRFz has a more N-S orientation than in the north, and mapped faults show a distribution of orientations that visually align with the orientations of the main fault, which has a largest mode of 357º. Three modes are evident in the fault's distribution: 1) parallel to the main fault (12.0% within ± 3º), 2) R shears (9.8% within ± 3º) and 3) P shears (12.0% within ± 3º). The bedrock-bound canyon reaches have a distribution of orientations with modes that align well with the main fault and its secondary structures. There are three main modes in the river's distribution: 1) parallel to the main fault (10.8% within ± 3º), 2) R shears (4.8% within ± 3º), and 3) P shears (13.3% within ± 3º). A fourth mode, which has a lesser magnitude, and is oriented WNW, cannot be explained by structures associated with the FRFz. Therefore 28.9% of the orientations can be predicted from the main fault orientation and wrench fault theory.

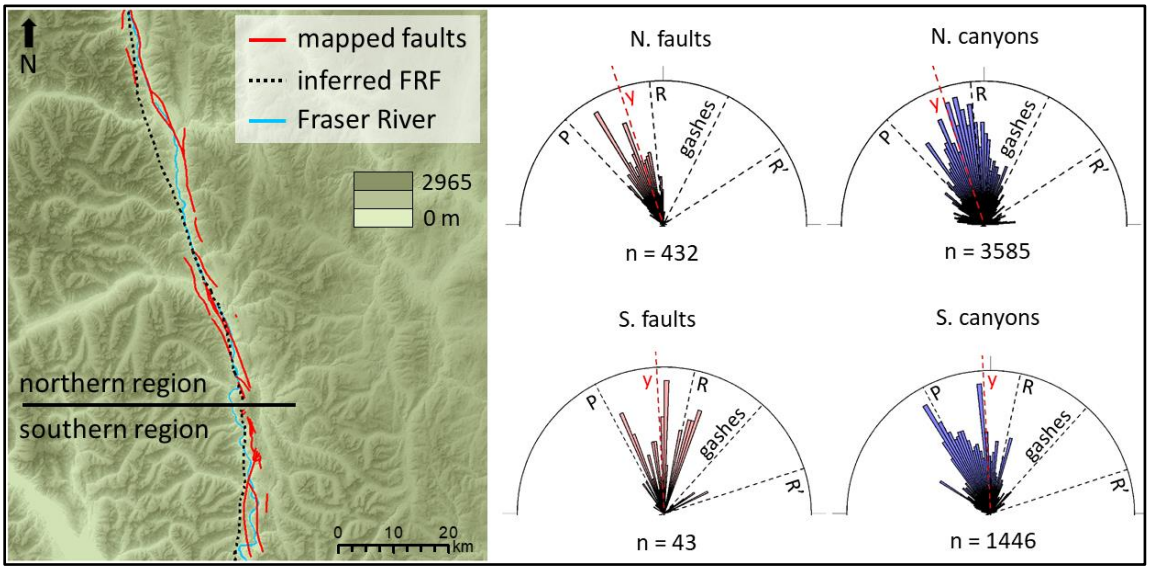

Figure 4. Rose diagrams showing orientations of 1 km segments of faults and 10 m segments of bedrock-bound reaches with expected orientations of secondary structures associated with wrench faulting in the FRFz overlain as dashed lines (Figure 3a). Map shows inferred and documented faults that lie within 2 km of the centerline of the river.

In the northern area, the main fault has a largest mode of 342º degrees, and mapped fault segments have one mode that centers around the orientation of the main fault plane (19.2% within ± 3º) and a second, unexplained mode that is oriented NW and contains 20.6% of the segments within ± 3º. The northern bedrock-bound canyons have a wide distribution that is centered around the main fault with its largest mode oriented at 343º.

The wide distribution of canyon orientations in the northern region is partly caused by large lateral sediment inputs to the river (e.g. glacial outwash channels or alluvial fans) which have created epigenetic gorges and thus displaced the channel from its alignment with the fault zone. Epigenetic canyons constitute 14 of the 42 named canyons; or 41% of the named bedrock-bound canyon reaches in the northern region. These canyons commonly have lobate shapes that align with the fans of lateral sediment inputs rather than fault structures (Figure 5).

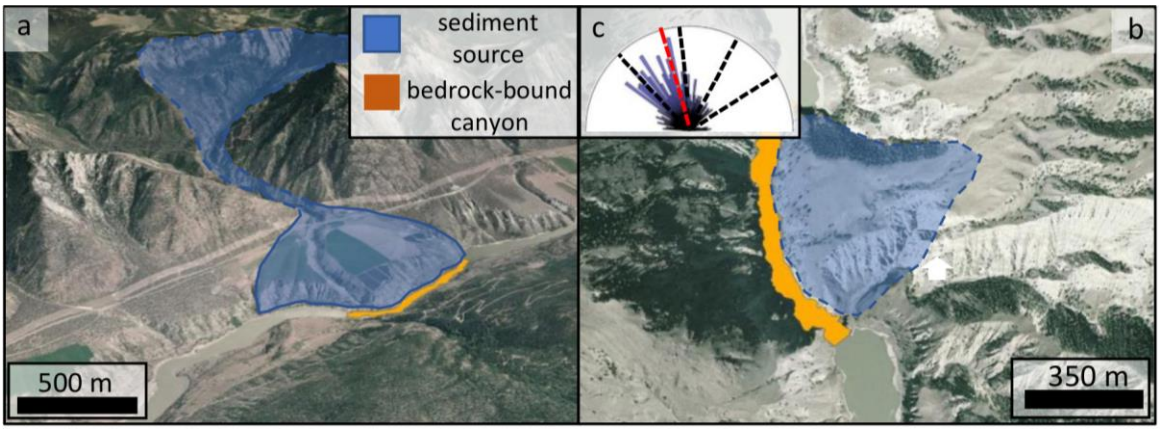

Figure 5. Examples of epigenetic canyons formed by major episodic sediment inputs. a) Lochore-Nesikep Canyon. b) Iron Canyon. c) Rose diagram of 10 m river segments orientations for all epigenetic canyons. Dashed lines show the expected orientations of secondary structures associated with the main fault (definitions as in Figure 3). See Appendix A for other examples.

Some canyons without epigenetic origins in both the north and south regions visibly align with local lineaments associated with the FRFz, suggesting that the alignment of the bedrock-bound canyons, where not influenced by large sediment inputs, is controlled by weakened zones associated with the main fault and secondary structures. Siska Canyon and Black Canyon, for example, align with the main fault and Riedel (R) and (P) shears (Figures 6a and 6b, respectively). Several other canyons that are not epigenetic have orientations that cannot be explained by the simple wrench faulting model of Reidel shearing (Figure 3a). White Canyon, the Fountain-Bridge River Canyon complex (Fountain Canyon East, Fountain Canyon West, West Fountain Canyon, Bridge River Rapid, and Bridge River Confluence Canyon) and Lillooet Canyon are a system of bedrock-bound canyons located at the intersection of the FRFz and Yalakom fault (Figure 6c). These canyons are located around an “S” shaped bend that appears to be a pull-apart basin where the two faults interact.

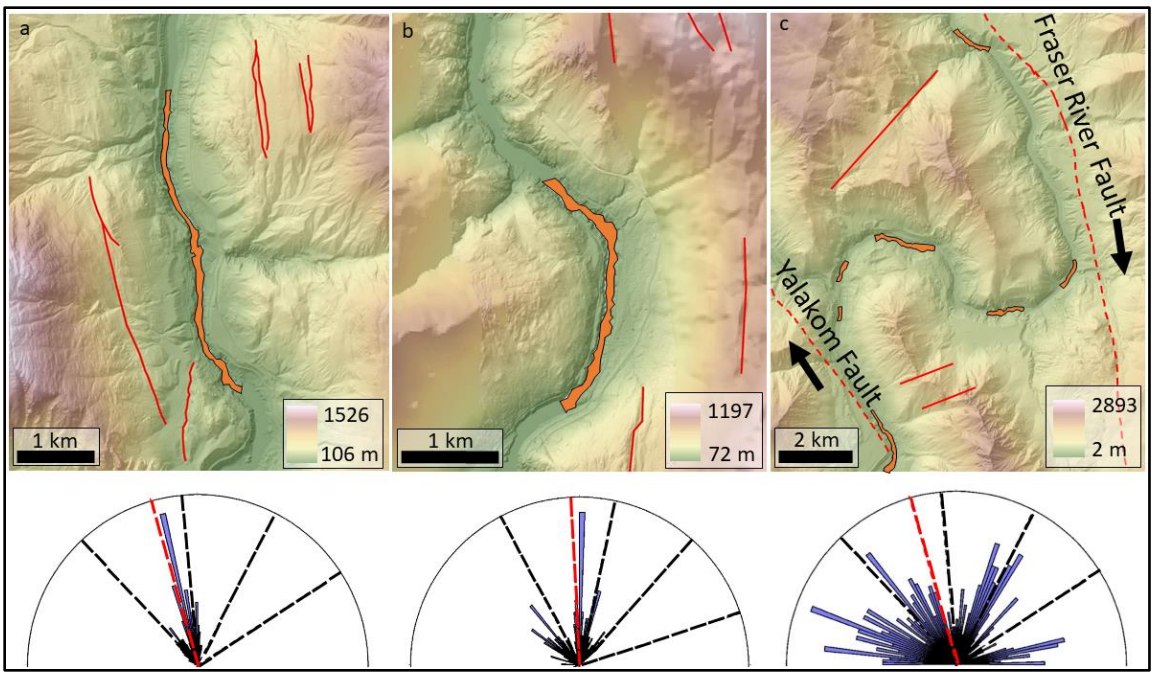

Figure 6. Canyons that visibly align with local structure: a) Siska Canyon. b) Black Canyon. c) Fountain-Bridge River Canyon complex. Bedrock canyons shaded in orange and lineaments highlighted in red. See Appendix A for other examples.

1.5. Discussion

Alignment of bedrock rivers with geologic structure

Bedrock rivers are commonly assumed to align with major geologic structures (unconformities, faults and folds) at large scale. Our investigation of the alignment of the Fraser River with the Fraser River Fault zone shows this is true. The river does roughly align with the fault zone, however, at the reach scale the main orientation of the FRFz only explains some of the river's alignment (~30% in the southern region and 19% in the northern region). Wrench faulting and associated secondary fault structures exert a first-order control on river orientations at the reach scale. Many reaches align with the expected orientations of Reidel shears associated with wrench faulting. Other differences are explained by epigenetic influence. Faulting associated with what appears to be a pull-apart basin at the intersection of the Yalakom and Fraser faults also contributes to the orientation differences. These results suggest that bedrock rivers do align with major geologic structures, but at the reach scale local characteristics of the fault zone can exert a first order control on alignment.

Differences in orientations of bedrock-bound canyons along other rivers that are structurally influenced likely also have epigenetic influences. The reaches just upstream and downstream of epigenetic canyons may align with the controlling structure in the region, but these canyons represent areas where the river has had to adjust to large inputs of sediment or other secondary phenomena. The epigenetic canyons of the Fraser River were forced to incise their bedrock walls either because landslides blocked the original channel or lobate sediment deposits were built out into the valley from tributaries. The 14 epigenetic Fraser River canyons deviate from the orientation of the FRFz, but their alignments suggest that the river was forced out of a channel aligned with the fault. These observations suggest that structure is the first-order control on the alignment of bedrock-bound canyons and that epigenetic processes locally overprint structure. This contention is consistent with Ouimette et al. (2008) who argue that the existence of epigenetic gorges can complicate the calculation of large-scale watershed incision rates. The large number of epigenetic gorges along the Fraser River suggests that this is an important consideration for the Fraser catchment.

Epigenetic canyons also provide a source of systematic variation in the morphology of bedrock-bound canyons in the Fraser River (Figure 7). Fault-controlled canyons have steeper valley wall slopes ($p < 0.05$) than epigenetic canyons, likely because greater glacial influences are conducive to epigenetic events. Fault controlled canyons also have steeper water surface slopes ($p < 0.05$), and greater mean depths. However, the maximum depth is the same in fault-controlled and epigenetic canyons. This may be explained by the type of erosion that occurs on the beds of bedrock-bound canyons and the amount of time that each canyon type has had for that process to work. Erosion on the beds of bedrock-bound canyons is focused where constrictions in the canyon walls cause backwaters and plunging flows (Venditti et al., 2014). Over time, deep scour pools develop directly downstream of constrictions. If epigenetic canyons are younger than the others, as the ordering of their alignment suggests, they may have had enough time to develop deep scour pools like the older fault controlled canyons, but not enough time to lower the whole bed to similar depths. This would occur through the formation and collapse of constriction-pool-sequences in multiple locations in the canyon over geologic time. Similarly, the greater slopes of epigenetic canyons are because they are younger, and erosion has not yet established a gentler gradient.

The FRFz is a wide shear zone along which movement was accommodated by an array of faults typical of large intracratonic strike-slip faults that deform adjacent crust in predictable but complex ways (Wilcox et al., 1973). Other major rivers, like the Indus and Red Rivers also follow major wrench fault systems. It is likely that the bedrock sections of these rivers are similarly controlled by the main orientations of their fault zones with interconnecting reaches that follow secondary structures like Reidel shears. In understanding the erosional patterns of similar rivers, it is important to consider the large variety of secondary structures that are commonly associated with wrench faults and how they may be expressed where the fault bends or interacts with other faults.

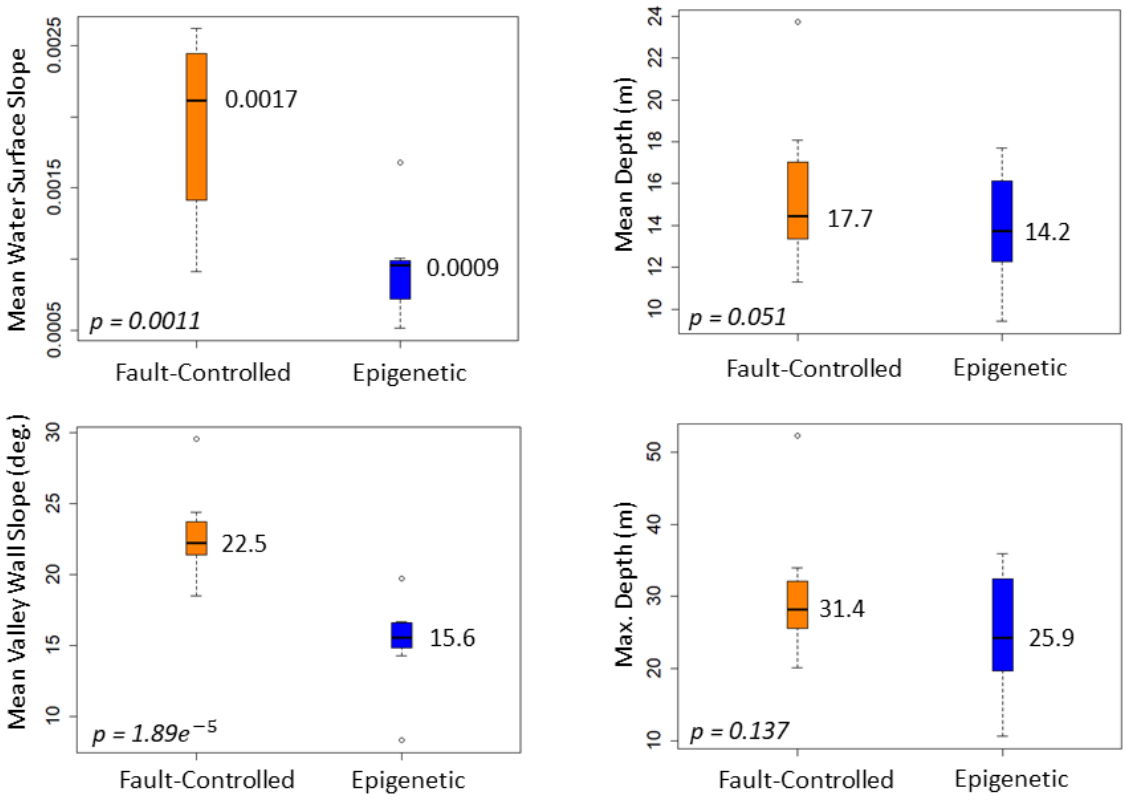

Figure 7. Box plots showing the morphological differences between epigenetic and fault-controlled bedrock-bound canyon reach types.

1.6. Conclusion

I conducted a reach-by-reach analysis of the Fraser River Canyon to investigate structural control on the alignment of the river on different scales. I confirmed that the Fraser River Fault zone controls river alignment at the large scale, but it varies by

channel type. Alluvial channels and bedrock-constrained channels are the most closely aligned with rock structure. Bedrock dominated channels have a much wider distribution of alignments. Individual bedrock-bound canyons often follow the main fault, but also often follow secondary fault structures and alignment is affected by episodic major sediment inputs that alter the course of the river. Epigenetic canyons created by these processes may be younger than the bedrock-bound canyons that align with faults. Bedrock rivers align with geologic structure intermittently – they follow the geologic fabric of a region and occasionally link up with local structures on a reach-by-reach basis.

Chapter 2.

2.1. Introduction

Bedrock rivers are the locus of incision in non-glaciated terrain and thus play a major role in determining the pace of landscape evolution. Their morphologies and rates of erosion on a watershed scale are well-constrained but lack clarity at the reach scale (Venditti et al., *in press*). When bedrock rivers are considered reach-by-reach, they form alternating alluvial, bedrock-constrained (bedrock on one bank), and bedrock-bound (bedrock on both sides) reaches, with different reach types present within the span of a few kilometers (see Rennie et al., 2018). The morphologies of individual bedrock-bound reaches are at least partially controlled by flow and sediment dynamics, and their interaction with the geometry of the walls (Venditti et al., 2014; Cao, 2018; Hunt et al., 2018). In order to better understand bedrock erosion on a large scale, we must understand it better at the reach scale. Here, I document a structural geologic control on the morphology of bedrock-bound canyons.

Although the controls on channel width in bedrock canyons are still poorly understood, it is generally agreed that local channel morphology reflects the characteristics of the bedrock. Channels narrow in areas of more competent bedrock (Wohl and Ikeda, 1998; Montgomery and Gran, 2001), and highly fractured bedrock enhances lateral erosion because of its lower rock mass strength (Wohl, 2008) or through the effects of subaerial weathering (Montgomery, 2004). It has also been shown that plucking can be a more effective erosional agent than abrasion and that fracture geometry can control channel width by affecting the style of erosion of channel walls (Spotilla et al., 2015). Dolan et al. (1978) documented reach-scale effects of geological structure on pool location and geometry in the Grand Canyon of the Colorado River, and Wohl and Legleiter (2002) showed that joint spacing influences the geometry and spacing of pools in a reach by controlling the ratio of width at the constricting feature and width at the downstream pool.

There is an established link between constrictions, flow patterns, and pools in bedrock canyons. Figure 8 shows a series of constrictions and pools in a bedrock-bound canyon of the Fraser River. Lateral constrictions cause plunging flows that promote scour by driving sediment into the bed (Venditti et al, 2014; Cao, 2018; Hunt et al., 2018). They also cause sediment deposition at the downstream end of the pool, where the

momentum of the plunging flow dissipates. This process also enhances lateral erosion, as sediment driven by the plunging flow is deflected off roughness elements on the bed and into the channel walls (Finnegan et al., 2007; Fuller et al., 2016; Li et al., in press). This process results in a constriction-pool-widening (hereinafter referred to as “CPW”) morphology that can be documented on the Fraser River (Figure 9). Constrictions along the Fraser River are located where the wall protrudes into the channel. Widenings are associated with cuspate lobes where the wall has failed. Multiple failures have produced larger widenings.

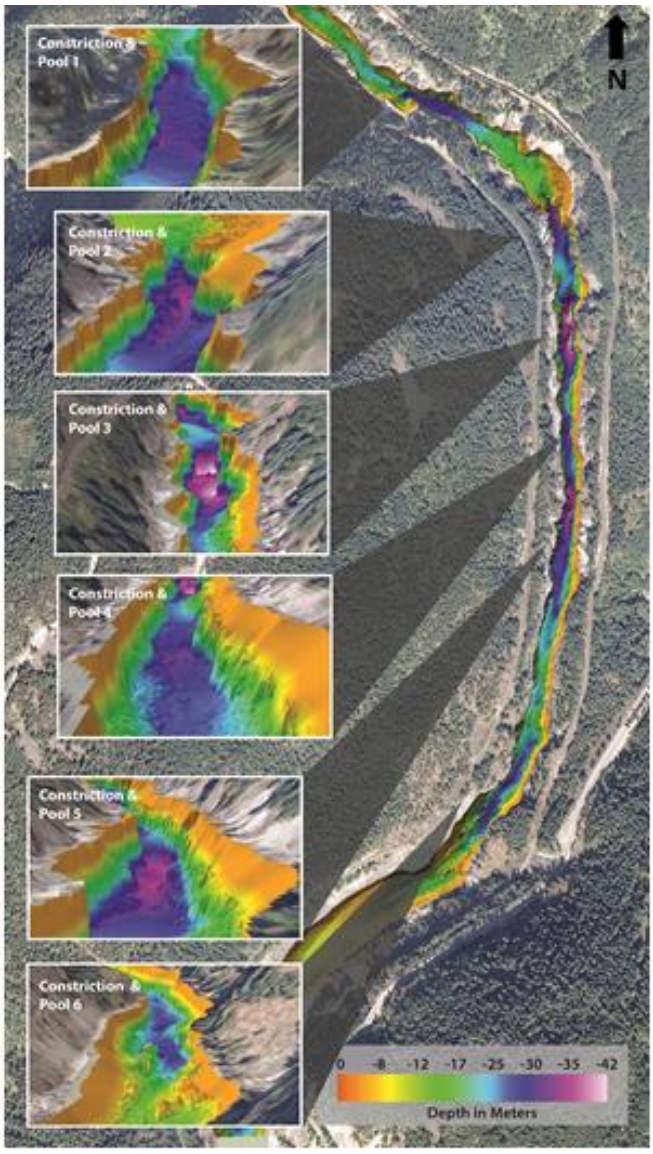

Figure 8. Black Canyon of the Fraser River (49º44’47.5” N 121º25’20.4” W). Province of British Columbia photo, 2003. Bathymetry derived from multibeam echo-soundings, August 31-September 1, 2016, at a discharge of 2190 m^3s^{-1}.

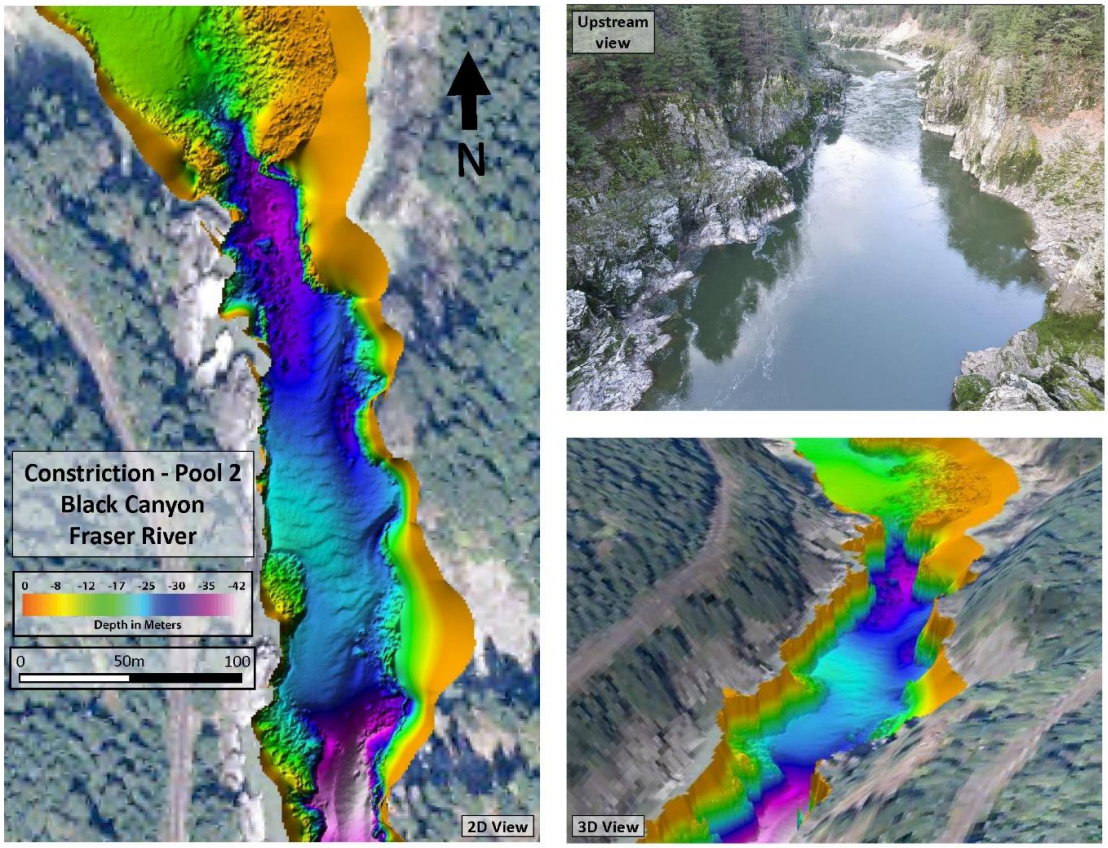

Figure 9. An example of alternating channel constriction and widening in Black Canyon. Drone image, January 21, 2019, at a discharge of 945 m^3s^{-1}.

Here, I explore why constrictions, scour pools, and widenings form in Fraser River bedrock canyons. One hypothesis is that scour pools are the result of the downstream propagation of plunging flows, induced by some upstream perturbation. Cao (2018) argues that the sediment deposit at the downstream end of a scour pool might create a backwater flow and induce a subsequent plunging flow and scour pool, thus autogenically creating a sequence of pools. A second hypothesis, explored here, is that the constrictions and scour pools are allogenic – controlled by the geological structure of the channel walls. Observations along the Fraser River suggest a connection between constrictions and widenings, and the geometrical characteristics of the joint sets within the channel walls (Figure 10).

I examine in detail local-scale structural geological controls on the morphology of Black Canyon, one of the bedrock canyons along the Fraser River in southern British Columbia (Figure 8). I investigate the relation between the joint sets and width. I propose a

conceptual model of bedrock canyon evolution, in which the joint set characteristics control the location of flow-inverting constrictions and create areas in the walls that are more susceptible to failure upon undercutting.

2.2. Study Area

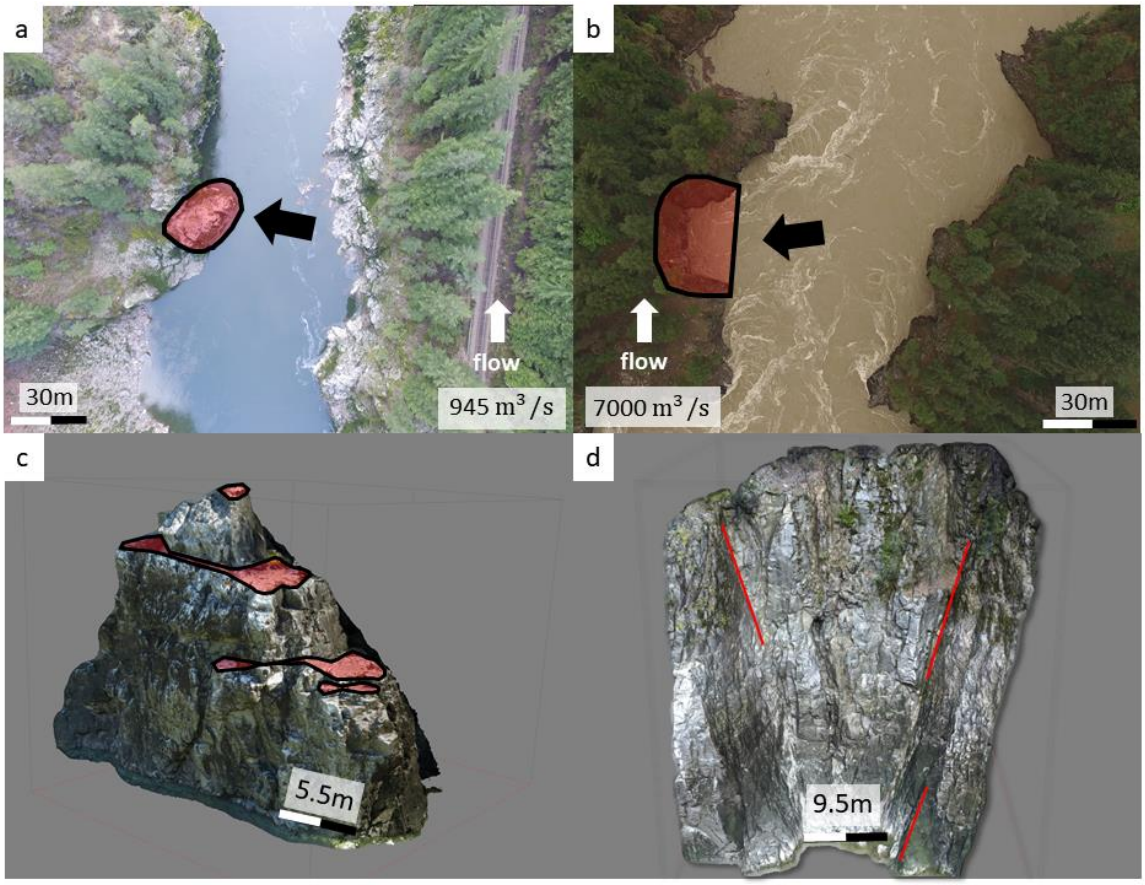

Figure 10. Joint set patterns in a) a constricted channel reach and b) a wide channel reach in Black Canyon. Black arrows show viewing angles for the corresponding windows below. c) and d) Point clouds generated from SfM showing dominantly sub-horizontal jointing in the constricted reach and sub-vertical jointing in the wide reach.

The Fraser River drains an area of ~232,000 km^2 in southern and central British Columbia, flowing 1375 km from its headwaters in the Rocky Mountains to its delta on the Salish Sea at Vancouver. The mean annual discharge at Hope, where the river exits the mountain front, is 2830 m^{3}s^{-1} and the mean annual flood is 8766 m^{3}s^{-1} (Venditti et al., 2015). The Fraser Canyon is a 375 km long portion of the Fraser River extending from Soda Creek in the north (RK 565) to Yale in the south (RK 190). Rennie et al. (2018) mapped the character of the river as it collects water from the southern Interior Plateau and flows between the Coast and Cascade mountain ranges. About 25.5% of the

canyon length is bedrock-bound (bedrock on both sides), although more is constrained by bedrock on one side. There are 42 bedrock-bound reaches (16% of the total reach length) that are considered long enough to be discrete bedrock canyons.

South of Boston Bar, the river incises into the Custer Gneiss – a gneissic granodiorite comprising multiple granitic intrusions. In the 43-km stretch where the river incises this rock, it traverses seven bedrock-bound canyons that are separated by bedrock-constrained and short alluvial reaches. The canyon is steep (1.5 m/km), has tall and steep valley walls, and some of the most imposing rapids in the river. The fourth canyon in this suite, Black Canyon (RK 217.2 to RK 214.4; river kilometers upstream of the ocean), is 2.8 km long and is constricted by ~50% from the reach above it, and the canyon widens downstream. A centerline survey in 2009 (Rennie et al. 2018) revealed that, within Black Canyon, the river had a mean depth of 19.5 m, a maximum depth of 39.2 m, and a mean width of 83.4 m at a discharge (Q) of 1620 m^3s^{-1}. The walls are vertical or near-vertical along most of the reach, but there are downstream differences in channel width from 43 m to 156 m (at Q = 2190 m^3s^{-1}). Much of this variation is expressed at six locations that show a CPW morphology (Figure 8).

2.3. Methods

In order to identify any structural geologic controls on CPW morphology, I first defined and identified constrictions, pools, and widenings. The pools stand out in the canyon bathymetry but identifying CPW morphologies is objectively difficult due to the large seasonal changes in the height of the water surface on the canyon walls. To overcome this problem, I used video data collected at a formative flow (8970 m^3s^{-1}) to identify where the walls were visually constricting the flow and causing convergence at the surface and upwelling downstream. I then compared these areas with observations of bathymetry and 3D velocity (collected between August 31 and September 1, 2017, at Q = 2175 m^3s^{-1}) to confirm that the constrictions are associated with scour pools and plunging flows. I then explored how these locations might change with discharge by measuring river widths (W) at three different flow stages (8970 m^3s^{-1}, 1800 m^3s^{-1}, and 945 m^3s^{-1}). Widenings were defined as areas where the walls retreat in a cuspate lobe as the result of rock slope failure(s).

I measured the high and low flow widths using orthophotograph imagery generated from structure from motion (SfM) data, and the medium flow widths from a LiDAR-generated DEM. The LiDAR topography was collected on December 7, 2016, using an airborne Riegl VQ-580 instrument, at a discharge of 1800 m^3s^{-1} (at Hope, British Columbia, 413 RK downstream). SfM topography was measured at 945 m^3s^{-1} on January 25, 2019, and 8970 m^3s^{-1} on June 16, 2017. I collected SfM data using a DJI Phantom 3 Professional unmanned aerial vehicle (UAV), which captured about 300 nadir images per survey from above the canyon. Ground control was established with 115 ground control points (GCPS) measured using a Trimble 5700 RTK GPS receiver, Trimble Zephyr base station antenna, and Trimble R8 rover antenna. I created orthomosaics using Agisoft Photoscan Professional and georeferenced them in ArcGIS using the LiDAR data and satellite imagery. Widths were measured as the perpendicular distance from the centerline to each bank by digitizing the banks, then creating a centerline following the thalweg as determined by the bed topography. Depths were extracted from a DEM of the bed along the centerline (Figure 1).

With the locations of the CPW units constrained, I documented the structural geological character of the bedrock at each of the six constrictions and on an equal number of widenings. I also identified rock slope failures as distinct cuspate embayments in the channel walls near constrictions and widenings (Figure 9). The structural geological character of all 12 of these constricting and cuspate features was determined using the circular window joint mapping method (Mauldon et al., 2001) with imagery collected at low flow when the features were most exposed above waterline. A circular window 10 m in diameter was selected near the middle of each of the 12 wall features. I mapped some of the widenings at their edges because their centers were covered by talus. Figure 11 shows an example of a window on a cuspate embayment and includes an image (Figure 11a), the generated point cloud (Figure 11b), and the mapping window (Figure 11c).

I measured joint planes using the QCompass plugin (Thiele et al., 2017) in the CloudCompare point-cloud editing software. Every visible joint plane within the window was measured. I plotted dips and dip direction of the joints in polar form on an equal area stereonet using DIPS 7.0 software. The dip and dip direction of the rock slope faces

were determined by fitting a plane to the point cloud representing each window in CloudCompare.

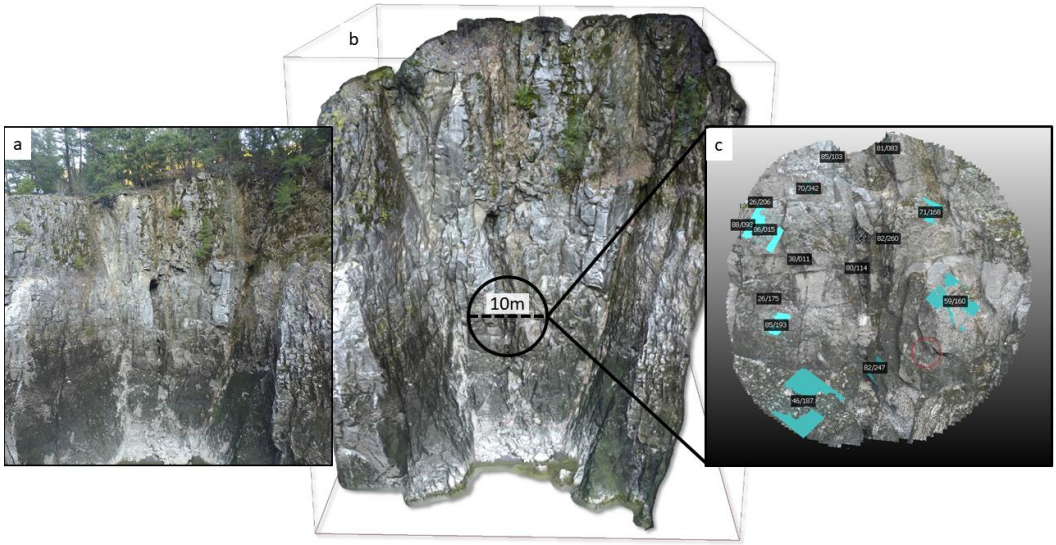

Figure 11. a) Image of a cuspate channel wall in Black Canyon captured with a UAV. b) Point cloud of the same feature created using Agisoft Photoscan. c) 10 m diameter circular sampling window showing joint planes measured using the Qcompass plugin in CloudCompare software.

2.4. Results

Average widths of the canyon differed by 40 m from high and low flow (Figure 12). At Q = 8970 m^3/s, the minimum and maximum widths are, respectively, 43.3 m and 155.7 m. At Q = 1800 m^3/s, the corresponding values are 35.3 m and 113.9 m. At Q = 2175 m^3/s, the minimum and maximum measured depths are 16 m and 41 m. Some of the identified CPW units appear to truncate the one above, with a constriction linking two pools. In the shorter CPW units, widenings are a single rock slope failure, whereas in the longer units, they can be an amalgamation of multiple failures. These widenings are most apparent at higher flows because at low flows the lower portions of walls are masked by a blanket of talus. The mean width at the six constrictions at low flow is 30.5 m and mean maximum width of all the CPW units at high water is 134 m (Table 2). At the six measured widening windows, the average width is 118 m, with a minimum of 85 m and a maximum of 153 m. In every CPW unit, the head of the scour pool has migrated headward, upstream of the constriction.

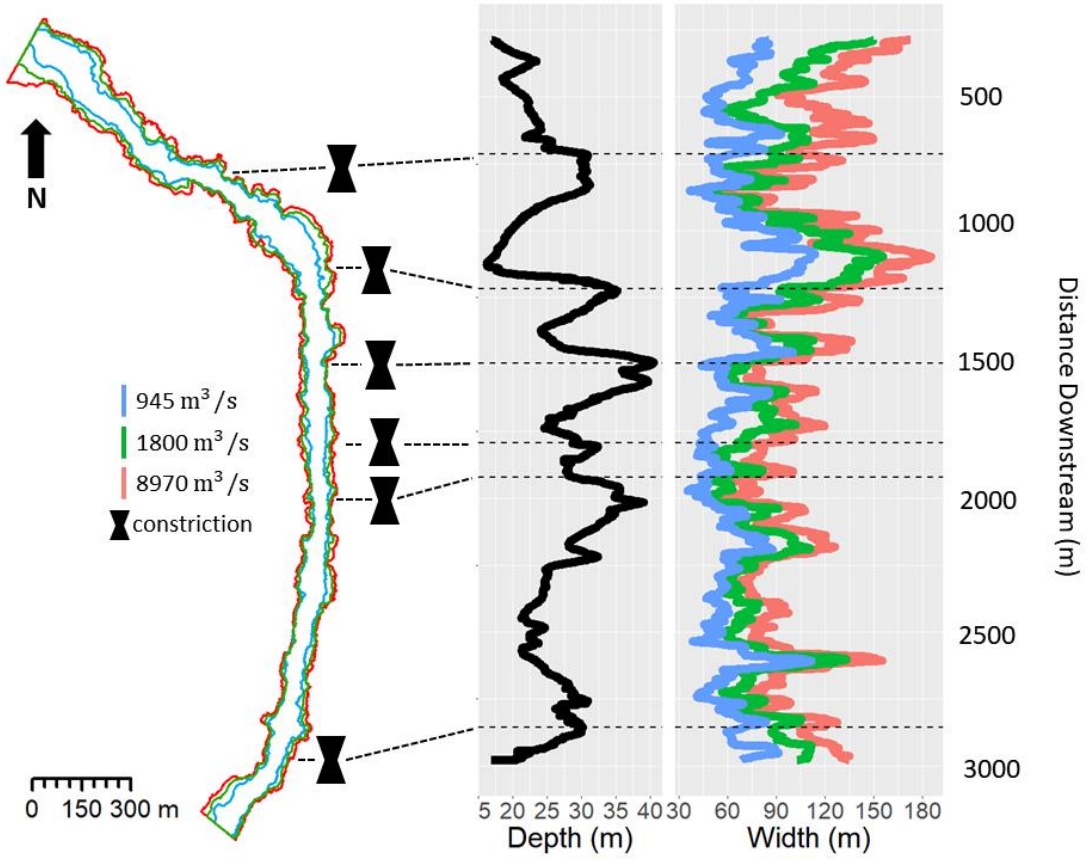

Figure 12. Width and depth differences in Black Canyon at three flow stages with the six constrictions marked.

Table 2. Morphological data for the six CPW morphologies identified in Black Canyon. w = width, h = depth.

	Q = 945 m^3s^{-1}				Q = 1800 m^3s^{-1}				Q = 8970 m^3s^{-1}				Q = 2190 m^3s^{-1}	
CPW	min w (m)	max w (m)	x (m)	constr. %	min w (m)	max w (m)	x (m)	constr. %	min w (m)	max w (m)	x (m)	constr. %	max h (m)	min h (m)
1	36	102	171	65	43	135	162	68	47	153	156	69	31	19
2	50	97	49	48	57	141	155	60	63	168	158	63	35	23
3	44	100	50	56	54	111	52	51	70	128	47	45	41	28
4	41	60	53	32	51	79	86	35	70	101	86	31	32	26
5	35	88	220	60	43	111	195	61	52	126	187	59	39	28
6	41	84	107	51	58	112	188	48	74	127	91	42	31	25

W is width; *h* is depth; x is downstream distance between the min. *w* and max. *w*; constr. % is constriction ratio calculated as: $\left(\frac{\max.w-\min.w}{max.w}\right)*100$.

Figure 13 shows equal area stereonets of joint orientations. Joint orientations in the walls differ between constrictions and widenings (detailed structural characterizations in Appendix B). The constrictions have dominantly horizontal or sub-horizontal joints, whereas the constrictions have largely vertical or sub-vertical joints. Two clear clusters are apparent in the plot of width against mean dip angle of the measured windows shown in Figure 13. The six constrictions have a mean joint dip of 67^0 and a mean width of 50 m, and the six widenings have a mean dip of 39^0 and a mean width of 92 m (at Q = 945 m^3/s).

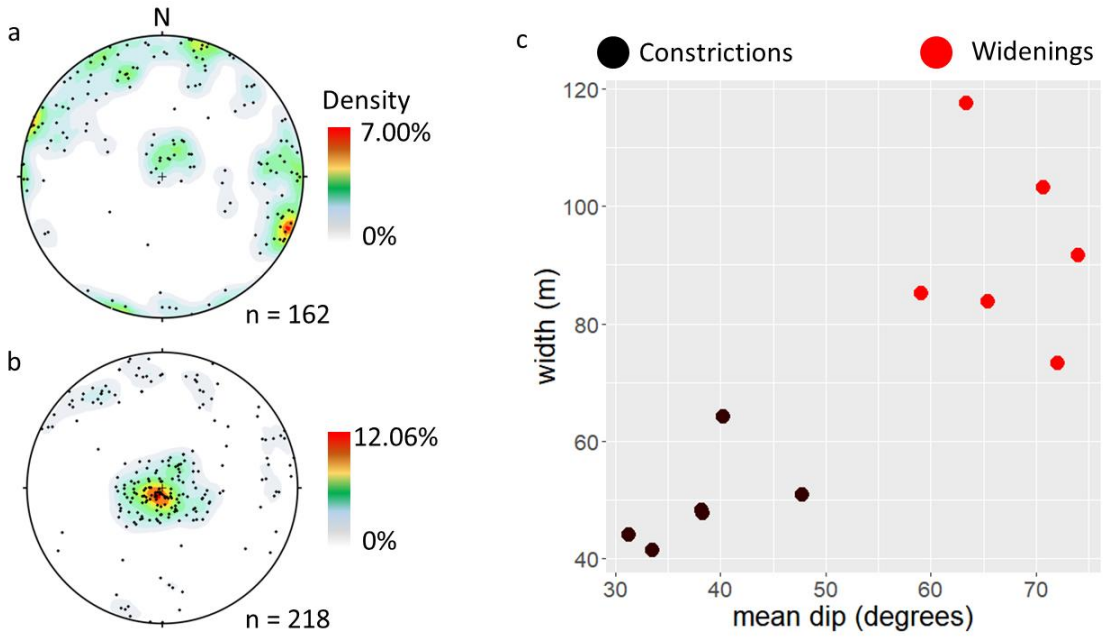

Figure 13. Joint orientations of constricted and wide bedrock channel reaches. a) Equal area stereonet plot of discontinuities for all the widening windows plotted together. b) Equal-area stereonet plot of discontinuities of all constricted reaches. Colors represent pole density determined by a Fisher contour distribution with a counting circle size of 1%. c) Plot of channel width against mean discontinuity dip angle.

2.5. Discussion

Our results suggest that joint set orientation determines the location of constrictions and widenings in Fraser River bedrock canyons because of differences in the resistance of the rock slope to collapse when undercut. Vertically jointed rock walls are more susceptible to collapse than horizontally jointed rock walls, therefore reaches with

pronounced vertical jointing tend to be wider than those with horizontal joints. Constrictions in horizontally jointed rock masses cause plunging flows that undercut walls, which tend to collapse where they are vertically jointed. This interpretation shows the coupled influence of rock discontinuity kinematics and flow dynamics in controlling the width of bedrock channels at the reach scale. It underpins a conceptual model for the link between discontinuity-controlled rock slope stability and channel morphology (Figure 14).

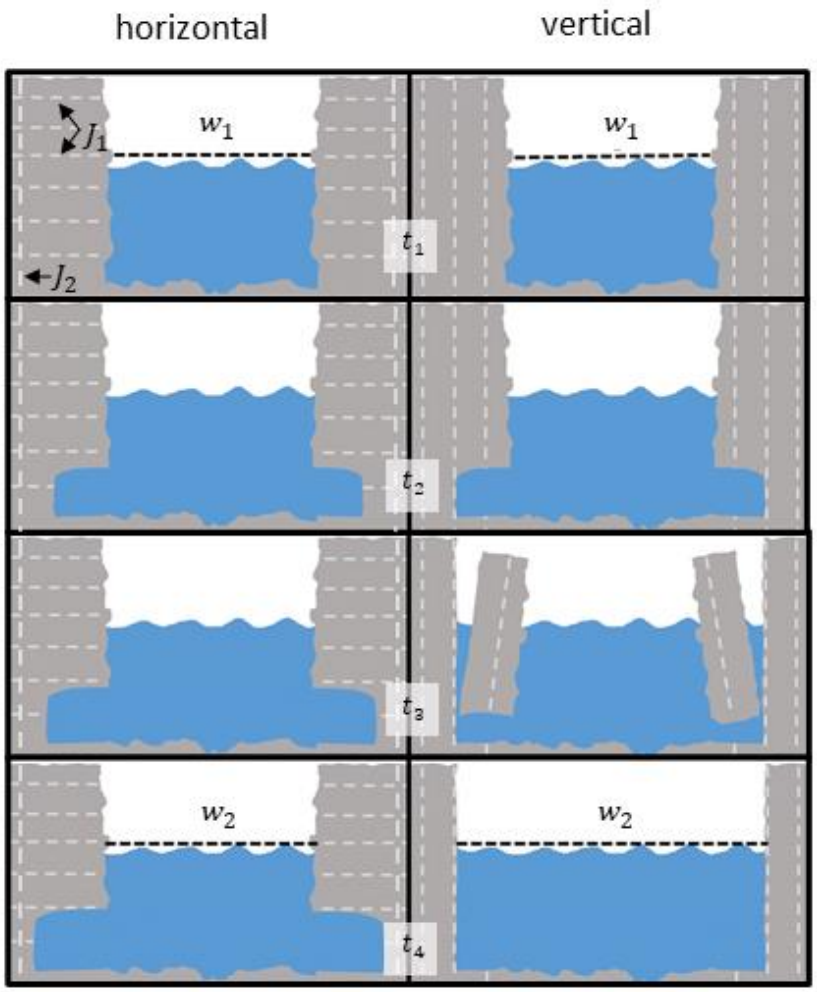

Figure 14. Conceptual model of the control of jointing on the evolution of bedrock canyon morphology. t_1: river incises into a jointed rock mass. t_2: Differences in wall geometry cause plunging flow structures that deflect sediment off the bed and into the walls, leading to undercutting. t_3: The vertically jointed rock mass fails after becoming undercut by a critical amount. The horizontally jointed rock mass is stable with the same amount of undercutting. t_4: A wide section of the canyon with vertically jointed bedrock walls is more stable than a section of canyon with horizontally jointed walls.

Vertical jointing makes a canyon wall more susceptible to failure when undercut because failure removes supporting rock and exposes new vertical joints. A horizontally jointed rock mass of similar lithology will persist longer when undercut at the same rate because there are no daylighting joints that are steep enough to induce failure. For rock slope failure to occur, the weight of the rock above a horizontal joint would have to overcome the tensile strength of that block (i.e. fail as a beam) or erode back to the nearest sub-vertical joint. Over time, this disparity in rock slope kinematics will lead to greater widths in areas where canyon walls are vertically jointed and constrictions in areas where the canyon walls are horizontally jointed as, horizontally jointed walls will collapse less frequently. In this way, the geometry of the walls and the topography of the bed will coevolve, with enhanced vertical incision downstream of constrictions and enhanced lateral erosion downstream of constrictions with vertically jointed walls. Cao (2018) describes a process of pool propagation whereby alluviation downstream of scour pools forces flow over the sediment and then back into the bed. The above-described model is consistent with this idea because widenings downstream of scour pools will enhance alluviation by reducing stress on the bed. Taking this into account, a canyon could evolve through the formation of multiple CPW morphological units that eventually either see collapse of the constrictions or become so deep that the plunging flows dissipate before they reach the bed, limiting pool growth.

Recent work has shown that the creation of a CPW morphology can be either autogenic or allogenic. Scheingross et al. (2019) shows that a series of constrictions and widenings can form autogenically in homogenous rock through the growth of undulating bedforms caused by flow instabilities. Cao (2018) suggests that both allogenic and autogenic processes might operate together — a forced constriction can create a scour pool that propagates through sediment dynamics. The results of this study provide a source for autogenic pool formation (i.e. constrictions) and allow for allogenic pool growth following an initial perturbation. I suggest a spectrum of behaviors that are dependent on the structural geological influence in otherwise similar rock (Figure 15). Where the discontinuity kinematic influence is strong, it will control the morphology of the canyon. Where the rock discontinuity orientations differ from reach to reach in a single canyon, the influence of the flow dynamics and the structure will compete. A pattern of CPWs can be either reinforced or dampened by the influence of differences in rock slope

stability dictated by joint geometry. In other words, bedrock structure can impose a control on a process that is otherwise self-occurring.

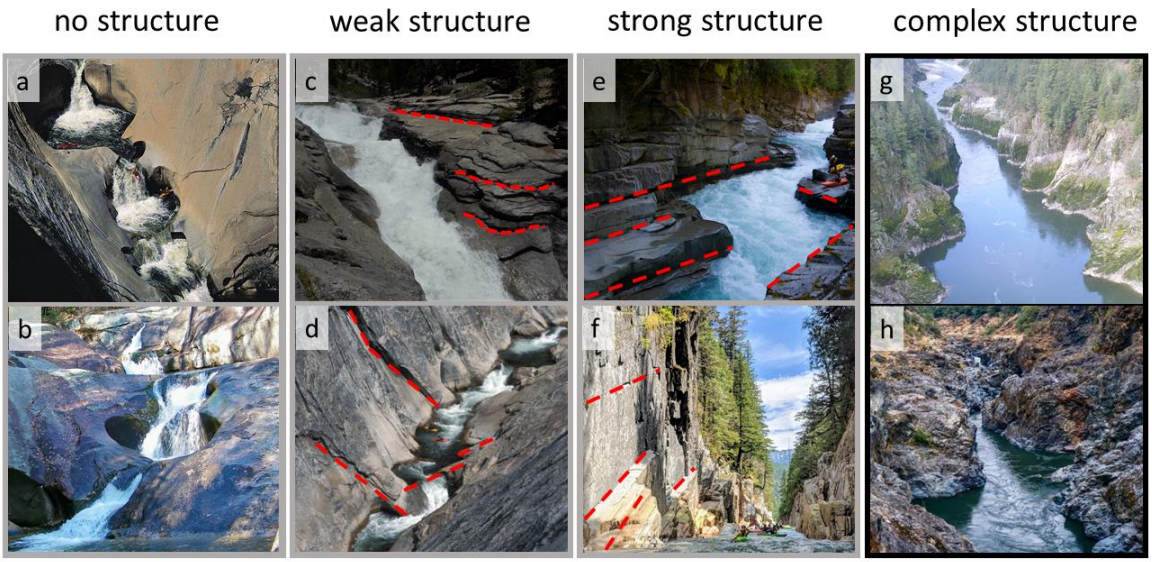

Figure 15. Bedrock canyon morphologies showing a spectrum of structural controls. a) Dry Meadow Creek, California. b) Silver Creek, North Carolina. c) South Silver Creek, California. d) Tuolomne River, California. e) Ashlu River, British Columbia. f) Big Silver Creek, British Columbia. g) Fraser River, British Columbia. h) Rogue River, Oregon). The morphologies of canyons with no structural control (a and b) are dominated by abrasional features, such as potholes. Canyons with weak structural control (c and d) show a mix of abrasional features and features that reflect structural geometry. Canyons with strong structural control (e and f) mimic the geometry of jointing. Canyons with complex structure (e.g. rivers that follow fault zones; (g and h) have convoluted geometries that coevolve with flow. The red dashed lines highlight structural discontinuities.

2.6. Conclusion

I examined bedrock discontinuities in Black Canyon to determine the role they play in the formation of constrictions, scour pools, and widenings. I found that a difference in rock slope stability due to joint geometry co-varies with width within the bedrock canyon. I propose a conceptual model based on the idea that vertical jointing leaves a rock slope more susceptible to failure when undercut, leading to channel widening over time. In contrast, horizontal jointing leads to lesser channel widening and constriction. These findings provide a new mechanism to explain reach-scale differences in bedrock canyon morphology.

References

Andrews, G.D.M., Russell, J.K., Brown, S.R., Enkin, R.J. (2012). Pleistocene reversal of the Fraser River, British Columbia. Geology, 40 (2), 111-114. https://doi.org/10.1130/G32488.1

Beer, A. R., Turowski, J. M., & Kirchner, J. W. (2017). Spatial patterns of erosion in a bedrock gorge. Journal of Geophysical Research: Earth Surface, 122(1), 191–214. https://doi.org/10.1002/2016JF003850

Bovis, M.J., Evans, S.G., (1996). Extensive deformation of rock slopes in southern Coast Mountains, southwest British Columbia, Canada. Engineering Geology, 44, 163-182.

Bovis, M.J., Jones, P., (1992). Holocene history of earthflow mass movements in south-central British Columbia: the influence of hydroclimatic changes. Canadian Journal of Earth Sciences, 29 (8), 1746-1755.

Burbank, D.W., Anderson, R.S. (2001). Tectonic Geomorphology. Malden (MA): Blackwell Pubishing.

Cao, Z.H., 2018. Scour Pool Incision in Bedrock Canyons. M.Sc. Thesis, Simon Fraser University, Burnaby, BC, 51 p.

Chatanantavet, P., Parker, G. (2009). Physically based modeling of bedrock incision by abrasion, plucking, and macroabrasion. Journal of Geophysical Research: Earth Surface, 114(4). https://doi.org/10.1029/2008JF001044

Clague, J.J. (1981). Late quaternary geology and geochronology of British Columbia, Part 2: Geological Survey of Canada, Paper 80-35, 41 p.

Clague, J.J., James, T.S. (2002). History and isostatic effects of the last ice sheet in southern British Columbia. Quaternary Science Reviews, 21 (1-3), 71-87.

Coleman, M. E., Parrish, R. R. (1991). Eocene dextral strike-slip and extensional faulting in the Bridge River Terrane, southwest British Columbia. Tectonics, 10(6), 1222–1238. https://doi.org/10.1029/91TC01078

Cui, Y., Miller, D., Schiarizza, P., Diakow, L.J., 2017. British Columbia digital geology. British Columbia Ministry of Energy, Mines and Petroleum Resources, Geological Survey Open File 2017-8, 9 p. Data version 2018-04-05.

Dilts, T.E. (2015) Polygon to Centerline Tool for ArcGIS. University of Nevada Reno. Available at: http://www.arcgis.com/home/item.html?id=bc642731870740aabf48134f90aa6165

Dolan, R., Howard, A., Trimble, D. (1978). Structural control of the rapids and pools of the Colorado River in the Grand Canyon. Science, 202(4368), 629-631. https://doi.org/10.1126/science.202.4368.629

Eyles, N., Arnaud, E., Scheidegger, A. E., Eyles, C. H. (1997). Bedrock jointing and geomorphology in southwestern Ontario, Canada: An example of tectonic predesign. Geomorphology, 19, 17-34.

Finnegan, N.J., Sklar, L.S., Fuller, T.K., (2007). Interplay of sediment supply, river incision and channel morphology revealed by the transient evolution of an experimental bedrock channel. Journal of Geophysical Research: Earth Surface, 112, F03S11. http://doi.org/10.1029/2006JF000569

Fuller, T.K., Gran, K.B., Sklar, L.S., Paola, C., 2016. Lateral erosion in an experimental bedrock channel: the influence of bed roughness on erosion by bed load impacts. Journal of Geophysical Research: Earth Surface, 121, 1084-1105.

Gallen, S.F., Wegmann, K.W. (2017). River profile response to normal fault growth and linkage: an example from the Hellenic forearc of south-central Crete, Greece. Earth Surface Dynamics, 5, 161-186. https://doi.org/10.5194/esurf-5-161-2017

Howes, D.E. (1975). *Quaternary stratigraphy and geomorphology of lower Bridge River valley, British Columbia* (unpublished MSc thesis). University of British Columbia, Vancouver, British Columbia.

Hunt, B., Venditti, J.G., Kwoll, E., (2017). Experiments on the morphological controls of velocity inversions in bedrock canyons. Earth Surface Processes and Landforms, 43(3), 654-668.

James, T. S., Clague, J. J., Wang, K., Hutchinson, I. (2000). Postglacial rebound at the northern Cascadia subduction zone. Quaternary Science Reviews, 19, 1527–1541. https://doi.org/10.1016/S0277-3791(00)00076-7

Judson, S., & Andrews, G. W. (1955). Pattern and form of some valleys in the Driftless area, Wisconsin. Journal of Geology, 63(4), 328–336. https://doi.org/10.1086/626270

Lamb, M. P., Finnegan, N. J., Scheingross, J. S., Sklar, L. S. (2015). New insights into the mechanics of fluvial bedrock erosion through flume experiments and theory. Geomorphology, 244, 33–55. https://doi.org/10.1016/j.geomorph.2015.03.003

Lanaro, F., Fredriksson, A., (2005). Rock Mechanics Model – Summary of the Primary Data. Preliminary Site Description Forsmark Area – Version 1.2. Swedish Nuclear Fuel and Waste Management Co., Stockholm, Sweden.

Maarouf, A. (1983). Relationship between basement faults and Colorado Plateau drainage. In Northern Paradox Basin - Uncompahgre Uplift (59–62). Grand Junction Geological Society, Grand Junction, Colorado.

Mauldon, M., Dunne, W.M., Rohrbaugh, Jr., (2001). Circular scanlines and circular windows: New tools for characterizing the geometry of fracture traces. Journal of Structural Geology, 23, 247-258. https://doi.org/10.1016/S0191-8141(00)00094-8

Molnar, P. (1975). Cenezoic tectonics of Asia: effects of a continental collision. Science, 189 (4201), 419-426.

Montgomery, D.R., (2004). Observations on the role of lithology in strath terrace formation and bedrock channel width. American Journal of Science, 305(5), 454-476. https://doi.org/10.2475/ajs.304.5.454

Montgomery, D.R., Gran, K.B., (2001). Downstream variations in the width of bedrock channels. Water Resources Research, 37,1841-1846. https://doi.org/10/1029/2000WR900393.

Ouimet, W. B., Whipple, † K X, Crosby, B. T., Johnson, J. P., Schildgen, T. F. (2008). Epigenetic gorges in fluvial landscapes. Earth Surface Processes and Landforms, 33(13). https://doi.org/10.1002/esp

Reiners, P.W., Ehlers, T.A., Garver, J.I., Mitchell, S.G., Montgomery, D.R., Vance, J.A., Nicolescu, S. (2002). Late Miocene exhumation an uplift of the Washington Cascade Range. Geology, 30 (9), 767-770.

Rennie, C., D., Church, M., Venditti, J. G. (2018). Rock control of river geometry: The Fraser canyons. Journal of Geophysical Research: Earth Surface, 123(8), 1860-1878. https://doi.org/10.1029/2017JF004458

River Dynamics Laboratory (2019). Fraser River atlas. Simon Fraser University, Department of Geography, Burnaby, British Columbia.

Ryder, J.M., Church, M. (1986). The Lillooet terraces of Fraser River: a paleoenvironmental enquiry. Canadian Journal of Earth Sciences, 23 (6), 869-884.

Scheidegger, A.E. (2004). Morphotectonics. Berlin: Springer Nature.

Scheingross, J.S., Lamb, M.P., Fuller, B.M., (2019). Self-formed bedrock waterfalls. Nature, 567, 229-233.

Sengor, C. A. M. (2017). Diversion of river courses across major strike-slip faults and keirogens. In Active Global Seismology Neotectonics and Earthquake Potential of the Eastern Mediterranean Region. American Geophysical Union, John Wiley & Sons.

Spotila, J. A., Moskey, K. A., Prince, P. S. (2015). Geologic controls on bedrock channel width in large, slowly-eroding catchments: Case study of the New River in eastern North America. Geomorphology, 230, 51–63. https://doi.org/10.1016/j.geomorph.2014.11.004

Thiele, S.T., Grose, L., Samsu, A., Micklethwaite, S., Vollger, S.A., Cruden, A.R. (2017). Rapid, semi-automatic fracture and contact mapping for point clouds, images and geophysical data. Solid Earth, http://doi.org/10.5194/se-8-1241-2017

Venditti, J.G., Domarad, N., Church, M., Rennie, C.D. (2015). The gravel-sand transition: Sediment dynamics in a diffuse extension. Journal of Geophysical Research: Earth Surface, 120 (6), 943-963.

Venditti, J.G., Li, T., Deal, E., Dingle, E., Church, M., (2019). Struggles with stream power: Connecting theory across scales. Geomorphology, in press.

Venditti, J.G., Rennie, C.D., Bromhof, J., Bradley, R.W., Little, M., Church, M. (2014). Flow in bedrock canyons. Nature, 513, 534-537.

Whipple, K. X., Hancock, G. S., Anderson, R. S. (2000). River incision into bedrock: Mechanics and relative efficacy of plucking, abrasion, and cavitation. Bulletin of the Geological Society of America, 112(3), 490–503.

Wilcox, R. E., Harding, T. P., & Seely, D. R. (1973). Basic wrench tectonics. American Association of Petroleum Geologists Bulletin, 57, 74-96.

Wohl, E. (2008). The effect of bedrock jointing on the formation of straths in the Cache la Poudre River drainage, Colorado Front Range. Journal of Geophysical Research: Earth Surface, 113(1), 1–12. https://doi.org/10.1029/2007JF000817

Wohl, E., Legleiter, C. J. (2003). Controls on pool characteristics along a resistant-boundary channel. Journal of Geology, 111(1), 103–114. https://doi.org/10.1086/344667

Wohl, E.E., Ikeda, H., (1997). Patterns of bedrock channel erosion on the Boso Peninsula, Japan. Journal of Geology, 106(3), 331-346. https://doi.org/10.1086/516026

Zernits, E.R. (1932). Drainage patterns and their significance. Journal of Geology, 40, 498-521.

Appendix A.

Explanation of Canyon Classification

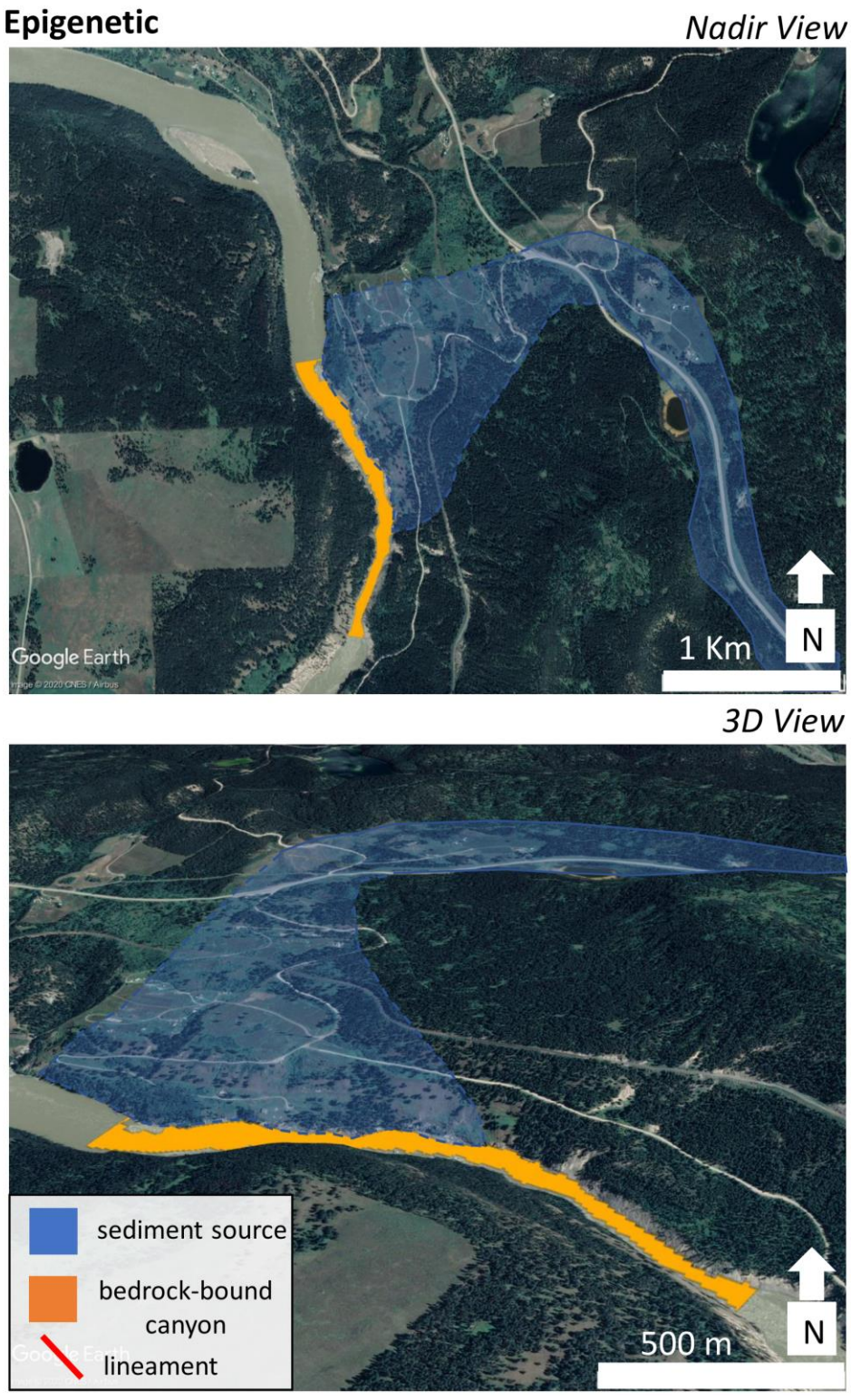

Figure A1: Soda Creek Canyon (imagery accessed in Google Earth; source: CNES/Airbus, 7/22/2019). Canyon was classified as epigenetic because of the large lateral sediment input associated with the relic channel. Dashed lines represent uncertainty in the boundaries of the sediment input.

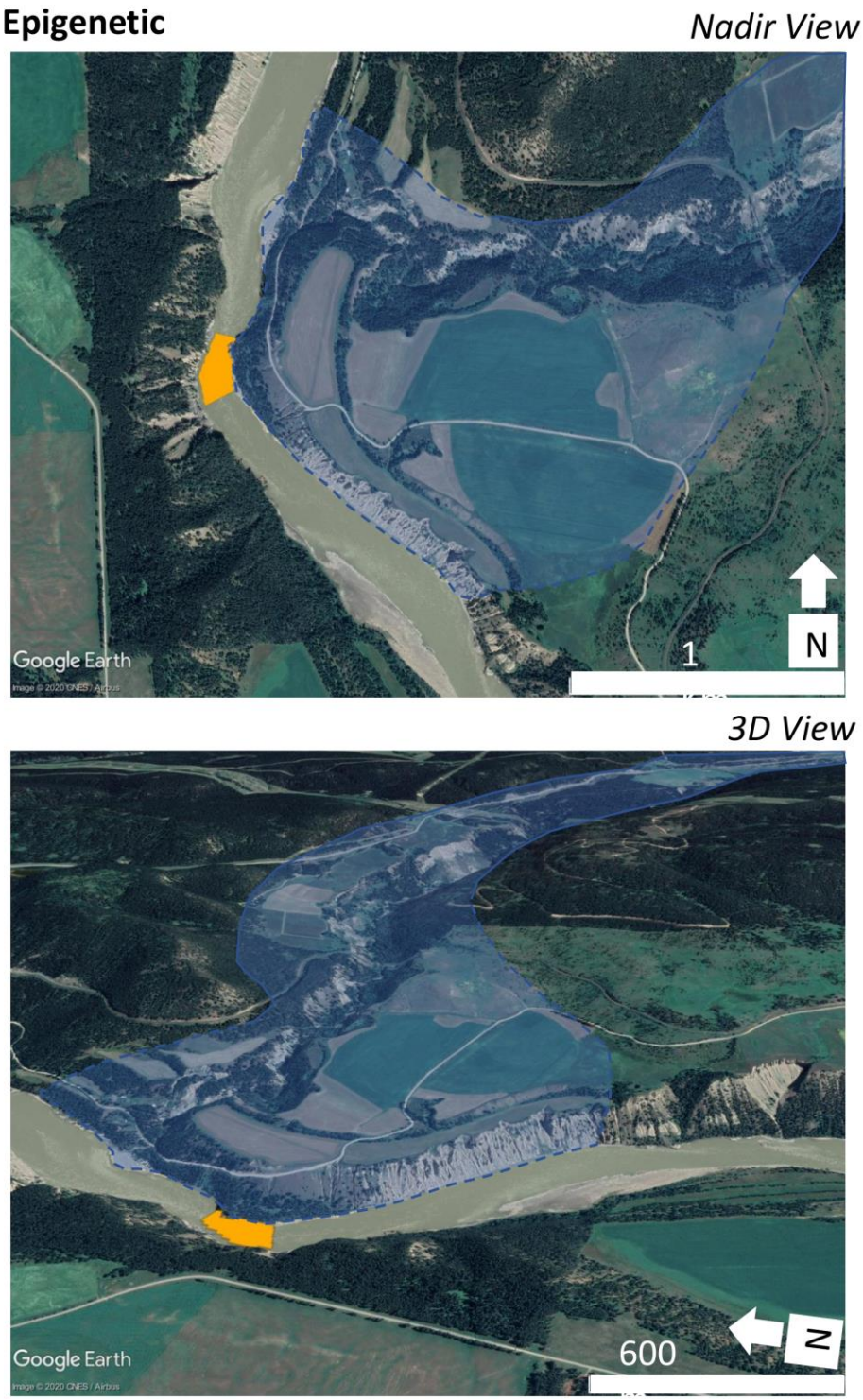

Figure A2: Hawk's Creek Canyon (imagery accessed in Google Earth; source: CNES/Airbus, 7/22/2019). Canyon was classified as epigenetic because of the large lateral sediment input associated with the relic channel. Dashed lines represent uncertainty in the boundaries of the sediment input.

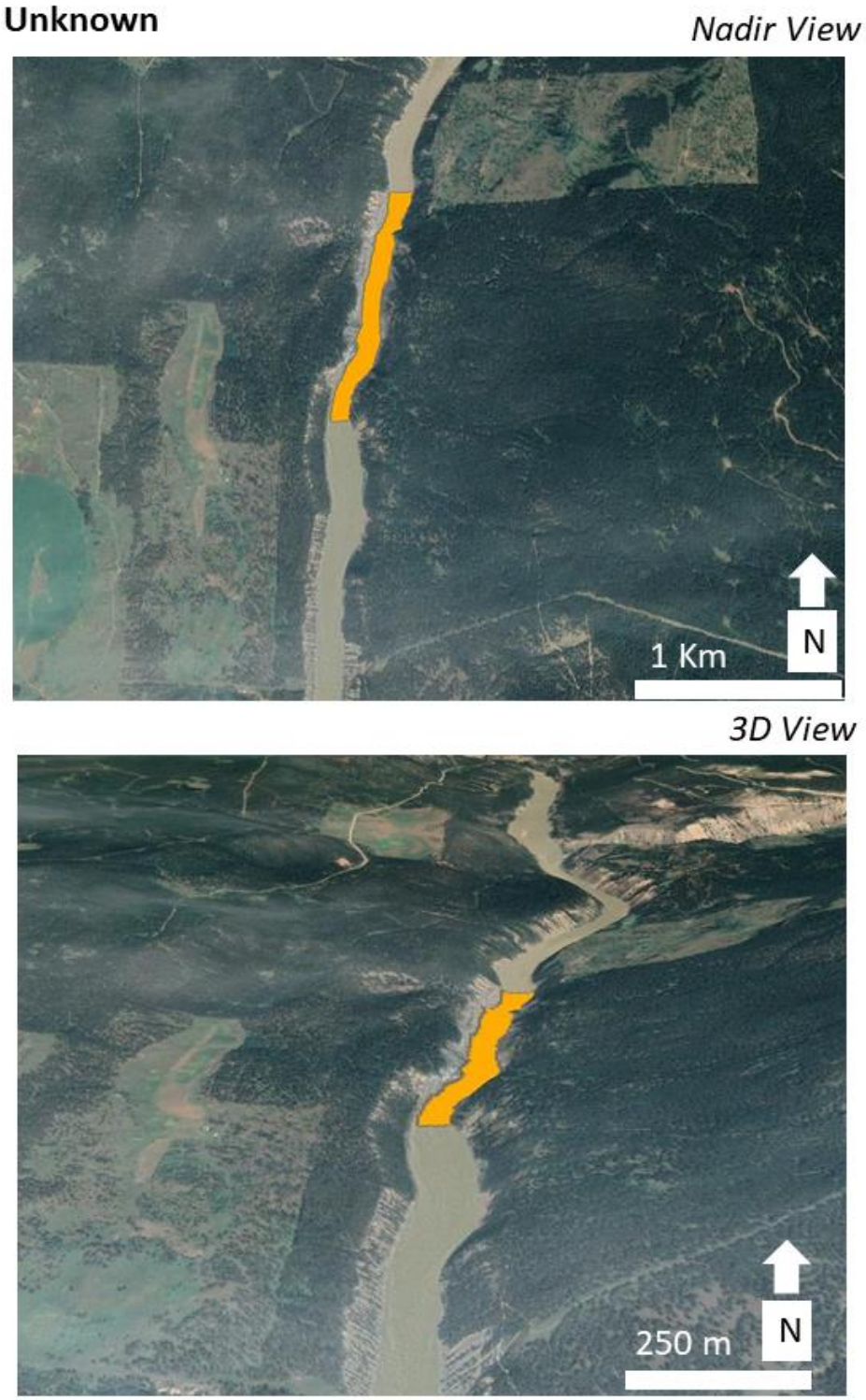

Figure A3: West Williams Canyon (imagery accessed in Google Earth; source: CNES/Airbus, 7/22/2019). Canyon was classified as unknown because there are no obvious proximal sediment inputs or lineaments.

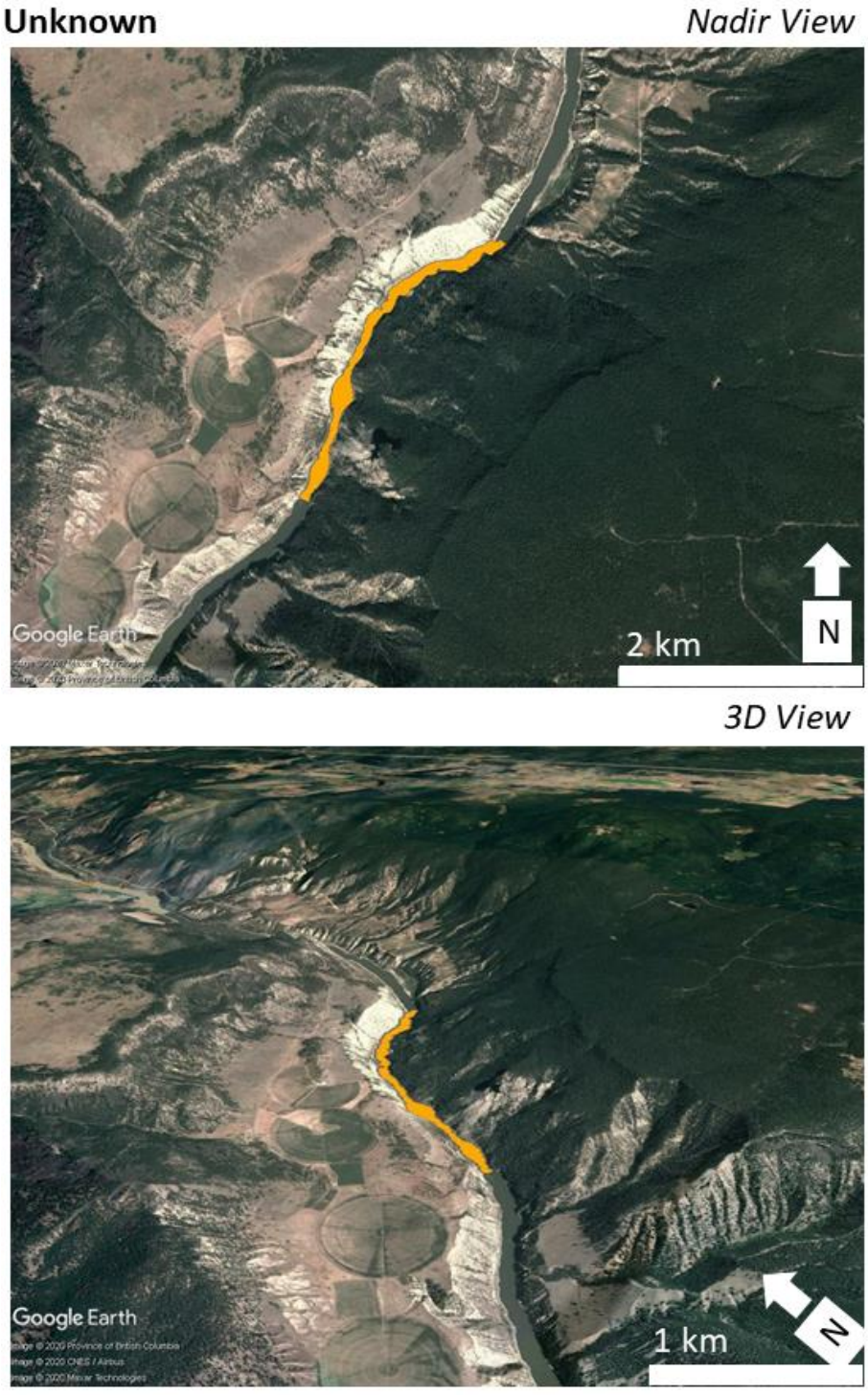

Figure A4: Doc English Canyon (imagery accessed in Google Earth; source: Province of British Columbia, CNES/Airbus, Maxar Technologies, 7/22/2019). Canyon was classified as unknown because there are no obvious proximal sediment inputs or lineaments.

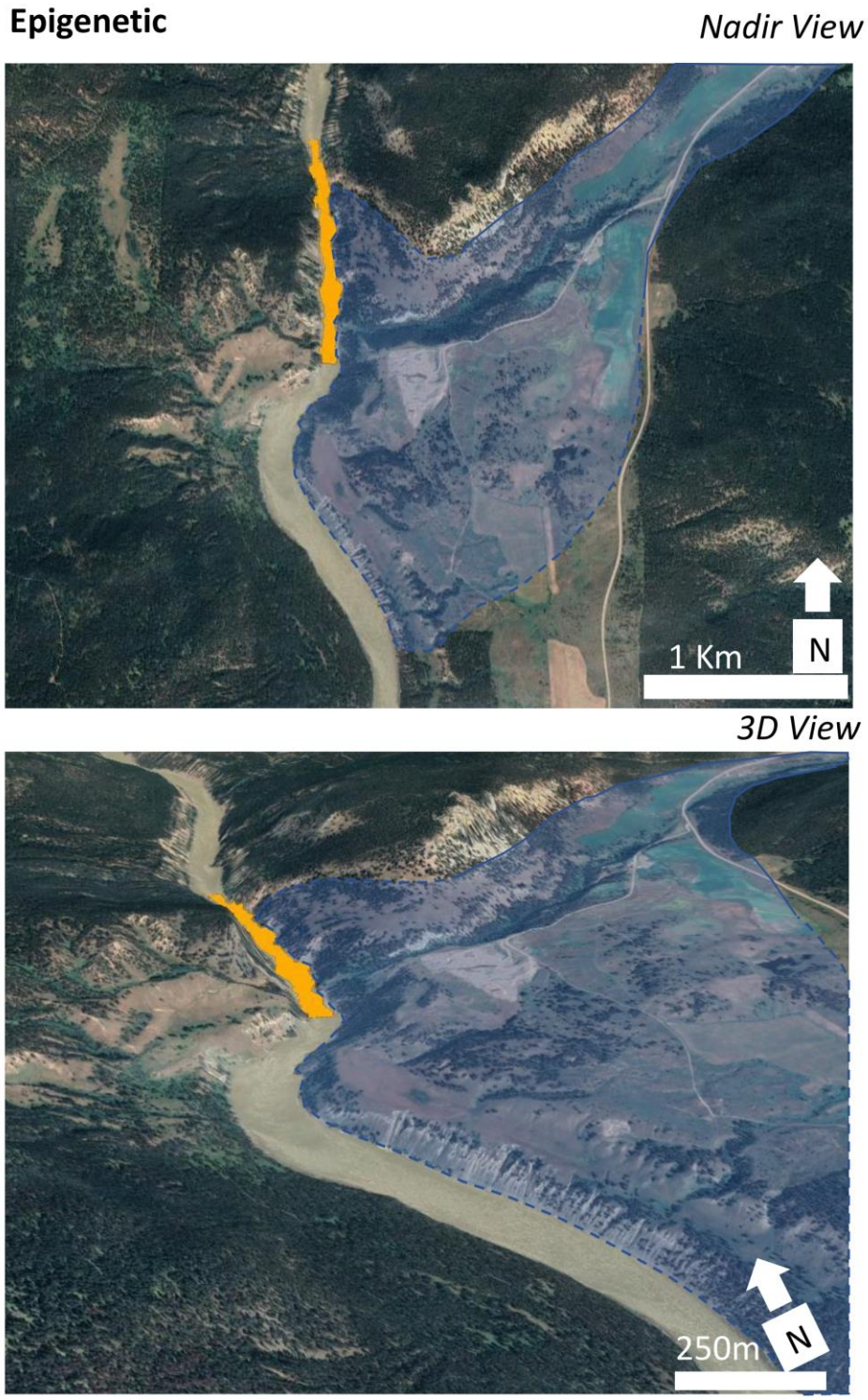

Figure A5: Chimney Creek Canyon (imagery accessed in Google Earth; source: CNES/Airbus, 7/22/2019). Canyon was classified as epigenetic because of the large lateral sediment input associated with the relic channel. Dashed lines represent uncertainty in the boundaries of the sediment input.

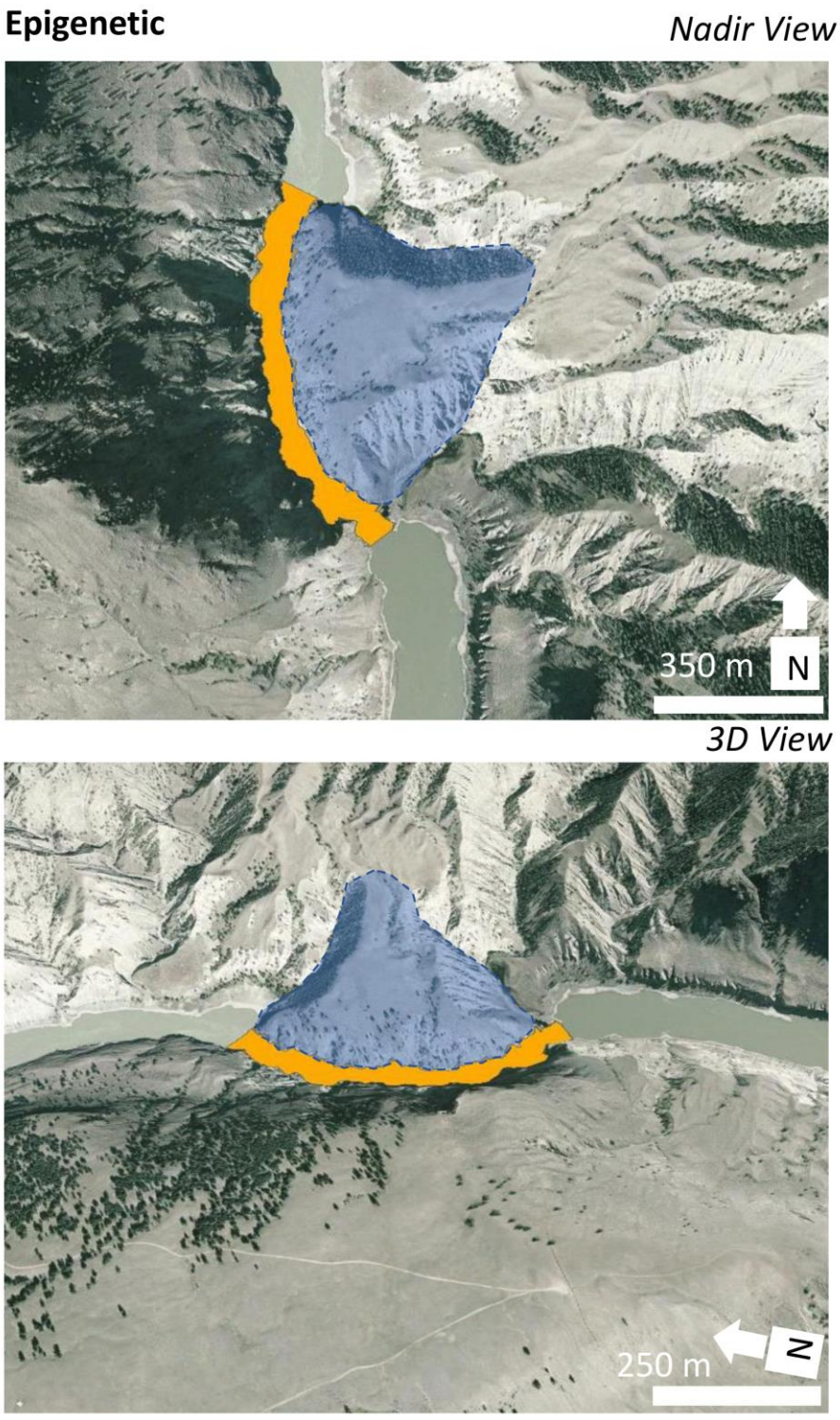

Figure A6: Iron Canyon (imagery accessed in Google Earth; source: Province of British Columbia, 7/22/2019). Canyon was classified as epigenetic because of the lobate lateral sediment input. Dashed lines represent uncertainty in defining the boundaries of what appears to be a mass movement.

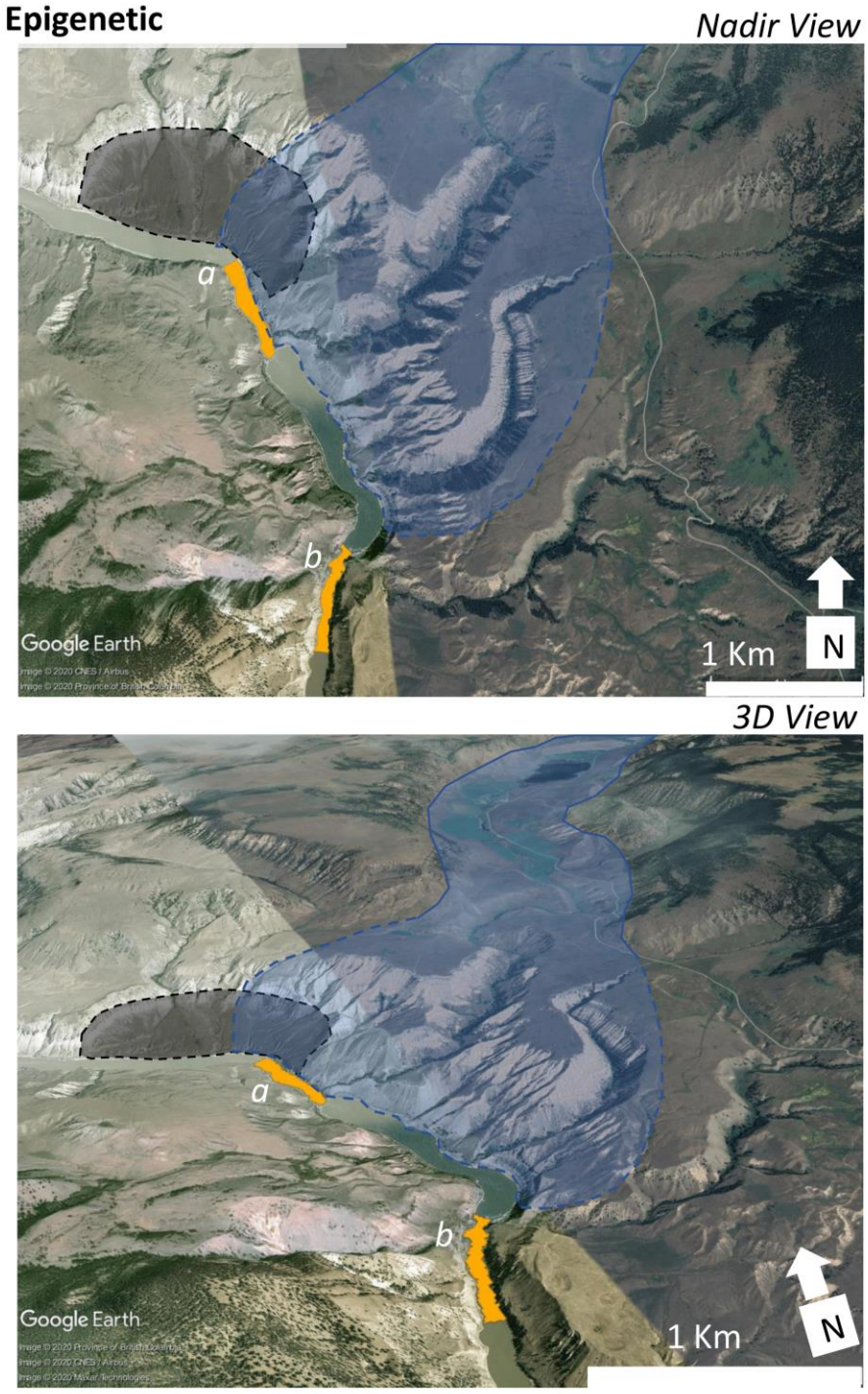

Figure A7: (*a*) Alki Rapids and (*b)* Mcewan Rapids canyons (imagery accessed in Google Earth; source: Province of British Columbia, CNES/Airbus, 7/22/2019). Canyons were classified as epigenetic because of the large lateral sediment input from the relic channel and what appears to be a mass movement (black polygon) adjacent to Alki Rapids Canyon. Dashed lines represent uncertainty in the boundaries of the sediment inputs.

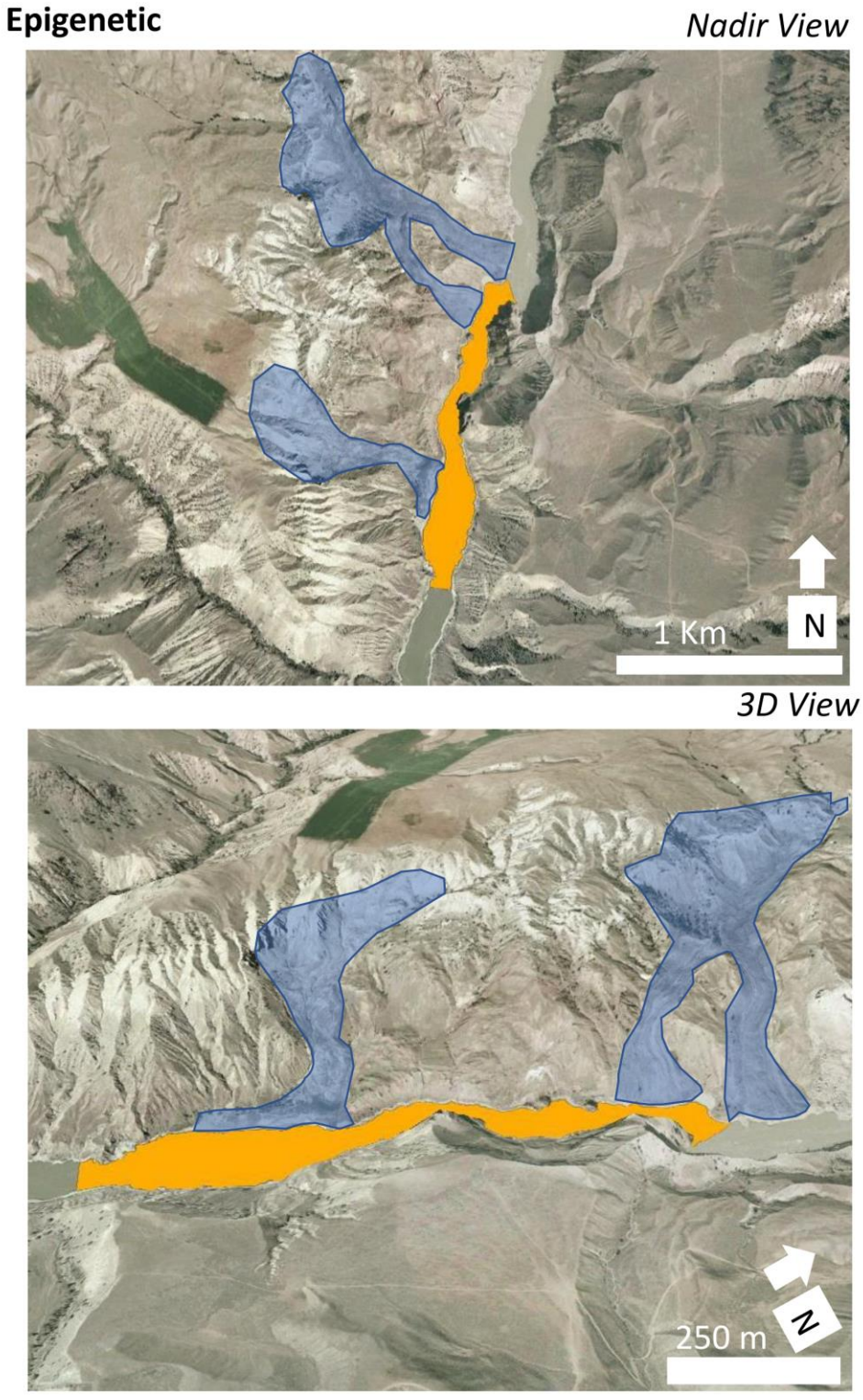

Figure A8: Grinder Creek North Canyon (imagery accessed in Google Earth; source: Province of British Columbia, 12,31,2004). Canyon was classified as epigenetic because of the Grinder Creek earthflows that have descended the western wall of the canyon and forced the channel to the east.

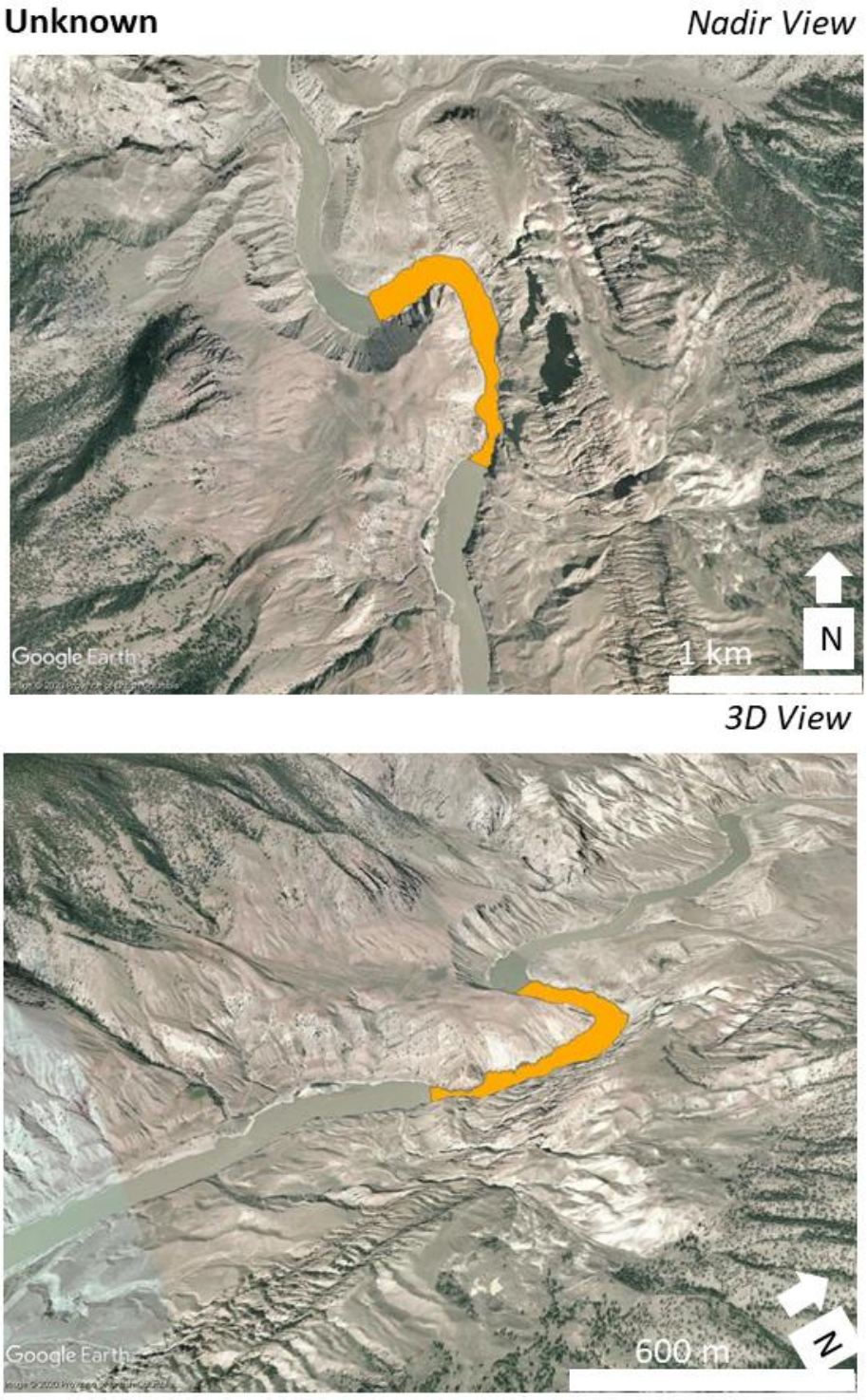

Figure A9: French Bar Canyon (imagery accessed in Google Earth; source: Province of British Columbia, 12/31/2004). Canyon was classified as unknown because there are no obvious proximal sediment inputs or lineaments.

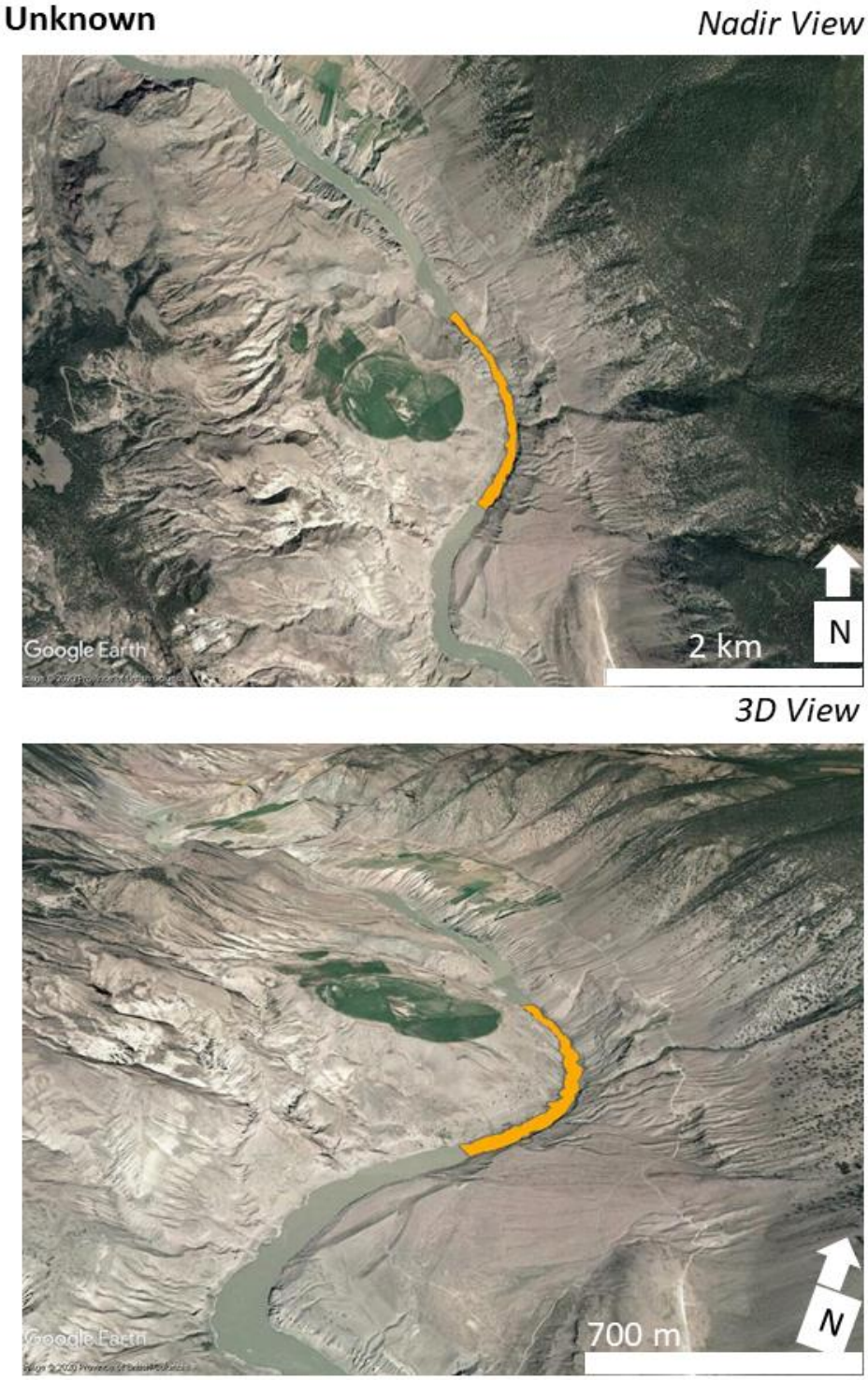

Figure A10: Chisolm Canyon (imagery accessed in Google Earth; source: Province of British Columbia, 12/31/2004). Canyon was classified as unknown because there are no obvious proximal sediment inputs or lineaments.

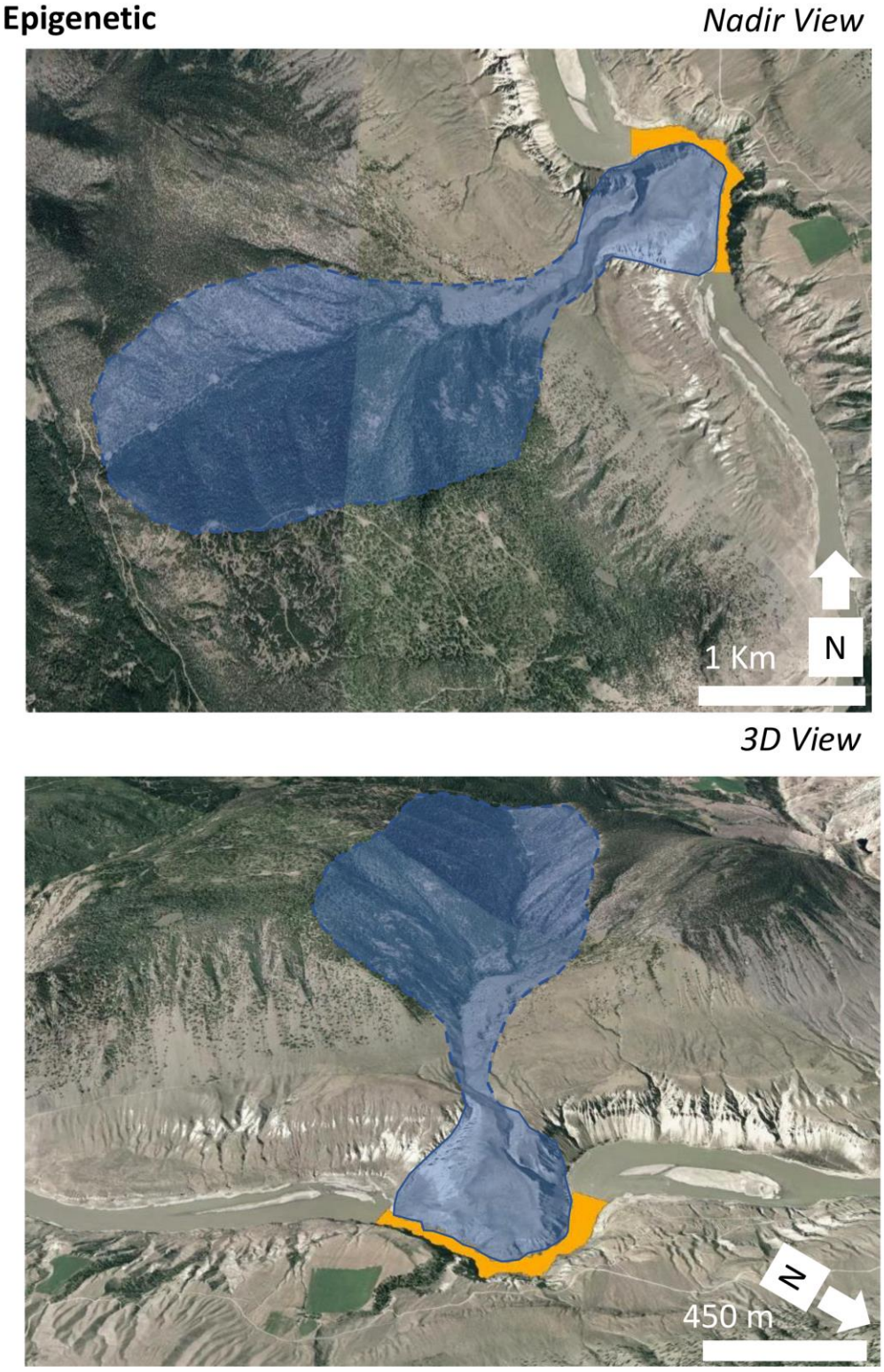

Figure A11: High Bar Canyon (imagery accessed in Google Earth; source: Province of British Columbia, 12/31/2004). Canyon was classified as epigenetic because of what appears to be a large mass movement that forced the channel to the northeast. Dashed lines represent uncertainty in defining the boundaries of the source area.

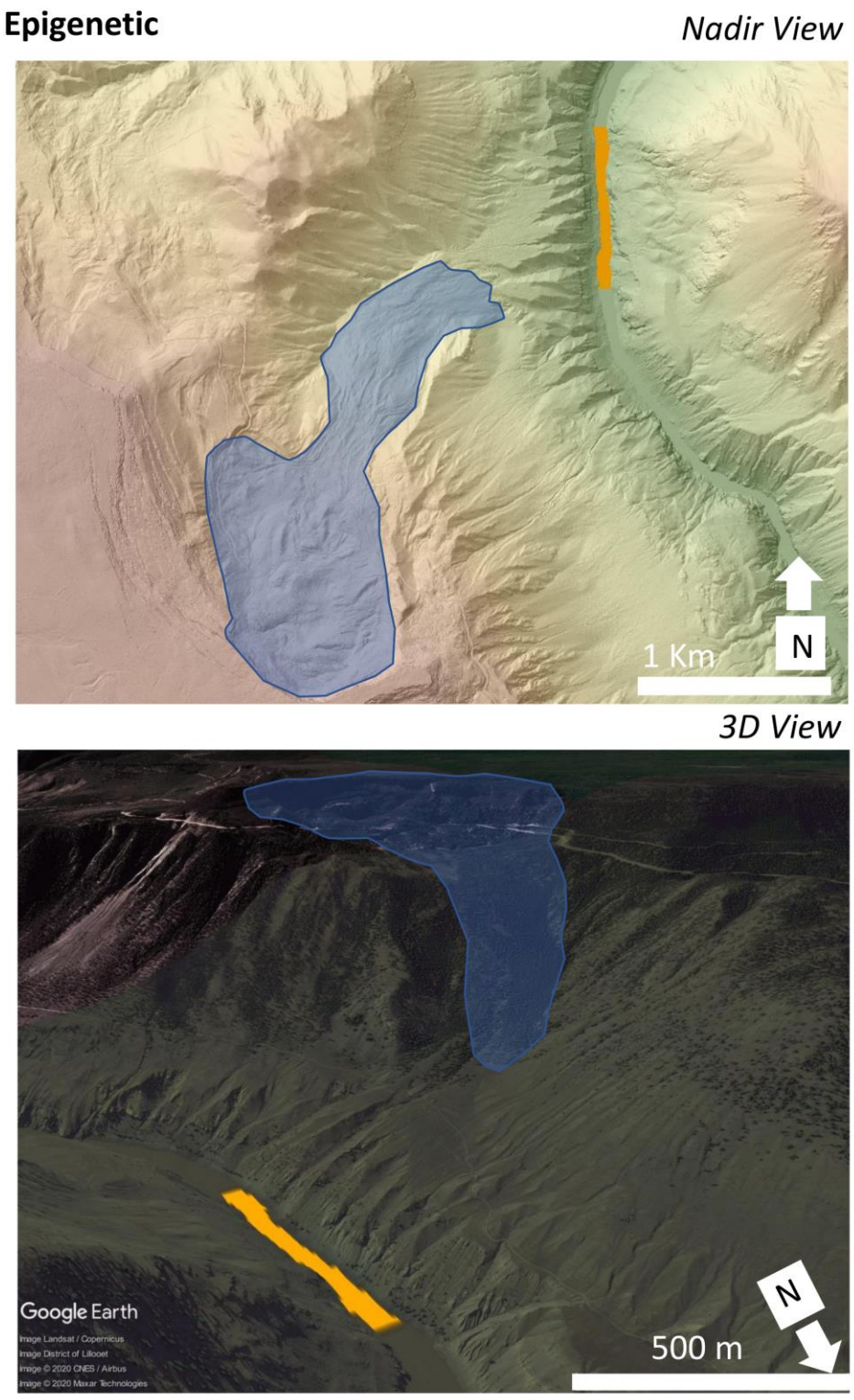

Figure A12: Chimney Creek Canyon (LiDAR collected Dec. 7, 2016, Imagery accessed in Google Earth; source: Maxar Technologies 3/26/2016). Canyon was classified as epigenetic because of the large lateral sediment input that originated on the western wall of the canyon.

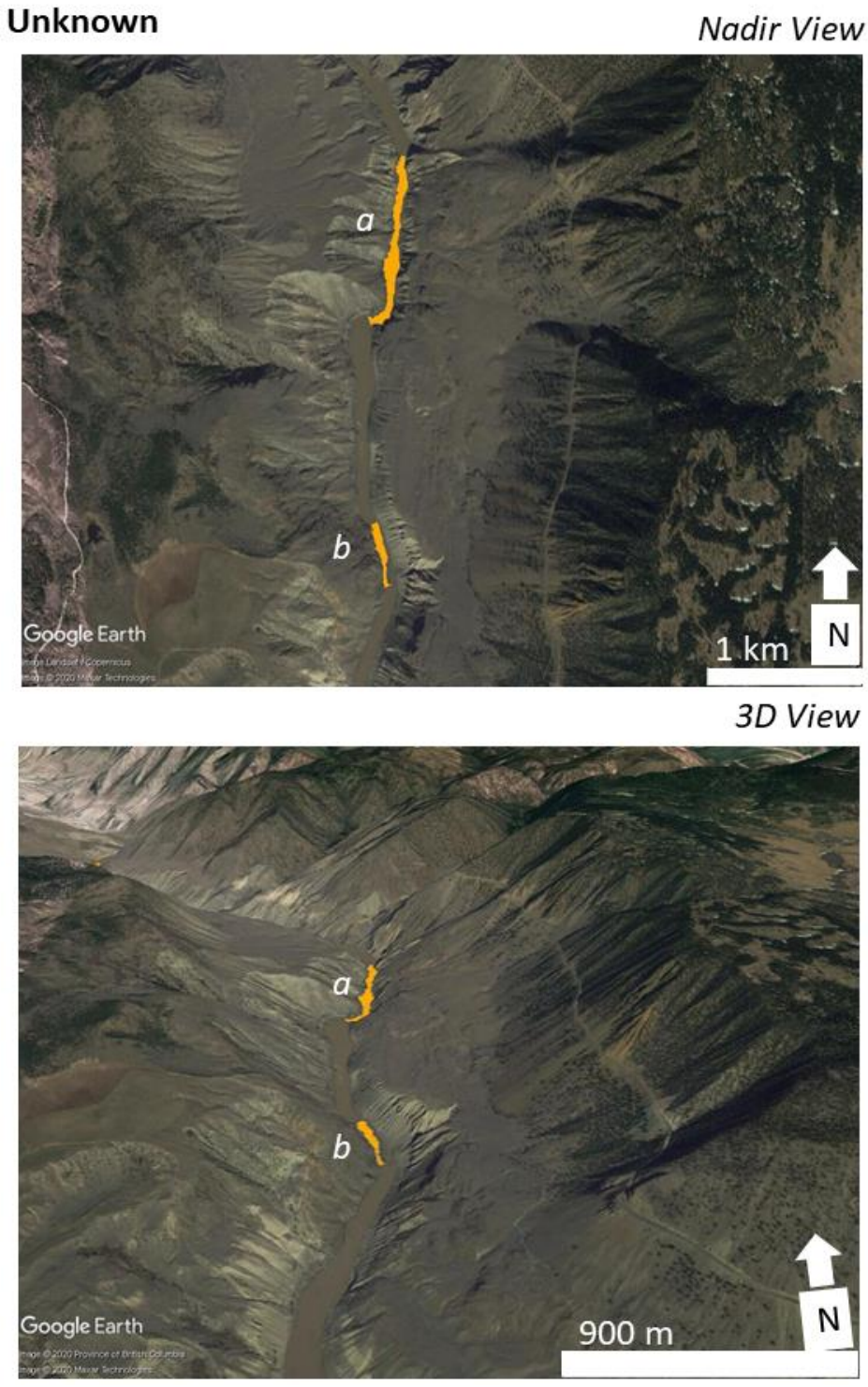

Figure A13: Kelly Creek (*a*) and North Pavillion (*b*) canyons (imagery accessed in Google Earth; source: Province of British Columbia, Maxar Technologies, Landsat/Copernicus, 3/26/2015). Canyon was classified as unknown because there are no obvious proximal sediment inputs or lineaments.

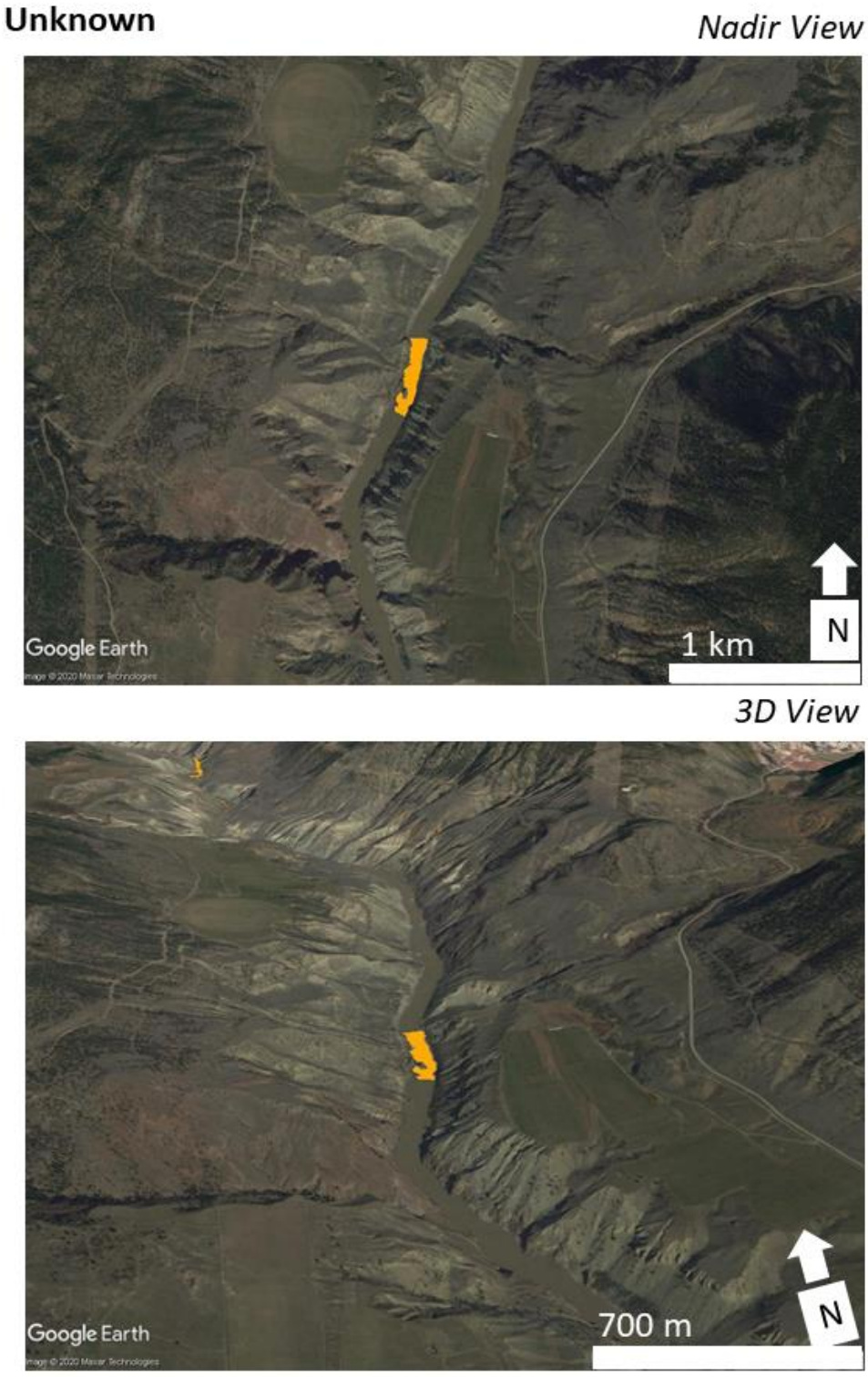

Figure A14: Powerline Rapids Canyon (imagery accessed in Google Earth; source: Maxar Technologies, 3/26/2015). Canyon was classified as unknown because there are no obvious proximal sediment inputs or lineaments.

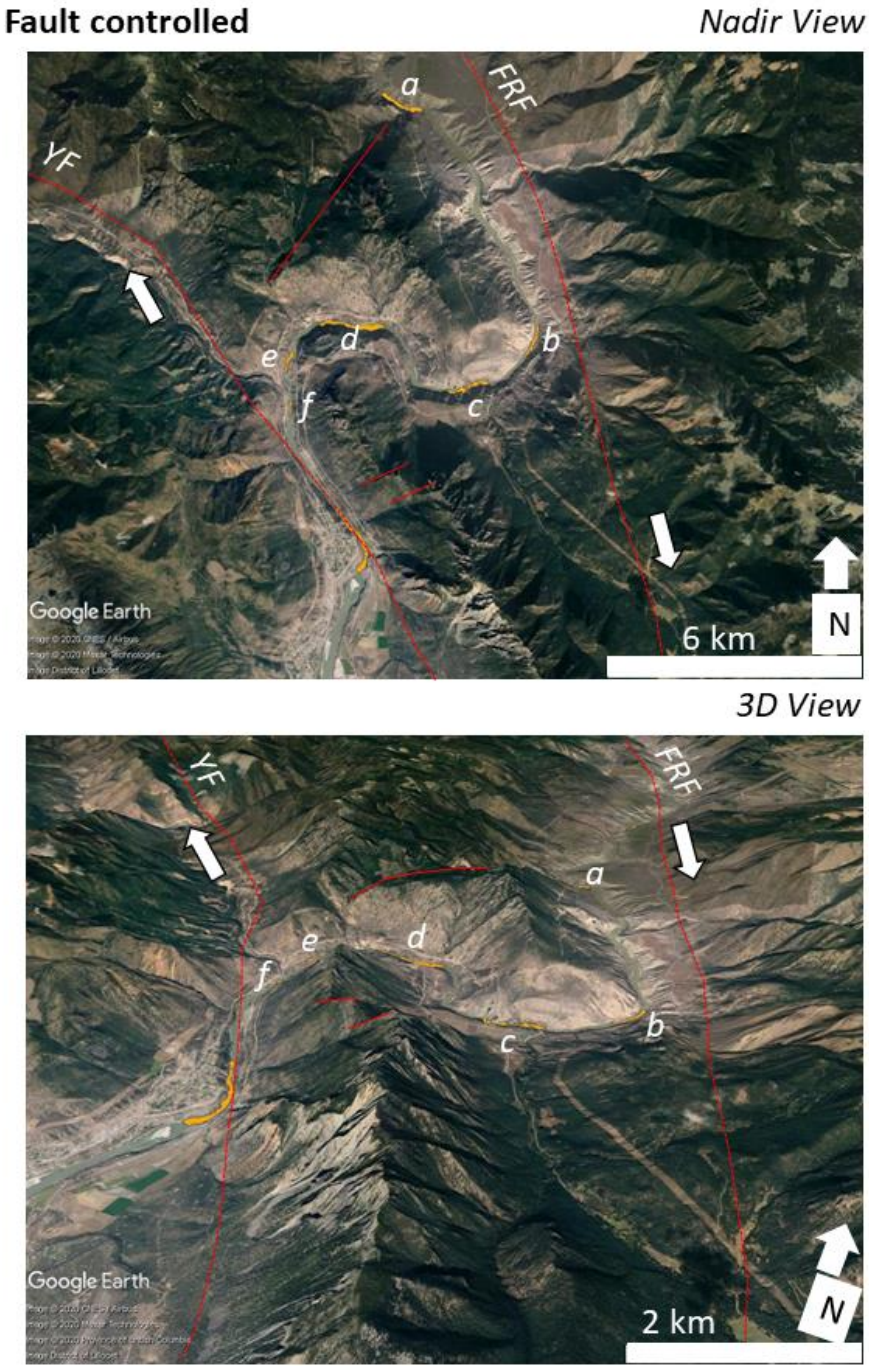

Figure A15: White *(a)*, Fountain East *(b)*, Fountain West *(c)*, West Fountain *(d)*, Bridge River Rapids *(e)*, and Bridge River Confluence Canyons *(f)* (imagery accessed in Google Earth; source: CNES/Airbus, Maxar Technologies, Province of British Columbia, District of Lillooet, 10/4/2019). Canyons were classified as fault controlled because of their unique geometry that aligns with proximal faults and lineaments. Dashed lines show inferred faults (BC Digital Geology), and arrows show sense of displacement on inferred faults.

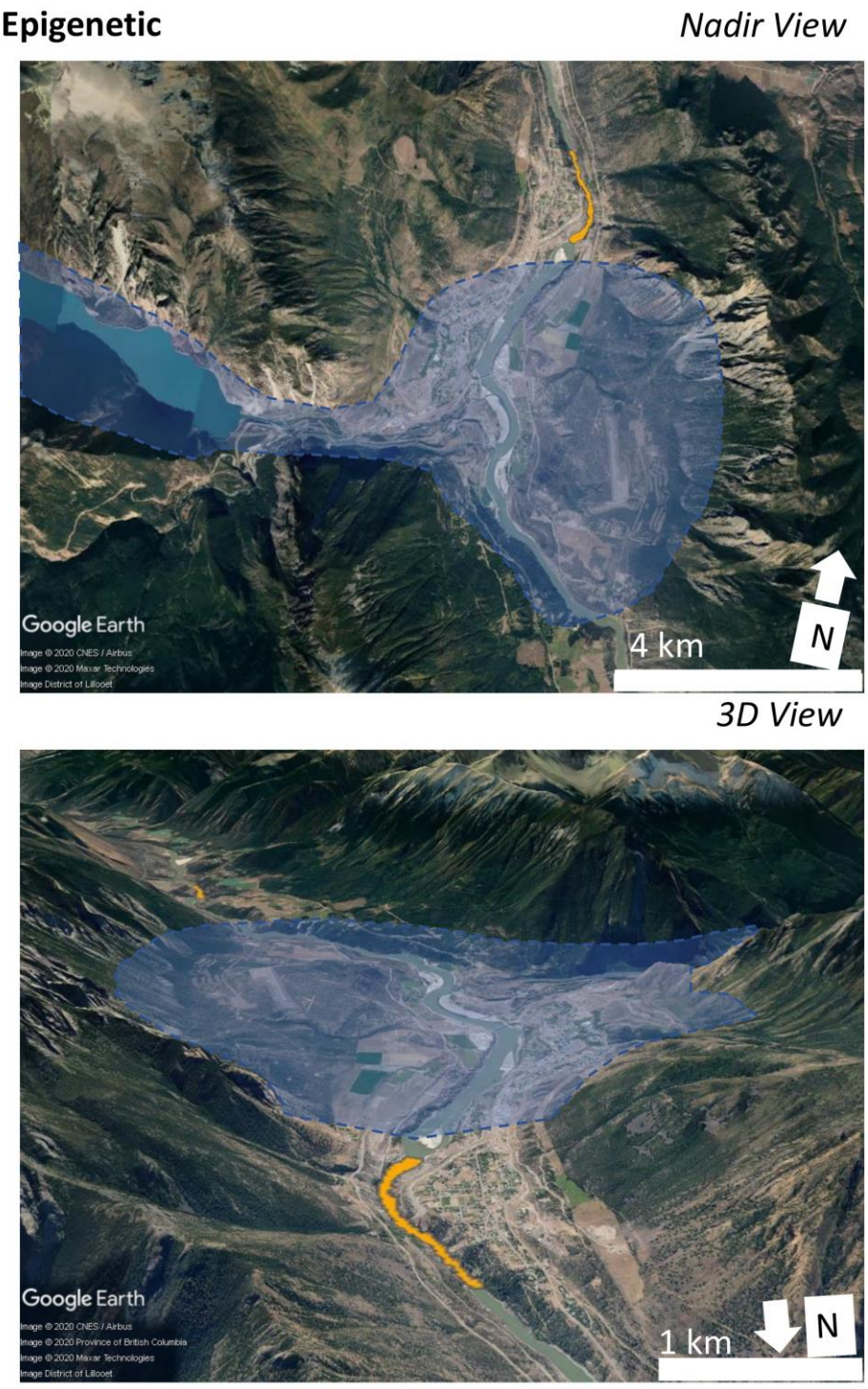

Figure A16: Lillooet Rapids Canyon (LiDAR flown Dec.,7, 2016). Canyon was classified as epigenetic because of the lobate shape of the canyon and the likely influence of the glacier that descended the Seton River canyon, whose influence can be seen crossing the river to the east side of the canyon. Dashed lines represent uncertainty in the boundaries of the glacier's influence.

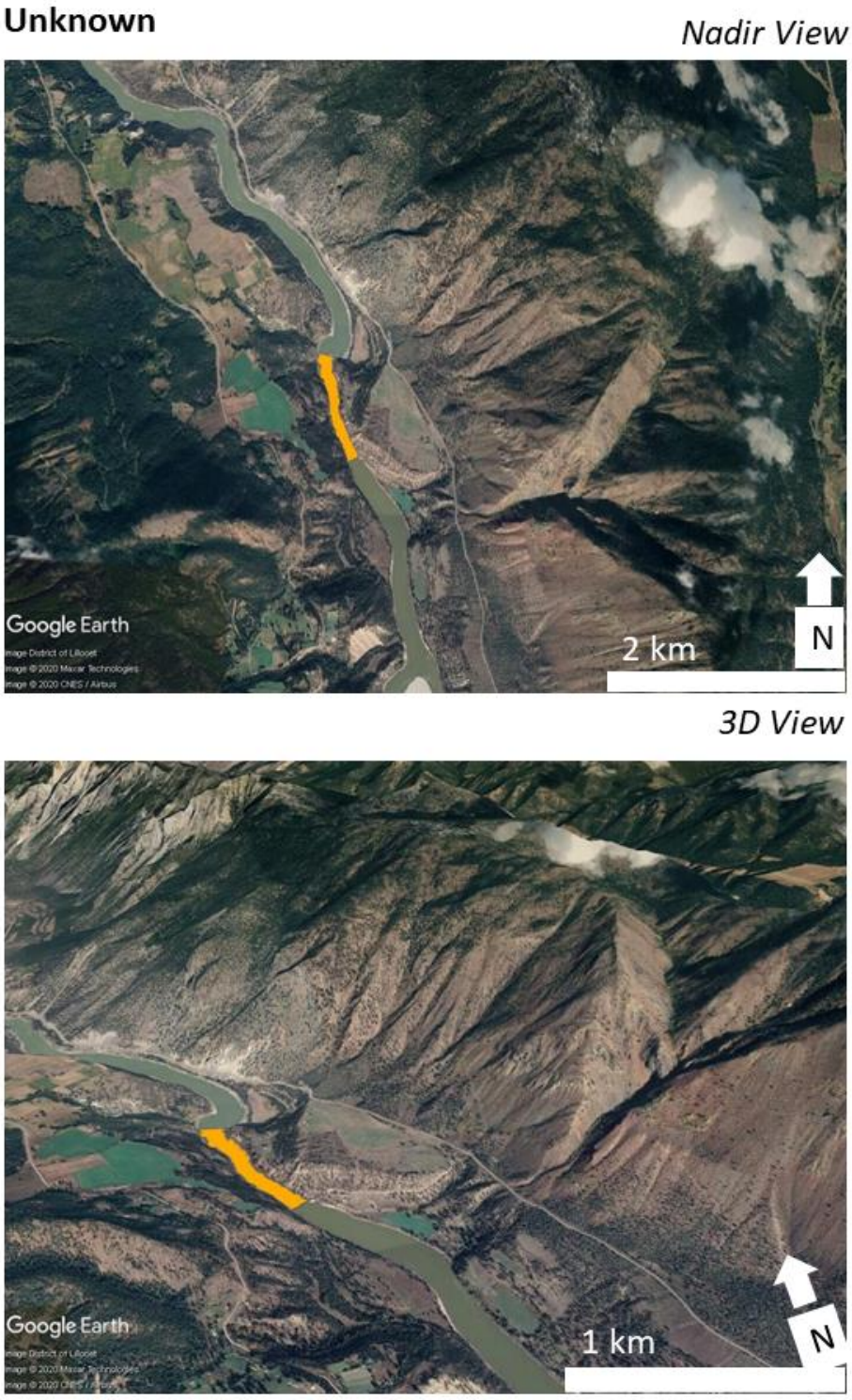

Figure A17: Powerline Rapids Canyon (imagery accessed in Google Earth; source: Maxar Technologies, District of Lillooet, CNEW/Airbus, 10/4/2019). Canyon was classified as unknown because there are no obvious proximal sediment inputs or lineaments.

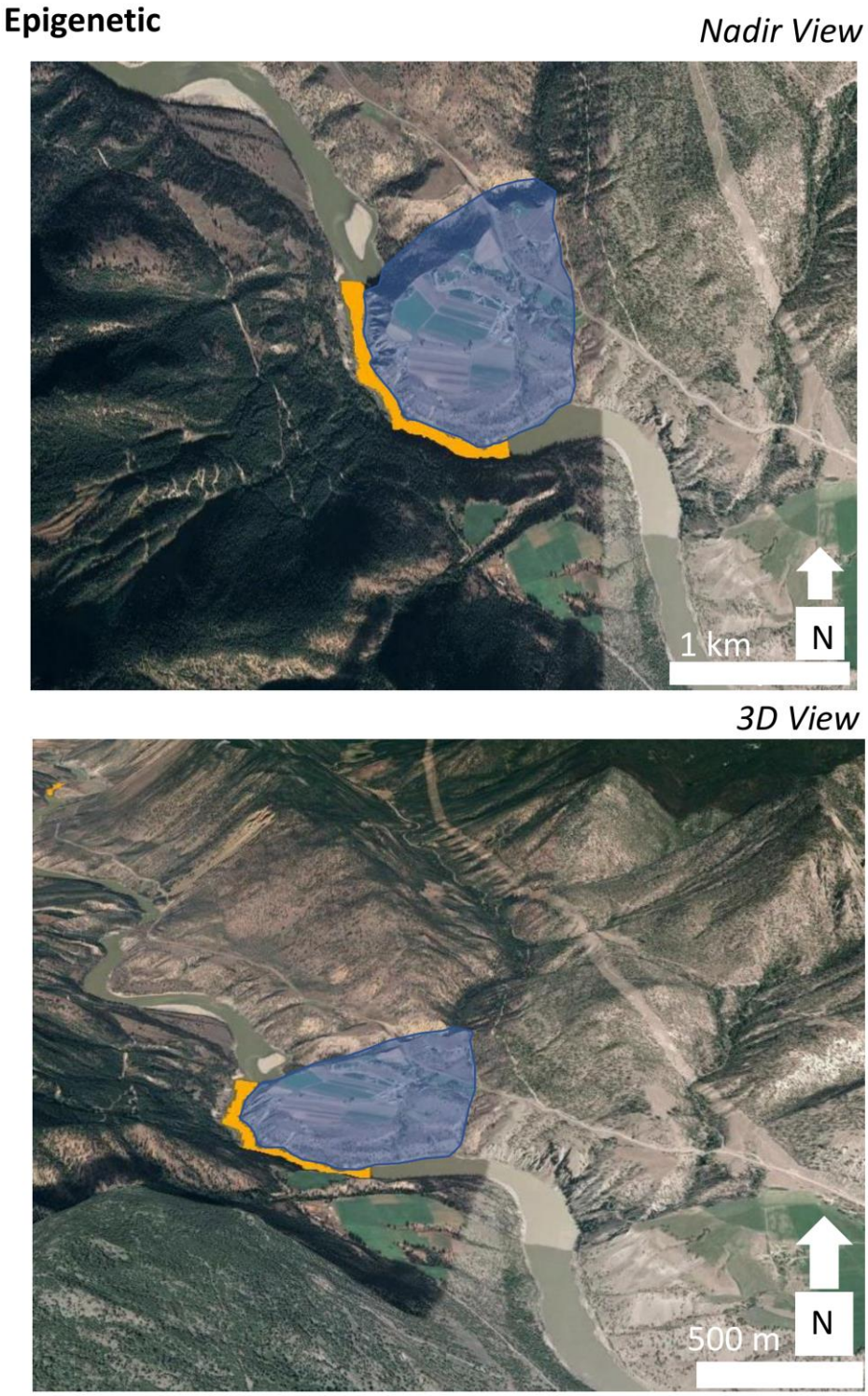

Figure A18: Lochore Nesikep Canyon (imagery accessed in Google Earth; source: Province of British Columbia, CNES/Airbus, 10/4/2019). Canyon was classified as epigenetic because of the lobate shape at the mouth a relic channel that appears to be a large lateral sediment input.

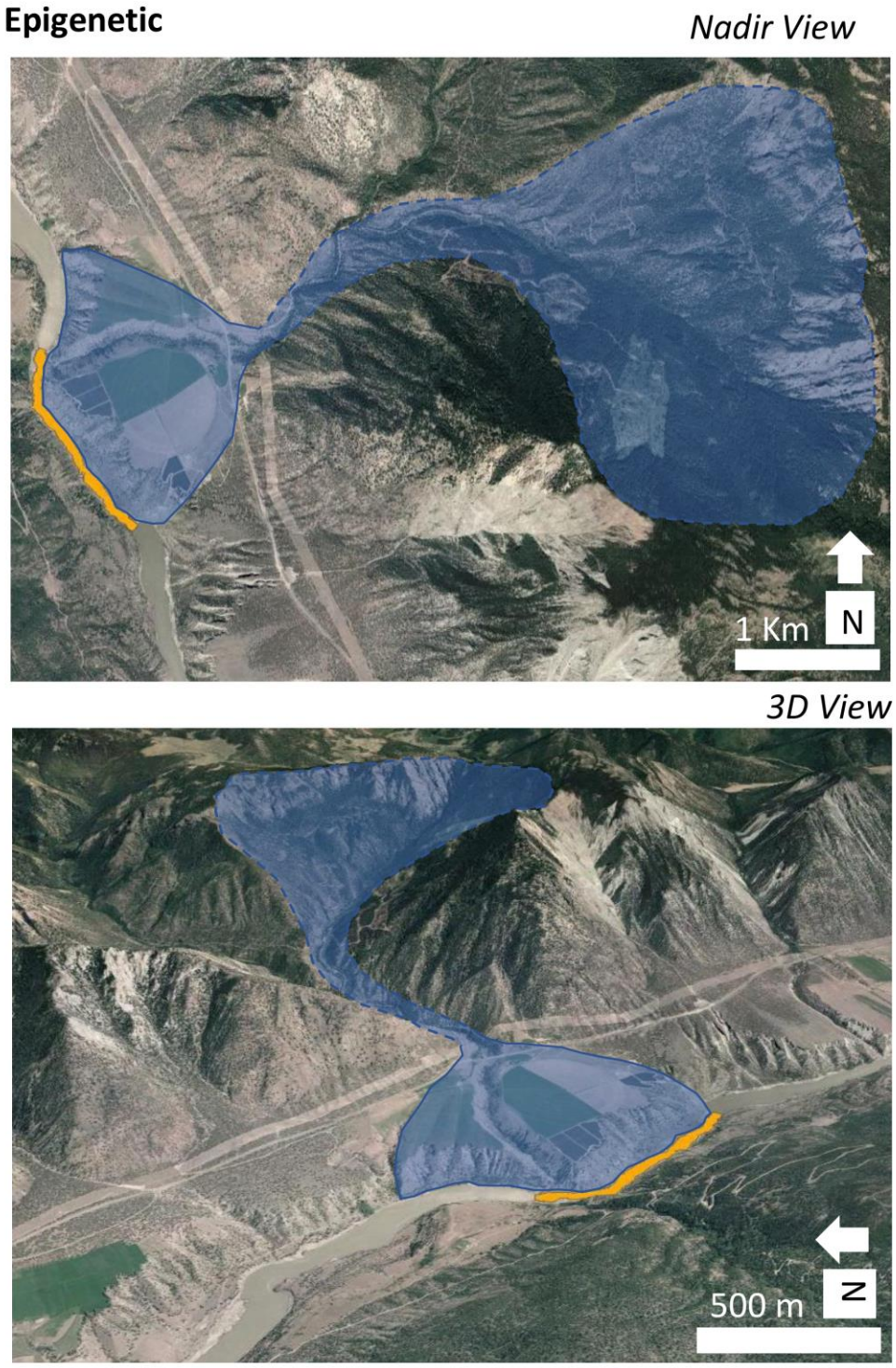

Figure A19: McGillivray Creek Canyon (imagery accessed in Google Earth; source: Province of British Columbia, Maxar Technologies, 12/31/2004). Canyon was classified as epigenetic because of the lobate shape associated with a large lateral sediment input from the eastern wall of the canyon. Dashed lines represent uncertainty in the boundaries of what appears to be the source of the sediment.

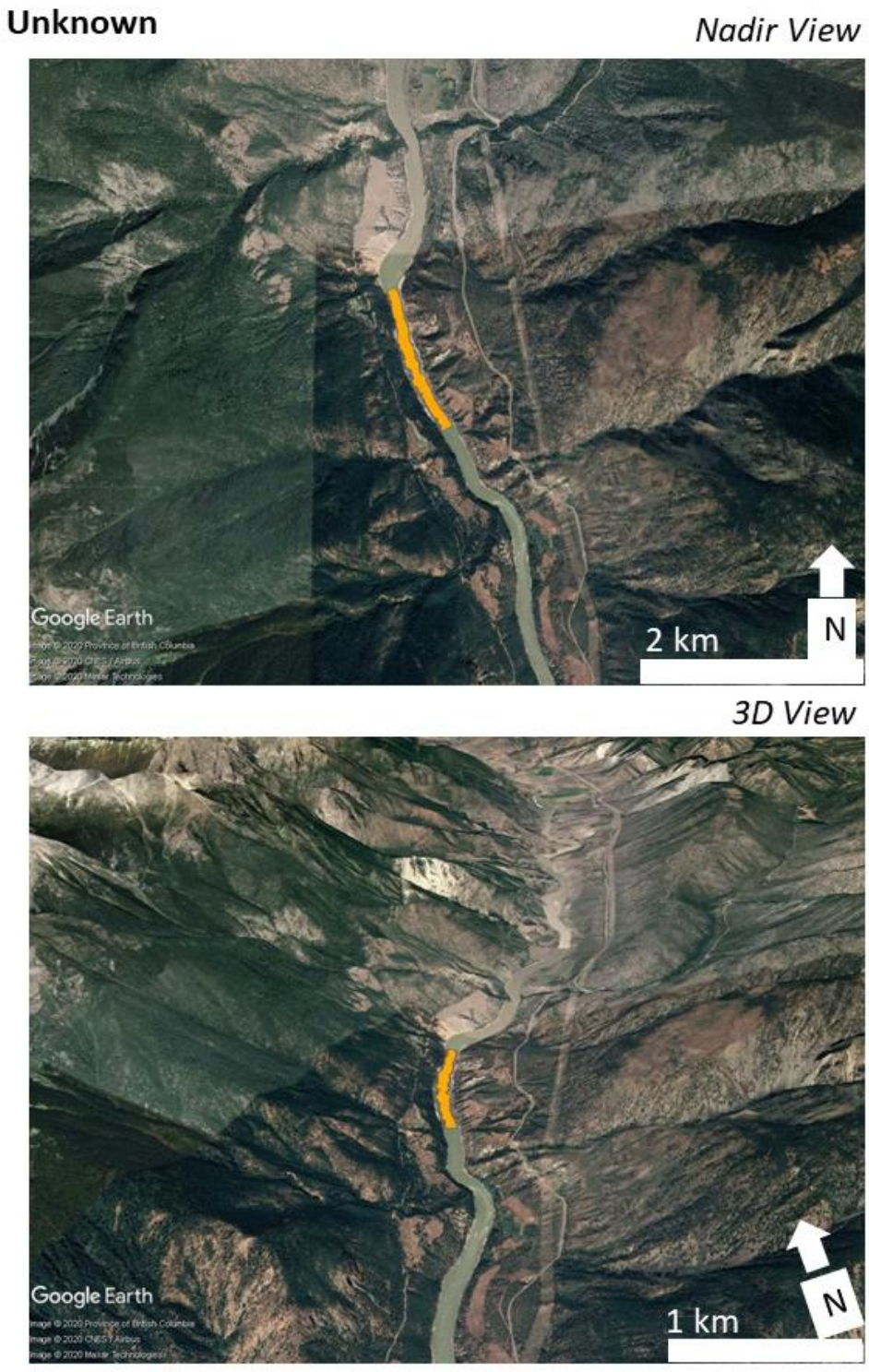

Figure A20: Spintlum Creek Canyon (imagery accessed in Google Earth; source: Maxar Technologies, Province of British Columbia, CNEW/Airbus, 10/4/2019). Canyon was classified as unknown because there are no obvious proximal sediment inputs or lineaments.

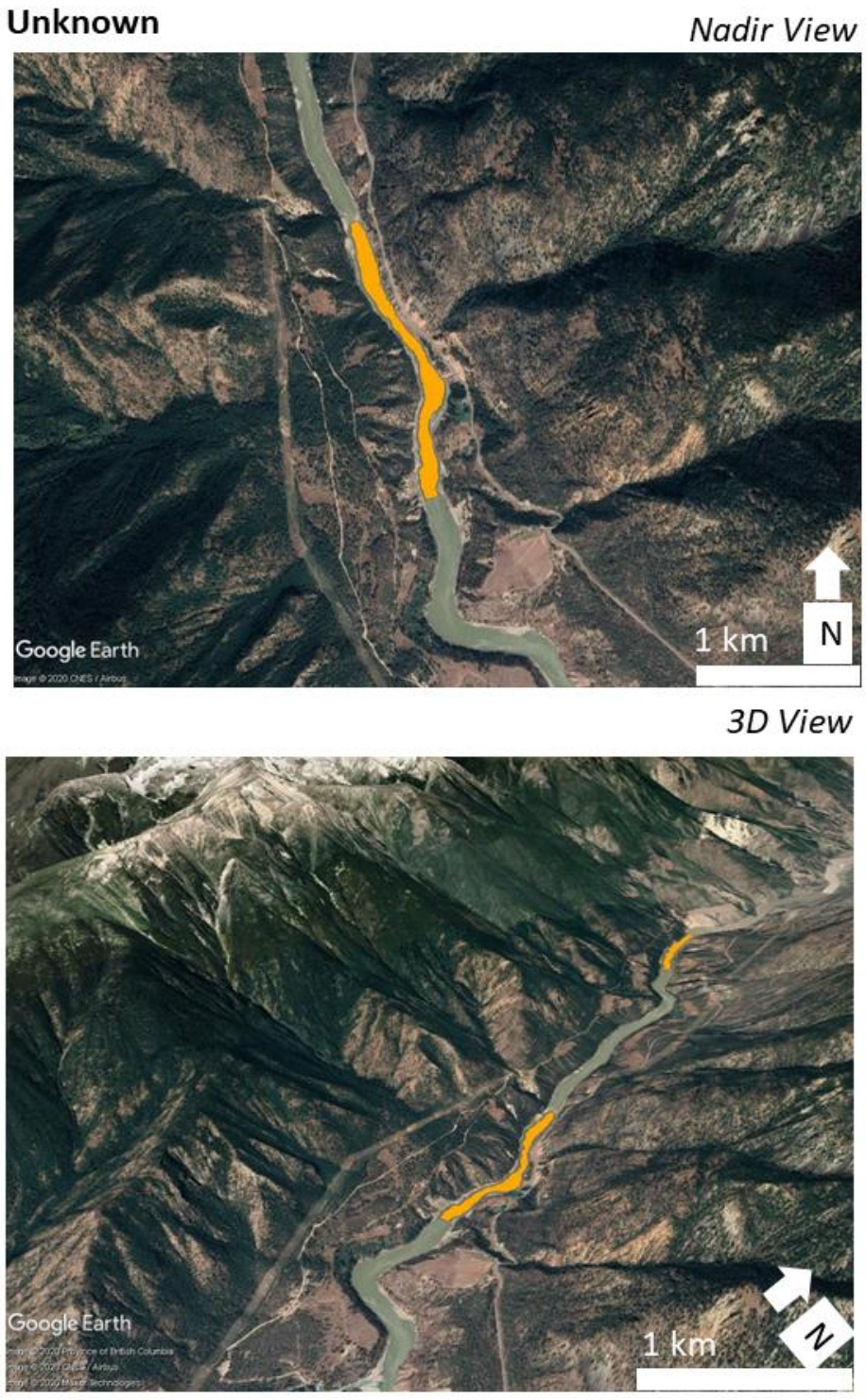

Figure A21: Hull Arden Canyon (imagery accessed in Google Earth; source: Maxar Technologies, Province of British Columbia, CNEW/Airbus, 9/2/2019). Canyon was classified as unknown because there are no obvious proximal sediment inputs or lineaments.

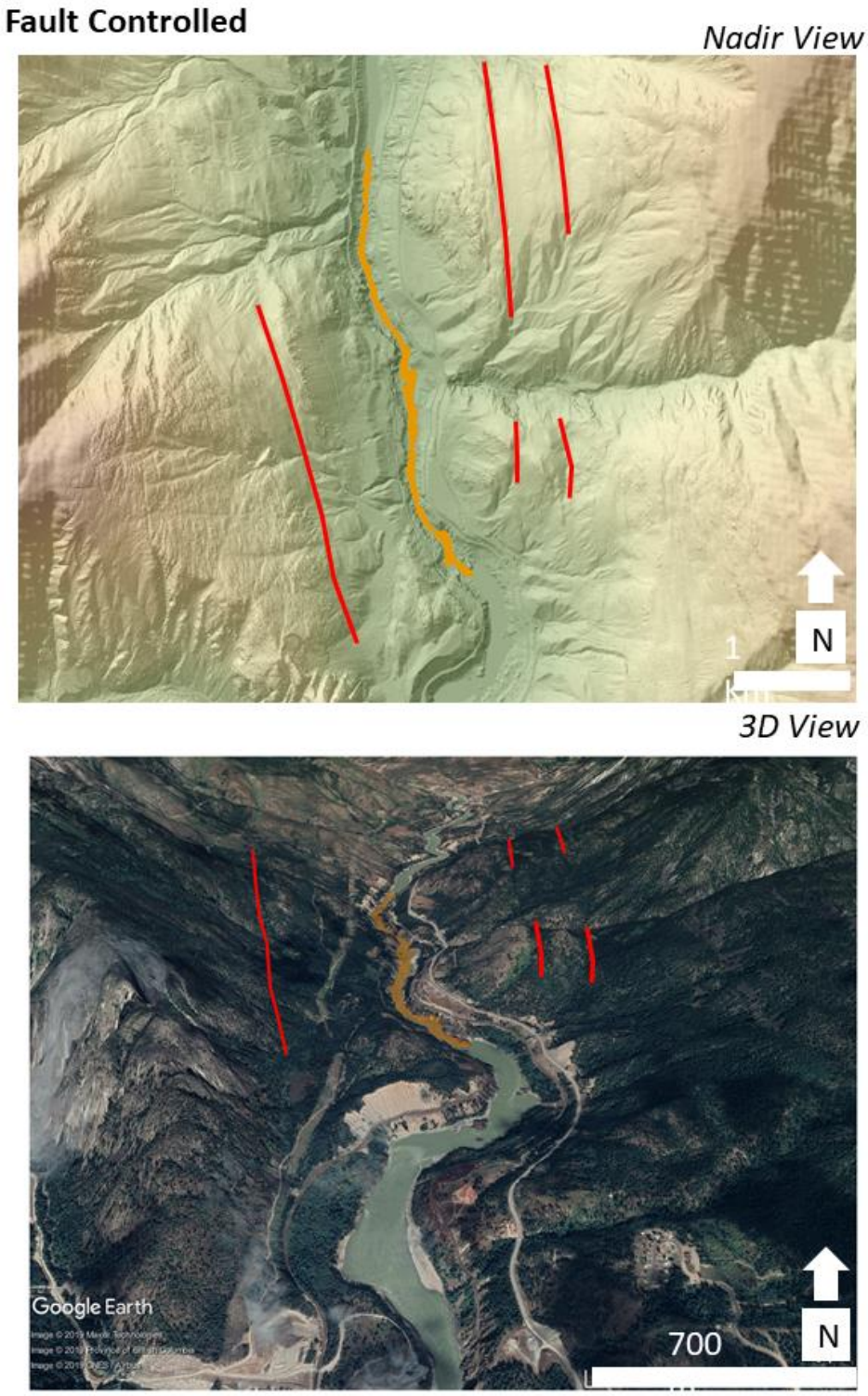

Figure A22: Siska Canyon (LiDAR flown Dec. 7th, 2016, imagery accessed in Google Earth; source: CNES/Airbus, 9/2/2019). Canyon was classified as fault controlled because of its alignment with proximal lineaments.

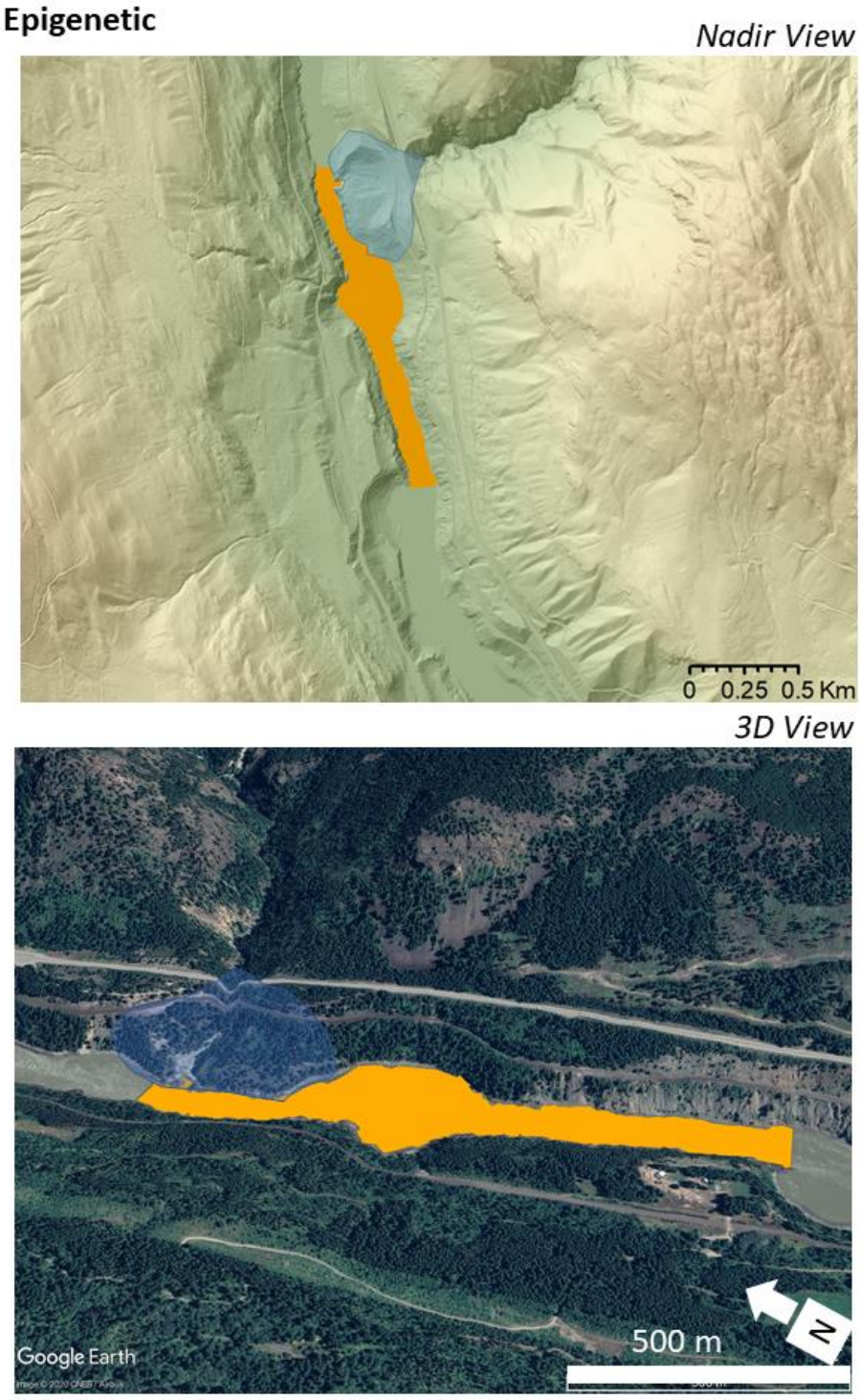

Figure A23: Keefer Canyon (imagery accessed in Google Earth; source: CNES/Airbus, Maxar Technologies, 7/25/2019). Canyon was classified as epigenetic because of the large amount of sediment at the mouth of Mowhokam Creek that appears to have influenced the channel.

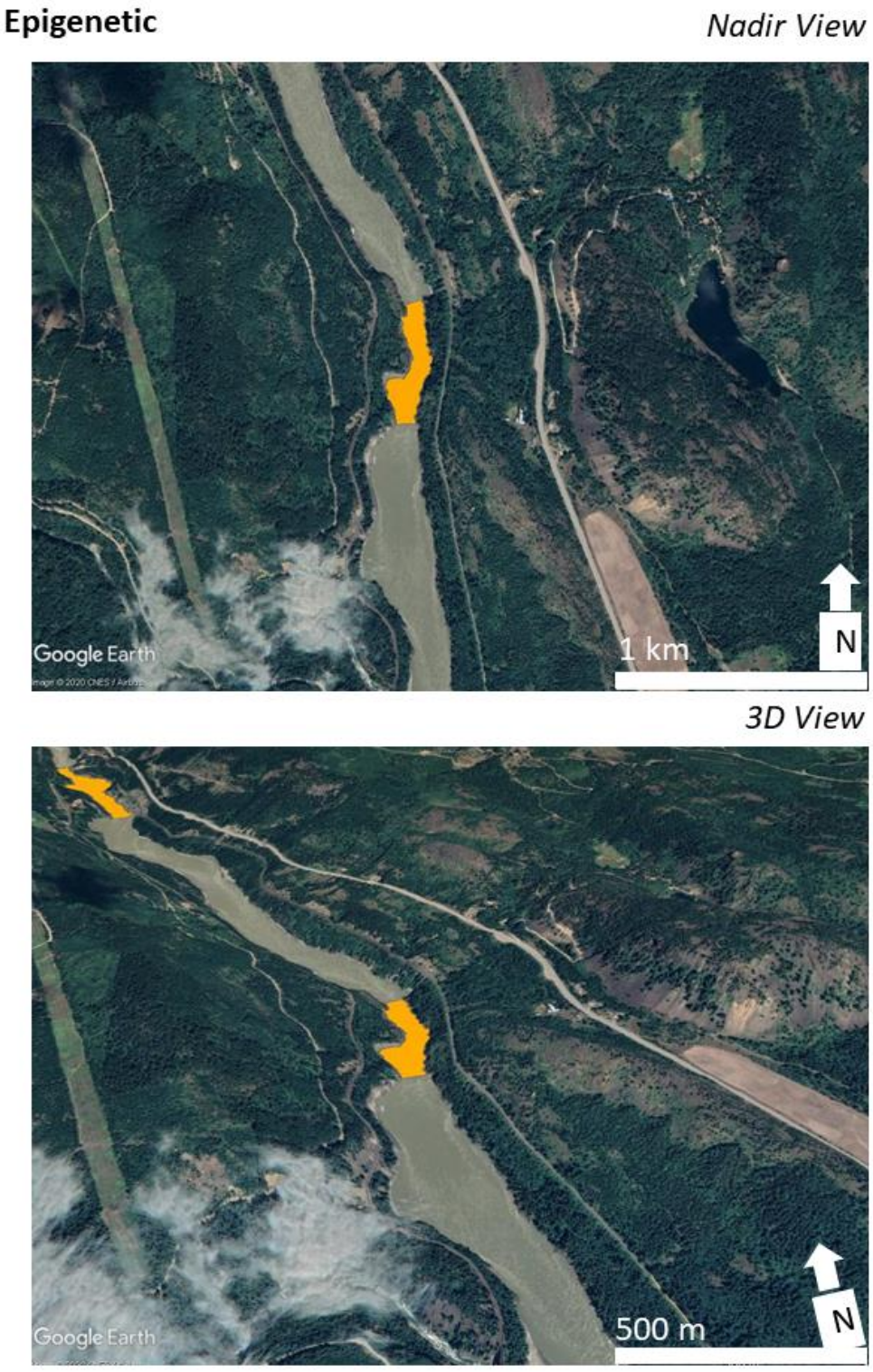

Figure A24: Inkahtsaph Canyon (imagery accessed in Google Earth; source: CNES/Airbus, 7/25/2019). Canyon was classified as unknown because there are no obvious proximal sediment inputs or lineaments.

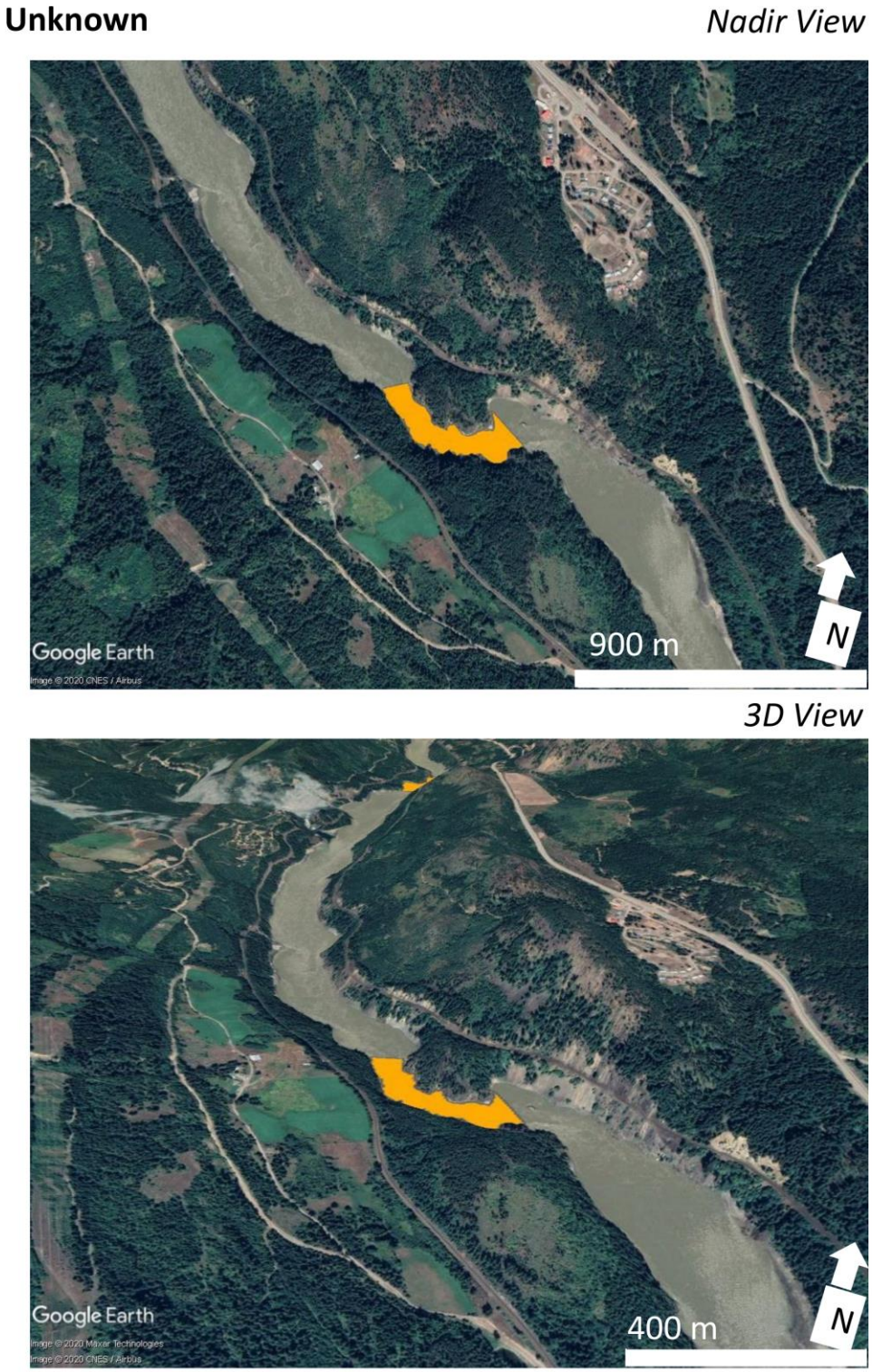

Figure A25: Kahmoose Canyon (imagery accessed in Google Earth; source: CNES/Airbus,Maxar Technologies, 7/25/2019). Canyon was classified as unknown because there are no obvious proximal sediment inputs or lineaments.

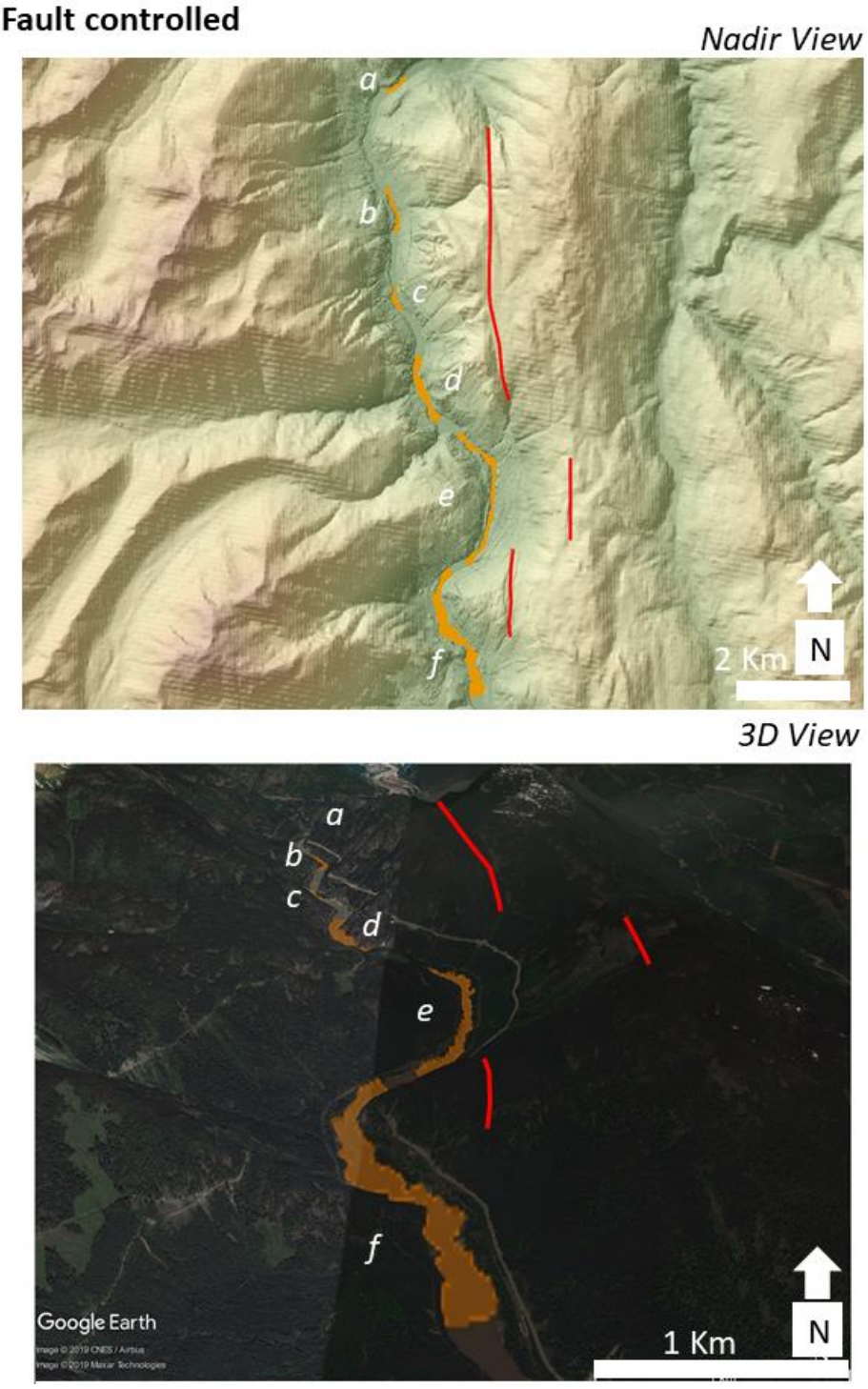

Figure A26: Scuzzy *(a),* Paul's Rapid *(b),* Hell's Gate *(c),* Little Hell's Gate *(d),* Black *(e),* and Black to Alexandra *(f)* Canyons (LiDAR flown Dec., 7, 2016, imagery accessed in Google Earth; source: CNES/Airbus, Maxar Technologies, 7/26/2016). Canyons were classified as fault controlled because of their obvious alignment with proximal lineaments.

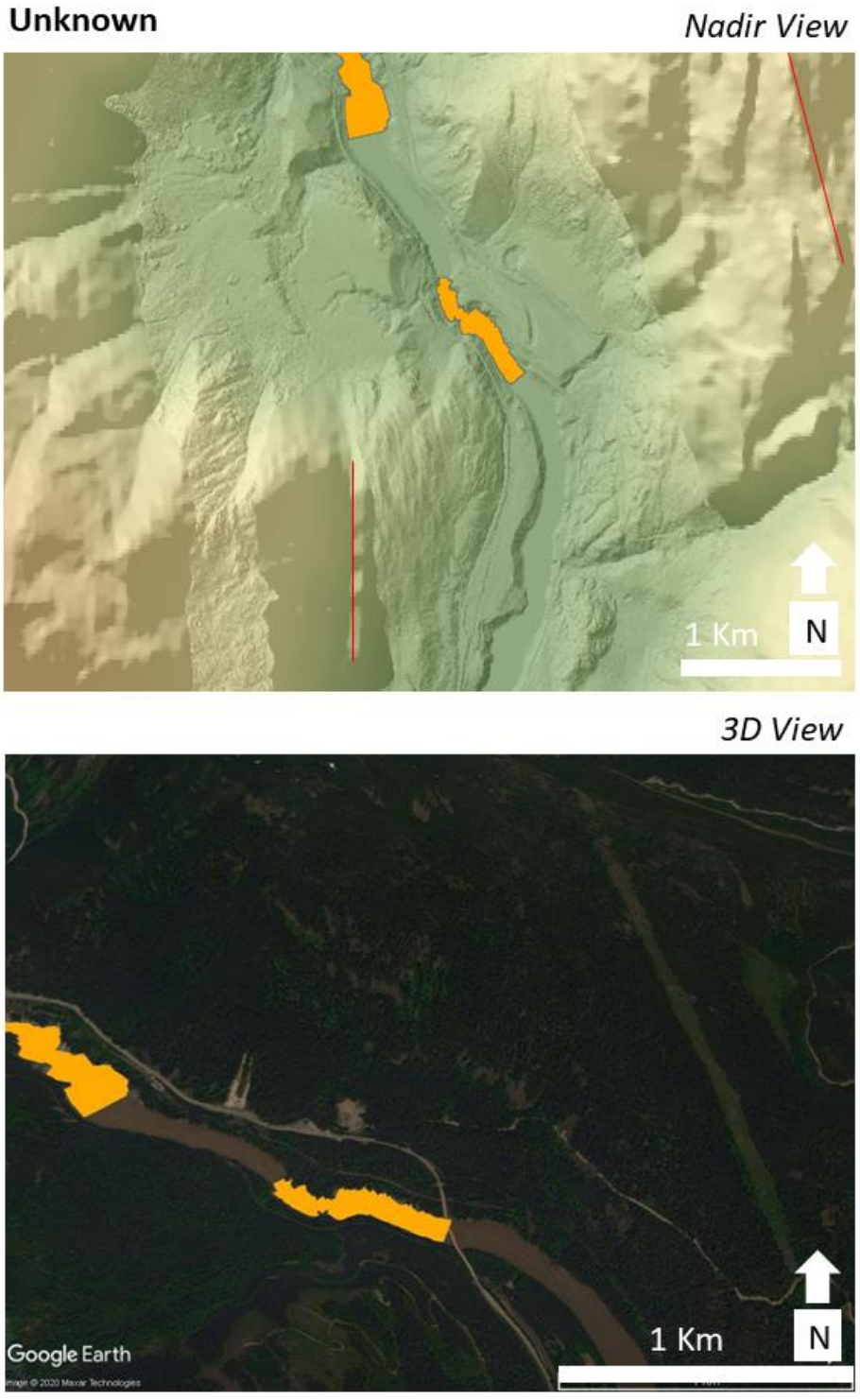

Figure A28: Yale Rapids Canyon (LiDAR flown Dec., 7, 2016, imagery accessed in Google Earth; source: CNES/Airbus, Maxar Technologies, 10/9/2019). Canyon was classified as fault controlled because of its alignment with the large lineament to the west.

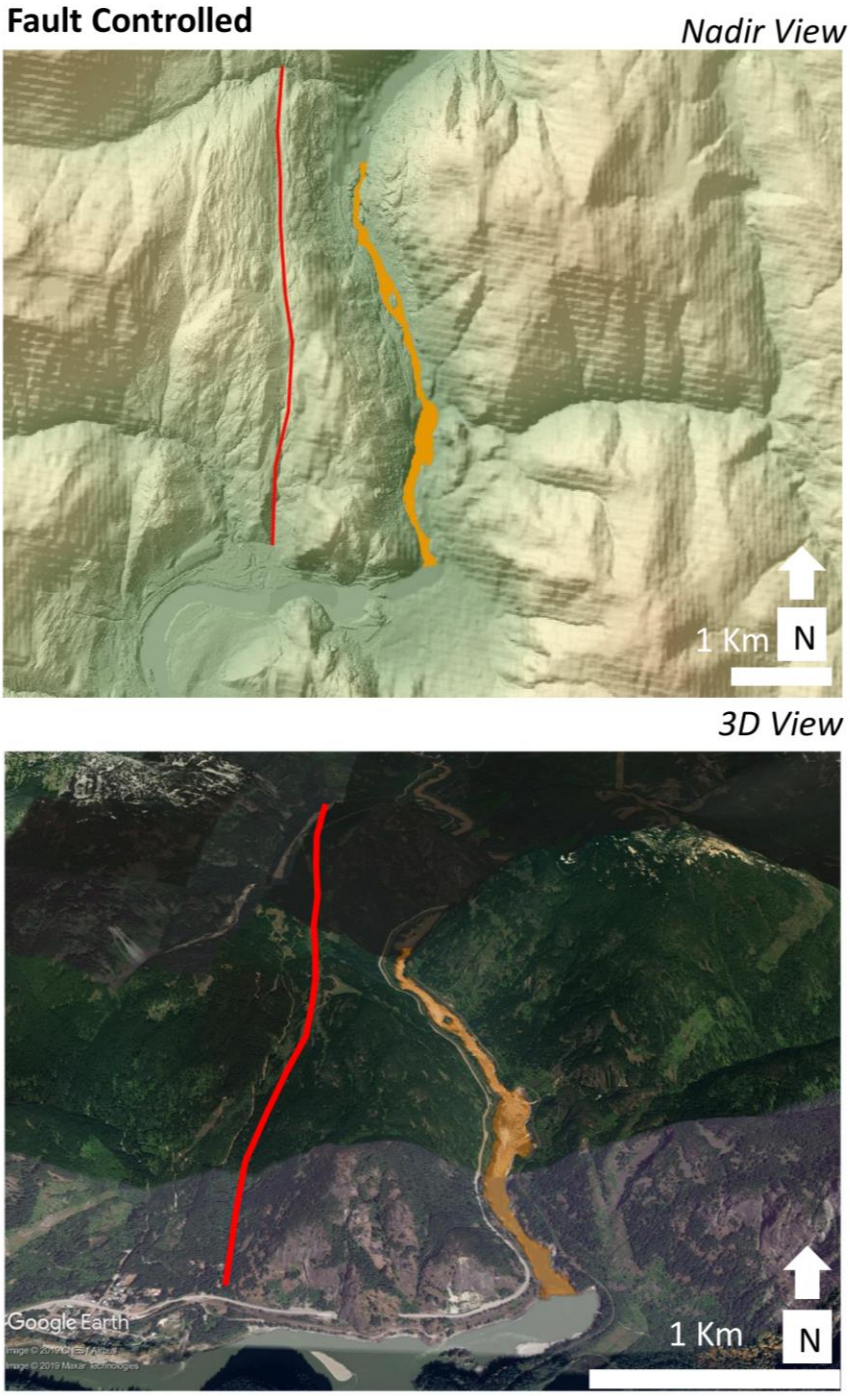

Figure A29: Yale Rapids Canyon (LiDAR flown Dec., 7, 2016, imagery accessed in Google Earth; source: CNES/Airbus, Maxar Technologies, 10/9/2019). Canyon was classified as fault controlled because of its alignment with a proximal lineament.

Appendix B.

Structural Characterizations of Constricting and Embayment Features

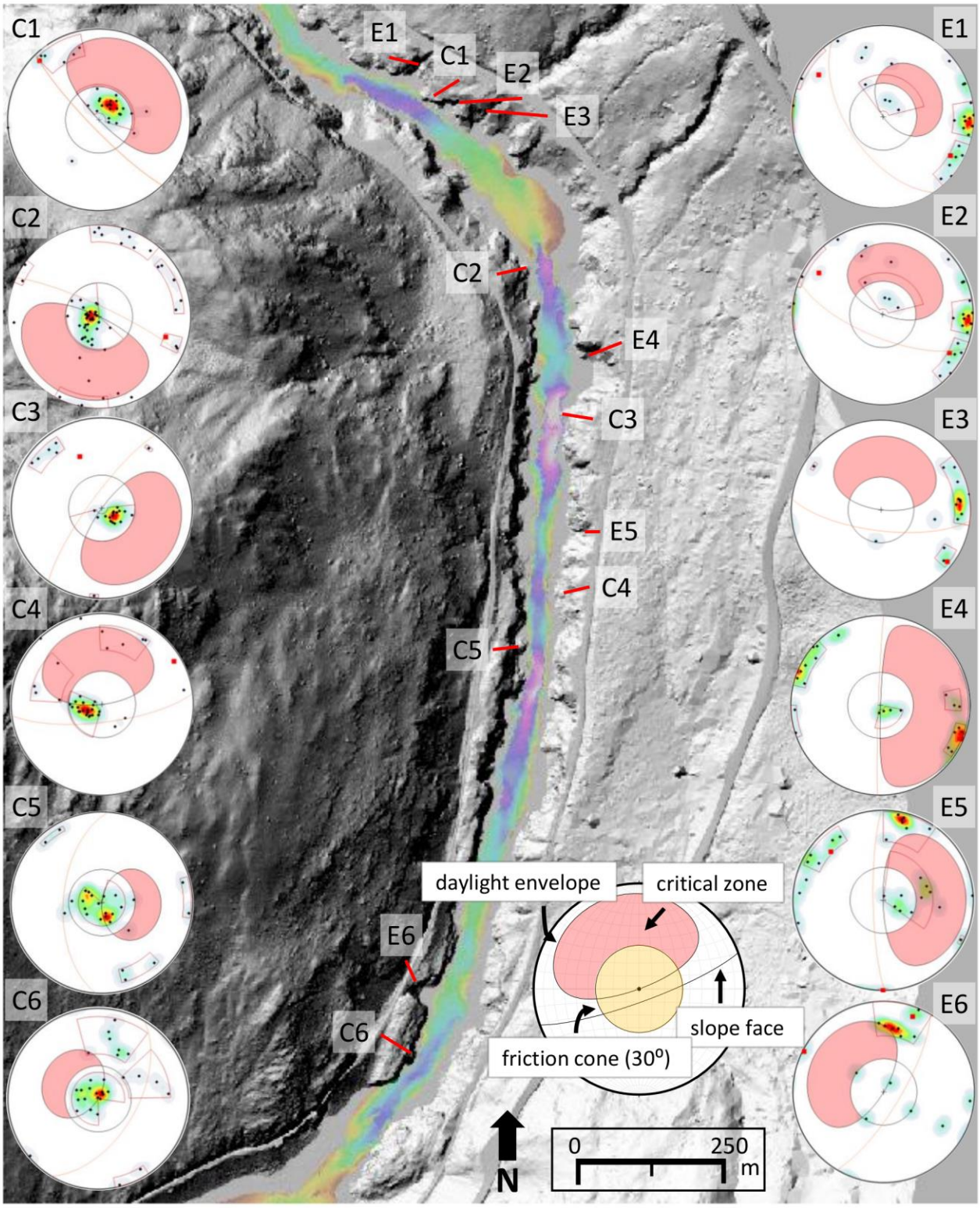

B1: Map and stereonets of the constricting and embayment features in Black Canyon. Slope stability analyses show potential for planar failure based on the angle and orientation of the slope of each feature's wall. In the feature labels, "C" stands for constricting features, and "E" stands for embayments, and the numbers are ordered from upstream to downstream.

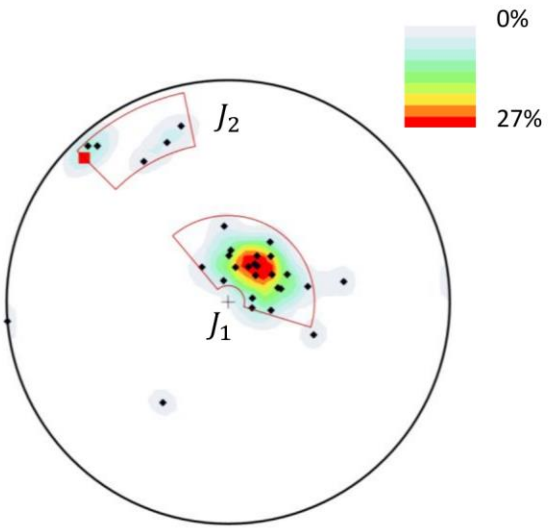

set	n	β^{o}	α^{o}	S (m)	P (m)
1	22	18	221	0.8	5.7
2	5	73	150	0.2	4.3

B2: C1. Above the high-water line on this constricting feature, medium-persistent joints intersect to create very large blocks sitting on a sub-horizontal surface. Below the high-water line, the jointing pattern is less clear, and the rock is intruded by a more competent granodiorite. The feature is bound on the downstream end by a major structure and on the upstream end by a rock slope failure. Red lines show major structures, which appear as red squares on the stereonets. β^{o} = mean dip angle; α^{o} = mean dip direction; S = mean spacing; P = mean persistence.

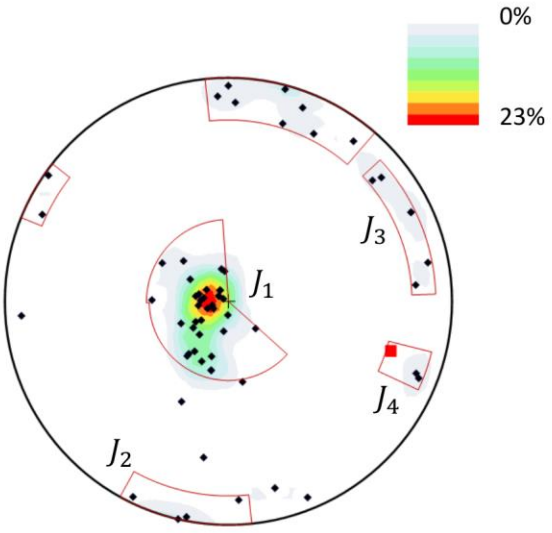

set	n	β^{o}	α^{o}	S (m)	P (m)
1	35	14	86	0.4	8.3
2	12	82	164	0.3	0.7
3	6	77	246	0.2	3.9
4	4	82	206	n/a	n/a

B3: C2. The dominant joint set in this constricting feature is sub-horizontal with medium persistence and very close spacing. It is intersected by two orthogonal sub-vertical joint sets, and a third that is parallel to a major structure that lies behind this constricting feature. The feature appears to be retreating by toppling or plucking of blocks on the left (downstream) side.

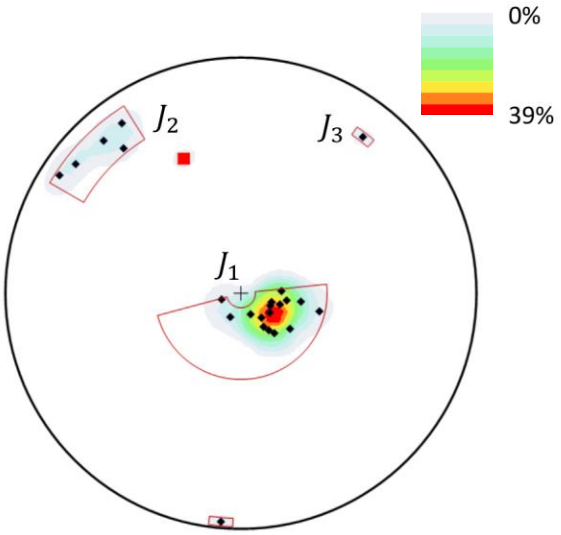

set	n	β°	α°	*S* (m)	*P* (m)
1	16	14	269	0.4	6.2
2	5	76	135	0.9	2.4
3	2	80	111		

B4: C3. This constricting feature is dominated by a sub-horizontal joint set with very close spacing and medium persistence. The two sub-vertical joint sets intersect with it to create blocks sitting on a sub-horizontal base. They appear to be retreating by toppling on the left (upstream side of the constriction (where undercutting would be greatest). A fault sits behind this outcrop, separating it from the wall in the background.

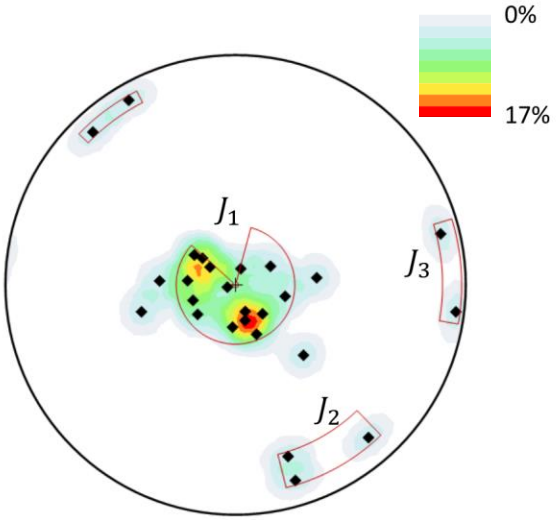

set	n	β°	α°	*S* (m)	*P* (m)
1	15	14	183	1.1	4.2
2	5	77	258	0.3	2.5
3	2	83	267	n/a	n/a

B5: C4. This constricting feature is dominated by a sub-horizontal joint set with wide spacing and medium persistence. The two sub-vertical joint sets intersect with it to create blocks sitting on a sub-horizontal base.

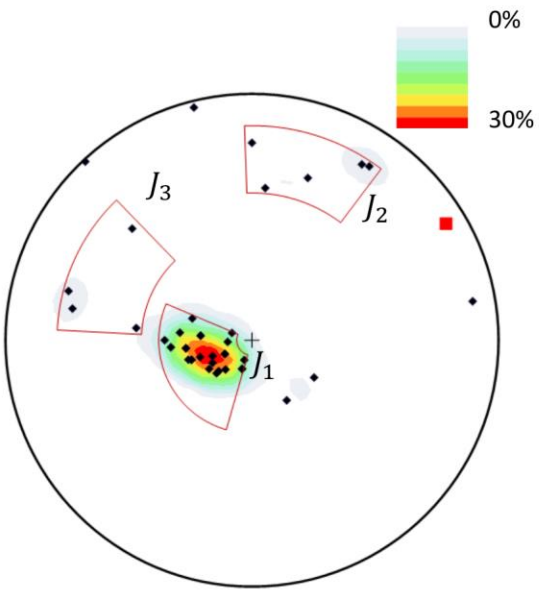

set	n	β°	α°	S (m)	P (m)
1	25	17	69	0.9	2.7
2	5	66	198	0.7	3.5
3	4	56	109	1.7	1.5

B6: C5. This constricting feature has three main joint sets that intersect to create columns sitting on a sub-horizontal base with low-medium persistence. The basal surface dips gently upstream and it appears that some columns on the downstream end of the outcrop have been removed by toppling or hydraulic plucking.The feature is bound by a fault, isolating it from the rest of the shoreline.

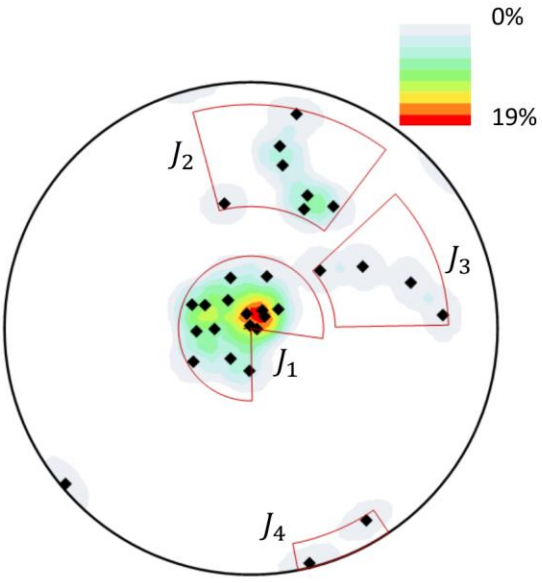

set	n	β°	α°	S (m)	P (m)
1	16	12	142	0.3	5.6
2	7	55	194	0.7	13.5
3	4	49	248	2.8	7.6
4	2	84	338	n/a	n/a

B7: C6. This constricting feature has four main joint sets with a dominant sub-horizontal joint set that forms the large bench feature in the bottom half of the wall. The overhanging joint faces on the right (upstream) end of the outcrop may have accommodated toppling of blocks.

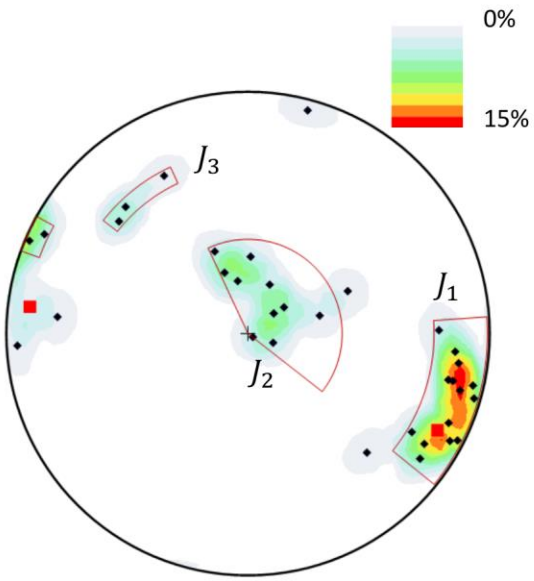

set	n	β°	α°	S (m)	P (m)
1	16	79	267	0.8	3.7
2	10	18	219	0.3	2.9
3	3	62	140	n/a	n/a

B8: E1. This embayment is bound by the major structures on the left (upstream) and a constricting feature on right. Two main sub-vertical joint sets run parallel to the main and intersect with the sub-horizontal joint set to form blocks. The joints have tighter spacing near the main structures. It is unclear if this wall retreated by the slow removal of blocks, or if it failed at once - sliding on the gently dipping surface seen in the foreground.

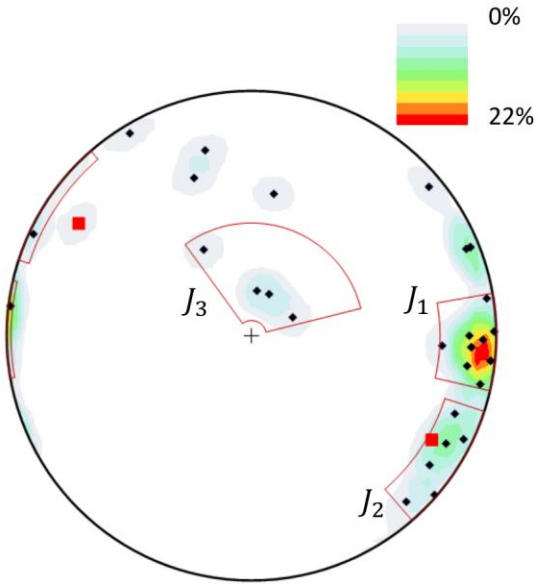

set	n	β°	α°	S (m)	P (m)
1	12	83	258	1.1	7.7
2	7	83	277	0.5	10.6
3	4	20	197	1.1	2.3

B9: E2. This embayment is bound both upstream and downstream by major structures and lies between more massive rock to the left (upstream), and more fractured rock to the right. The hole in the cliff and the rubble pile below may demonstrate the method of failure, with the toppling of columns created by the intersection of three mapped joint sets. If undercut, it may have failed as one event on the two major structures and a fracture parallel to the current face. A fresh surface suggests recent failure in the top left corner of the embayment.

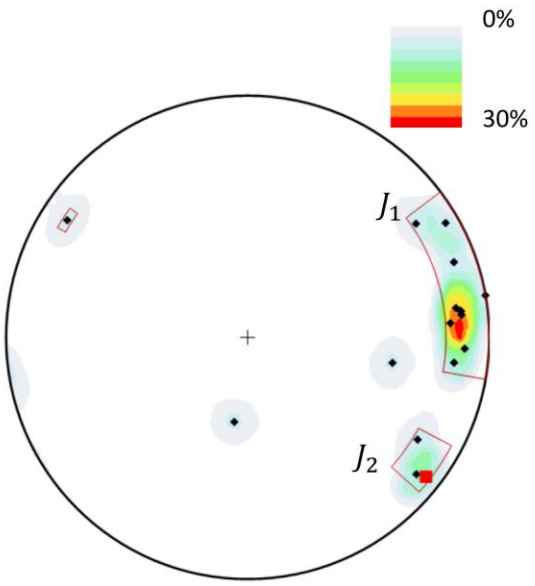

set	n	β°	α°	*S* (m)	*P* (m)
1	10	78	259	1.6	8.0
2	3	76	244	0.4	5.1

B10: E3. The main sub-vertical joint sets in this embayment are of close to very close spacing and medium persistence. There is another joint set, sub-parallel to the face of the outcrop that was unmeasurable because it rarely daylights but has extremely close spacing. The two measured joint planes are parallel or sub-parallel to the major structure that the waterfall traces.

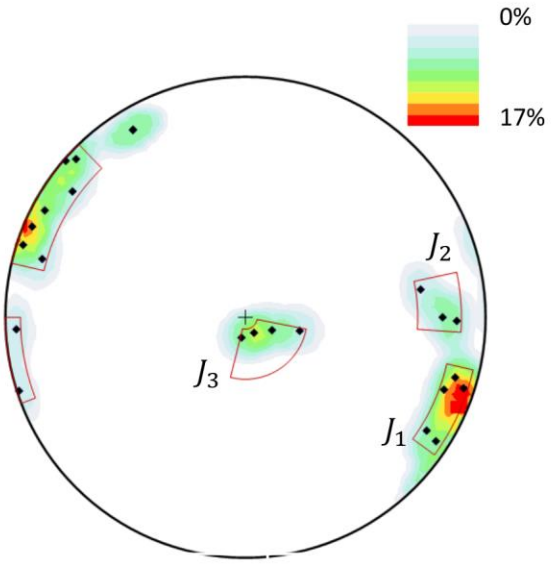

set	n	β°	α°	*S* (m)	*P* (m)
1	12	83	192	n/a	n/a
2	5	77	192	n/a	n/a
3	4	11	231	n/a	n/a

B11: E4. Measurements of this embayment feature were taken on the tower-like feature on the left (upstream) end of this photo because the bedrock in the embayment itself is mostly overlain with talus. The two dominant sub-vertical joint sets on this feature intersect with the sub-horizontal joint set to create columns that may fail through toppling or planar failure. Fresh rock surfaces suggest recent failures above and below waterline. It is unclear if this embayment formed through stages of retreat, or all at once.

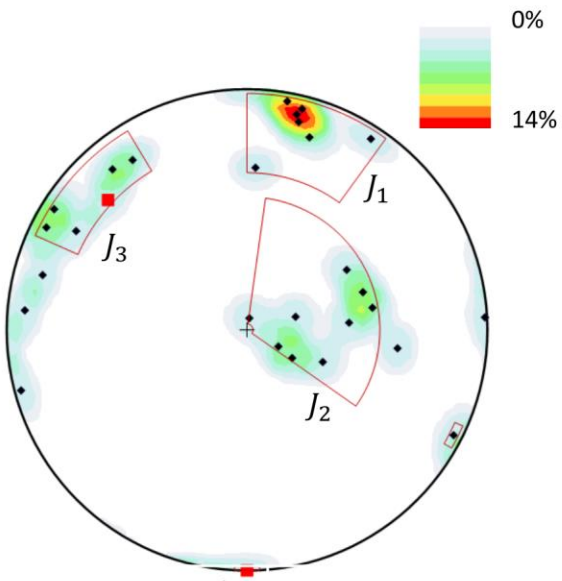

set	n	β°	α°	*S* (m)	*P* (m)
1	7	78	195	0.5	11.9
2	9	27	262	2.1	11.7
3	6	79	157	0.7	2.9

B12: E5. On the left of the outcrop, close to very closely spaced sub-vertical joints interact with sub-horizontal joints to create tall, thin columns. Evidence of their retreat is seen in the small basal features at the bottom of the outcrop. The right side of the outcrop shows similar kinematics of failure on more persistent joints of the same orientations. The deepest part of the embayment is bound by subvertical structures.

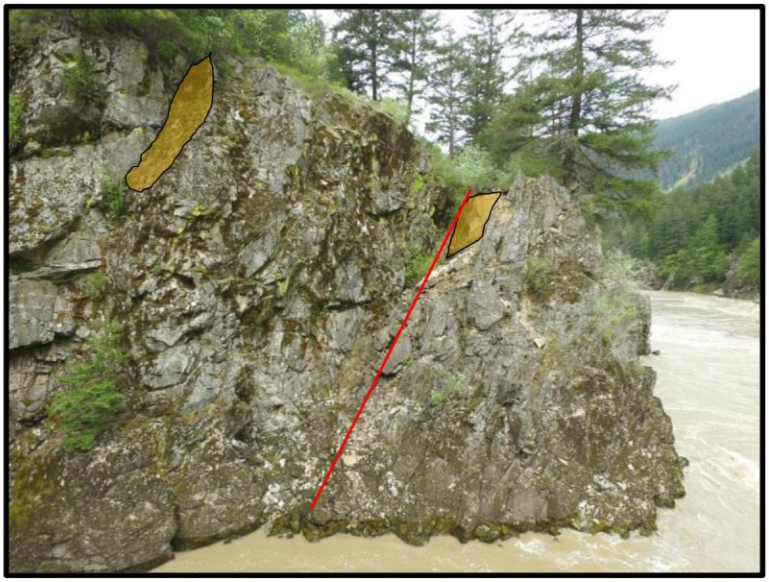

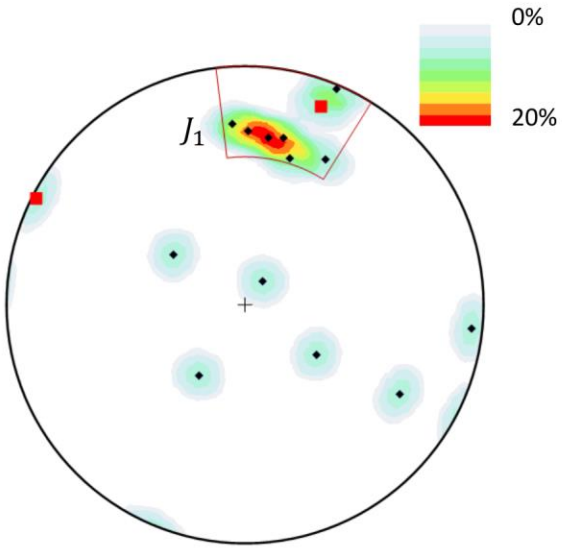

set	n	β°	α°	*S* (m)	*P* (m)
1	7	64	192	1.9	8.1

B13: E6. This embayment has two dominant sub-vertical joint sets that each align with major structures that bound the upstream and downstream ends of the feature. While The kinematics of failure are unclear here; it appears that the rock between the two major structures failed when undercut.